

Dear handling editor,

Thanks for giving us the opportunity to revise our manuscript following reviewers' comments. We have taken into account all of reviewers' comments in revising our manuscript.

Among their major comments,

- 1) we have rearranged the manuscript by moving budget equations to the appendix, and moving the description of all parameterizations to the main text,
- 2) moved Figure 1, which showed the original structure of the model, from main text to the appendix
- 3) added additional discussion of various BNF parameterizations, and parameterizations that related leaf N to V_{cmax} , in the discussion section
- 4) added equations that describe how the model treats upper limit of C:N ratios of different plant components,
- 5) included an additional plot (now Figure 10c) which shows zonally-averaged GPP ratios to illustrate how downregulation works differently in the original model and the model version with N cycle, and
- 6) included a sentence about prioritizing immobilization versus plant N uptake in section 3.3.6 (on page 27 of this document).
- 7) Reorganized figures such that fertilizer input and N deposition are considered inputs, plotted in a separate figure, and discussed in inputs while BNF is considered a model output, plotted separately than specified N inputs of fertilizer and N deposition, and discussed in the model results section.

In addition, we also took into account all of minor comments that reviewers made as mentioned in our reply to the reviewers in the discussion section.

This document tracks all the changes that we have made since our last version.

Best regards,
Vivek.

Implementation of nitrogen cycle in the CLASSIC land model

Ali Asaadi and Vivek. K. Arora

Canadian Centre for Climate Modelling and Analysis, Environment Canada, University of Victoria,
Victoria, B.C., V8W 2Y2, Canada

1 **Abstract**

2

3 A terrestrial nitrogen (N) cycle model is coupled to carbon (C) cycle in the framework of the Canadian Land
4 Surface Scheme Including biogeochemical Cycles (CLASSIC). CLASSIC currently models physical and
5 biogeochemical processes and simulates fluxes of water, energy, and CO₂ at the land-atmosphere
6 boundary. Similar to most models, gross primary productivity in CLASSIC increases in response to
7 increasing atmospheric CO₂ concentration. In the current model version, a downregulation
8 parameterization emulates the effect of nutrient constraints and scales down potential photosynthesis
9 rates, using a globally constant scalar, as a function of increasing CO₂. In the new model when nitrogen
10 (N) and carbon (C) cycles are coupled, cycling of N through the coupled soil-vegetation system facilitates
11 the simulation of leaf N content and maximum carboxylation capacity (V_{cmax}) prognostically. An increase
12 in atmospheric CO₂ decreases leaf N content, and therefore V_{cmax} , allowing the simulation of
13 photosynthesis downregulation as a function of N supply. All primary N cycle processes, that represent
14 the coupled soil-vegetation system, are modelled explicitly. These include biological N fixation, treatment
15 of externally specified N deposition and fertilization application, uptake of N by plants, transfer of N to
16 litter via litterfall, mineralization, immobilization, nitrification, denitrification, ammonia volatilization,
17 leaching, and the gaseous fluxes of NO, N₂O, and N₂. The interactions between terrestrial C and N cycles
18 are evaluated by perturbing the coupled soil-vegetation system in CLASSIC with one forcing at a time over
19 the 1850-2017 historical period. These forcings include the increase in atmospheric CO₂, change in
20 climate, increase in N deposition, and increasing crop area and fertilizer input, over the historical period.
21 Increase in atmospheric CO₂ increases the C:N ratio of vegetation; climate warming over the historical
22 period increases N mineralization and leads to a decrease in vegetation C:N ratio; N deposition also
23 decreases vegetation C:N ratio; and fertilizer input increases leaching, NH₃ volatilization, and gaseous
24 losses of N₂, N₂O, and NO. These model responses are consistent with conceptual understanding of the
25 coupled C and N cycles. The simulated terrestrial carbon sink over the 1959-2017 period, from the
26 simulation with all forcings, is 2.0 Pg C/yr and compares reasonably well with the quasi observation-based
27 estimate from the 2019 Global Carbon Project (2.1 Pg C/yr). The contribution of increasing CO₂, climate
28 change, and N deposition to carbon uptake by land over the historical period (1850-2017) is calculated to
29 be 84%, 2%, and 14%, respectively.

30

Deleted: to these forcings is

32 1. Introduction

33 The uptake of carbon (C) by land and ocean in response to the increase in anthropogenic
34 fossil fuel emissions of CO₂ has served to slow down the growth rate of atmospheric CO₂ since
35 the start of the industrial revolution. At present, about 55% of total carbon emitted into the
36 atmosphere is taken up by land and ocean (Le Quéré et al., 2018; Friedlingstein et al., 2019). It is
37 of great policy, societal, and scientific relevance whether land and ocean will continue to provide
38 this ecosystem service. Over land, as long as photosynthesis is not water limited, the uptake of
39 carbon in response to increasing anthropogenic CO₂ emissions is driven by two primary factors,
40 1) the CO₂ fertilization of the terrestrial biosphere, and 2) the increase in temperature, both of
41 which are associated with increasing [CO₂]. The CO₂ fertilization effect increases photosynthesis
42 rates for about 80% of the world's vegetation that uses the C₃ photosynthetic pathway and is
43 currently limited by [CO₂] (Still et al., 2003; Zhu et al., 2016). The remaining 20% of vegetation
44 uses the C₄ photosynthetic pathway that is much less sensitive to [CO₂]. Warming increases
45 carbon uptake by vegetation in mid-high latitude regions where growth is currently limited by
46 low temperatures (Zeng et al., 2011).

47 Even when atmospheric CO₂ is not limiting for photosynthesis, and near surface air
48 temperature is optimal, vegetation cannot photosynthesize at its maximum possible rate if
49 available water and nutrients (most importantly nitrogen (N) and phosphorus (P)) constrain
50 photosynthesis (Vitousek and Howarth, 1991; Reich et al., 2006b). In the absence of water and
51 nutrients, photosynthesis simply cannot occur. N is a major component of chlorophyll (the
52 compound through which plants photosynthesize) and amino acids (that are the building blocks
53 of proteins). The constraint imposed by available water and nutrients implies that the carbon

Deleted: C₃

Deleted: since photosynthesis for plants

56 uptake by land over the historical period in response to increasing [CO₂] is lower than what it
57 would have been if water and nutrients were not limiting. This lower than maximum theoretically
58 possible rate of increase of photosynthesis in response to increasing atmospheric CO₂ is referred
59 to as downregulation (Faria et al., 1996; Sanz-Sáez et al., 2010). Typically, however, the term
60 downregulation of photosynthesis is used only in the context of nutrients and not water.

61 Downregulation is defined as a decrease in photosynthetic capacity of plants grown at elevated
62 CO₂ in comparison to plants grown at baseline CO₂ (McGuire et al., 1995). However, despite the
63 decrease in photosynthetic capacity, the photosynthesis rate for plants grown at elevated CO₂ is
64 still higher than the rate for plants grown and measured at baseline CO₂ because of higher
65 background CO₂.

Deleted: McGuire et al. (1995) define d

Deleted: ,

Deleted: although

Deleted: rate of

Deleted: and measured at

Deleted: .

66 Earth system models (ESMs) that explicitly represent coupling of the global carbon cycle
67 and physical climate system processes are the only tools available at present that, in a physically
68 consistent way, are able to project how land and ocean carbon cycles will respond to future
69 changes in [CO₂]. Such models are routinely compared to one another under the auspices of the
70 Coupled Model Intercomparison Project (CMIP) every 6-7 years. The most recent and sixth phase
71 of CMIP (CMIP6) is currently underway (Eyring et al., 2016). Interactions between carbon cycle
72 and climate in ESMs have been compared under the umbrella of the Coupled Climate-Carbon
73 Cycle Model Intercomparison Project (C⁴MIP) (Jones et al., 2016) which is an approved MIP of
74 the CMIP. Comparison of land and ocean carbon uptake in C⁴MIP studies (Friedlingstein et al.,
75 2006; Arora et al., 2013, 2020) indicate that the inter-model uncertainty in future land carbon
76 uptake across ESMs is more than three times than the uncertainty for the ocean carbon uptake.

Deleted: varies widely and

Deleted: as much

77 The reason for widely varying estimates of future land carbon uptake across models is that our

86 understanding of biological processes that determine land carbon uptake is much less advanced
87 than the physical processes which primarily determine carbon uptake over the ocean. In the
88 current generation of terrestrial ecosystem models, other than photosynthesis for which a
89 theoretical framework exists, almost all of the other biological processes are represented on the
90 basis of empirical observations and parameterized in one way or another. In addition, not all
91 models include N and P cycles. In the absence of an explicit representation of nutrient constraints
92 on photosynthesis, land models in ESMs parameterize downregulation of photosynthesis in other
93 ways that reduce the rate of increase of photosynthesis to values below its theoretically
94 maximum possible rate, as [CO₂] increases (e.g., Arora et al., 2009). Comparison of models across
95 5th and 6th phase of CMIP shows that the fraction of models with land N cycle is increasing (Arora
96 et al., 2013, 2020).

97 The nutrient constraints on photosynthesis are well recognized (Vitousek and Howarth,
98 1991; Arneeth et al., 2010). Terrestrial carbon cycle models neglect of nutrient limitation on
99 photosynthesis has been questioned from an ecological perspective (Reich et al., 2006a) and it
100 has been argued that without nutrient constraints these models will overestimate future land
101 carbon uptake (Hungate et al., 2003). Since in the real world photosynthesis downregulation does
102 indeed occur due to nutrient constraints, it may be argued that more confidence can be placed
103 in future projections of models that explicitly model the interactions between the terrestrial C
104 and N cycles rather than parameterize it in some other way.

105 Here, we present the implementation of N cycle in the Canadian Land Surface Scheme
106 Including biogeochemical Cycles (CLASSIC) model, which serves as the land component in the
107 family of Canadian Earth System Models (Arora et al., 2009, 2011; Swart et al., 2019). Section 2

Deleted: s

109 briefly describes existing physical and carbon cycle components and processes of the CLASSIC
110 model. The conceptual basis of the new N cycle model and its parameterizations are described
111 in Section 3, Section 4 outlines the methodology and data sets that we have used to perform
112 various simulations over the 1850-2017 historical period to assess the realism of the coupled C
113 and N cycles in CLASSIC in response to various forcings. Results from these simulations over the
114 historical period are presented in Section 5 and finally discussion and conclusions are presented
115 in Section 6.

Deleted: and in the appendix

116 **2. The CLASSIC land model**

117 **2.1 The physical and carbon biogeochemical processes**

118 The CLASSIC model is the successor to, and based on, the coupled Canadian Land Surface
119 Scheme (CLASS; Verseghy, 1991; Verseghy et al., 1993) and Canadian Terrestrial Ecosystem
120 Model (CTEM; Arora and Boer, 2005; Melton and Arora, 2016). CLASS and CTEM model physical
121 and biogeochemical processes in CLASSIC, respectively. Both CLASS and CTEM have a long history
122 of development as described in Melton et al. (2019) who also provide an overview of the CLASSIC
123 land model and describe its new technical developments that launched CLASSIC as a community
124 model. CLASSIC simulates land-atmosphere fluxes of water, energy, momentum, CO₂, and CH₄.
125 The CLASSIC model can be run at a point scale, e.g. using meteorological and geophysical data
126 from a FluxNet site, or over a spatial domain, that may be global or regional, using gridded data.
127 We briefly summarize the primary physical and carbon biogeochemical processes of CLASSIC here
128 that are relevant in the context of implementation of the N cycle in the model.

129 **2.1.1 Physical processes**

131 The physical processes of CLASSIC which simulate fluxes of water, energy and momentum,
 132 are calculated over vegetated, snow, and bare fractions at a sub-daily time step of 30 minutes.
 133 The vegetation is described in terms of four plant functional types (PFTs); needleleaf trees,
 134 broadleaf trees, crops, and grasses. The fractional coverage of these four PFTs are specified in
 135 the current study over the historical period. The structural attributes of vegetation are described
 136 by leaf area index (LAI), vegetation height, canopy mass, and rooting distribution through the soil
 137 layers and these are all simulated dynamically by the biogeochemical module of CLASSIC. In the
 138 model version used here, 20 ground layers starting with 10 layers of 0.1 m thickness are used.
 139 The thickness of layers gradually increases to 30 m for a total ground depth of over 61 m. The
 140 depth to bedrock varies geographically and is specified based on a soil depth data set. Liquid and
 141 frozen soil moisture contents, and soil temperature, are determined prognostically for
 142 permeable soil layers. CLASSIC also prognostically models the temperature, mass, albedo, and
 143 density of a single layer snow pack (when the climate permits snow to exist), Interception and
 144 throughfall of rain and snow by the canopy, and the subsequent unloading of snow, are also
 145 modelled. The energy and water balance over the land surface, and the transfer of heat and
 146 moisture through soil, affect the temperature and soil moisture content of soil layers all of which
 147 consequently affect the carbon and nitrogen cycle processes.

149 2.1.2 Biogeochemical processes

150 The biogeochemical processes in CLASSIC are based on CTEM, and described in detail in
 151 the appendix of Melton and Arora (2016). The biogeochemical component of CLASSIC simulates

- Deleted:** that
- Deleted:** based on CLASS, operate at
- Deleted:** . A time step
- Deleted:** is typically used to avoid numerical instabilities
- Deleted:** Water, energy, and momentum fluxes are calculated over vegetated, snow, and bare fractions, and the fractional vegetation cover is specified for each grid cell.
- Deleted:** in the operational version of the model
- Deleted:** either
- Deleted:** or may be dynamically simulated using competition between PFTs, calculations for which are performed in the biogeochemical module (CTEM).
- Deleted:** rooting
- Deleted:** depth and distribution that determine the fraction of roots in each of the model's soil layers. These structural vegetation attributes
- Deleted:** may be specified or
- Deleted:** of CLASSIC as a function of the driving meteorological data and [CO₂]
- Deleted:** The number of permeable soil and non-permeable bedrock layers in CLASSIC can be varied depending on its application. The
- Deleted:** standard offline
- Deleted:** that is driven with reanalysis meteorological data, like
- Deleted:** in this study, uses
- Deleted:** ,
- Deleted:** ing
- Deleted:** a
- Deleted:** thick layer
- Deleted:** For application within the Canadian Earth system model currently three ground layers with thicknesses of 0.1, 0.25 and 3.75 m are used.
- Deleted:** Above this depth, the layers are considered soil and therefore permeable allowing movement of water between the layers for which I
- Deleted:** Below the permeable soil, the bedrock rock layers are considered impermeable and therefore their soil moisture content is zero. Soil and bedrock temperatures are found for each ground layer.
- Deleted:** , the temperature and depth of ponded water on the soil, and the temperature of the vegetation canopy
- Deleted:** Energy and water balance of each grid cell evolves independently and there is no lateral transfer of heat or moisture between them.

196 the land-atmosphere exchange of CO₂ and while doing so simulates vegetation as a dynamic
197 component. The biogeochemical module of CLASSIC uses information about net radiation, and
198 liquid and frozen soil moisture contents of all the soil layers along with air temperature to
199 simulate photosynthesis and prognostically calculates amount of carbon in the model's three live
200 (leaves, stem, and root) and two dead (litter and soil) carbon pools for each PFT. The litter and
201 soil carbon pools are not tracked for each soil layer. Litter is assumed to be near surface and an
202 exponential distribution for soil carbon is assumed with values decreasing with soil depth.
203 Photosynthesis in CLASSIC is modelled at the same sub-daily time as the physical processes. The
204 remainder of the biogeochemical processes are modelled at a daily time step. These include: 1)
205 autotrophic and heterotrophic respirations from all the live and dead carbon pools, respectively,
206 2) allocation of photosynthate from leaves to stem and roots, 3) leaf phenology, 4) turnover of
207 live vegetation components that generates litter, 5) mortality, 6) land use change (LUC), 7) fire
208 (Arora and Melton, 2018), and 8) competition between PFTs for space (not switched on in this
209 study).

Deleted: The physics module (CLASS) provides the biogeochemical module (CTEM) with physical land surface information including net radiation, and liquid and frozen soil moisture contents of all the soil layers.

Deleted: this

210 Figure A1 in the appendix shows the existing structure of CLASSIC's carbon pools along
211 with the addition of non-structural carbohydrate pools for each of the model's live vegetation
212 components. The non-structural pools are not yet represented in the current operational version
213 of CLASSIC (Melton et al., 2019). The addition of non-structural carbohydrate pools is explained
214 in Asaadi et al. (2018) and helps improve leaf phenology for cold deciduous tree PFTs. The N cycle
215 model presented here is built on the research version of CLASSIC that consists of non-structural
216 and structural carbon pools for the leaves (L), stem (S), and root (R) components and the two
217 dead carbon pools in litter or detritus (D) and soil or humus (H) (Figure A1). We briefly describe

Deleted: ¶

224 these carbon pools and fluxes between them, since N cycle pools and fluxes are closely tied to
225 carbon pools and fluxes. The gross primary productivity (GPP) flux enters the leaves from the
226 atmosphere. This non-structural photosynthate is allocated between leaves, stem, and roots. The
227 non-structural carbon then moves into the structural carbohydrates pool. Once this conversion
228 occurs structural carbon cannot be converted back to non-structural labile carbon. The model
229 attempts to maintain a minimum fraction of non-structural to total carbon in each component of
230 about 0.05 (Asaadi et al., 2018). Non-structural carbon is moved from stem and root components
231 to leaves, at the time of leaf onset for deciduous PFTs, and this is termed reallocation. The
232 movement of non-structural carbon is indicated by red arrows. Maintenance and growth
233 respiration (indicated by subscript *m* and *g* in Figure A1), which together constitute autotrophic
234 respiration, occur from the non-structural components of the three live vegetation components.
235 Litterfall from the structural and non-structural components of the vegetation components
236 contributes to the litter pool. Leaf litterfall is generated due to normal turnover of leaves as well
237 as cold and drought stresses, and reduction in day length. Stem and root litter is generated due
238 to their turnover based on their specified life spans. Heterotrophic respiration occurs from the
239 litter and soil carbon pools depending on soil moisture and temperature, and humified litter is
240 moved from litter to the soil carbon pool.

241 All these terrestrial ecosystem processes and the amount of carbon in the live and dead
242 carbon pools are modelled explicitly for nine PFTs that map directly onto the four base PFTs used
243 in the physics module of CLASSIC. Needleleaf trees are divided into their deciduous and
244 evergreen phenotypes, broadleaf trees are divided into cold deciduous, drought deciduous, and
245 evergreen phenotypes, and crops and grasses are divided based on their photosynthetic

246 pathways into C₃ and C₄ versions. The sub-division of PFTs is required for modelling
247 biogeochemical processes. For instance, simulating leaf phenology requires the distinction
248 between evergreen and deciduous phenotypes of needleleaf and broadleaf trees. However, once
249 LAI is known, a physical process (such as the interception of rain and snow by canopy leaves) does
250 not need to know the underlying evergreen or deciduous nature of leaves.

251 The prognostically determined biomasses in leaves, stem, and roots are used to calculate
252 structural vegetation attributes that are required by the physics module. Leaf biomass is used to
253 calculate LAI using PFT-dependent specific leaf area. Stem biomass is used to calculate vegetation
254 height for tree and crop PFTs, and LAI is used to calculate vegetation height for grasses. Finally,
255 root biomass is used to calculate rooting depth and distribution which determines the fraction of
256 roots in each soil layer. Only total root biomass is tracked; fine and coarse root biomasses are not
257 separately tracked. Fraction of fine roots is calculated as a function of total root biomass, as
258 shown later.

259 The approach for calculating photosynthesis in CLASSIC is based on the standard Farquhar
260 et al. (1980) model for C₃ photosynthetic pathway, and Collatz et al. (1992) for the C₄
261 photosynthetic pathway and presented in detail in Arora (2003). The model calculates gross
262 photosynthesis rate that is co-limited by the photosynthetic enzyme Rubisco, by the amount of
263 available light, and by the capacity to transport photosynthetic products for C₃ plants or the CO₂-
264 limited capacity for C₄ plants. In the real world, the maximum Rubisco limited rate (V_{cmax}) depends
265 on the leaf N content since photosynthetic capacity and leaf N are strongly correlated (Evans,
266 1989; Field and Mooney, 1986; Garnier et al., 1999). In the current operational version of
267 CLASSIC, the N cycle is not represented and the PFT-dependent values of V_{cmax} are therefore

Deleted: Other than these structural vegetation attributes the biogeochemical module also calculates canopy resistance (in conjunction with photosynthesis) that is used by the physics module in calculating transpiration.

272 specified based on Kattge et al. (2009) who compile V_{cmax} values using observation-based data
273 from more than 700 measurements. Along with available light, and the capacity to transport
274 photosynthetic products, the GPP in the model is determined by specified PFT-dependent values
275 of V_{cmax} .

Deleted: strongly

276 In the current CLASSIC version a parameterization of photosynthesis downregulation is included
277 which, in the absence of the N cycle, implicitly attempts to simulate the effects of nutrient
278 constraints. This parameterization, based on approaches which express GPP as a logarithmic
279 function of $[CO_2]$ (Cao et al., 2001; Alexandrov and Oikawa, 2002), is explained in detail in Arora
280 et al. (2009) and briefly summarized here. To parameterize photosynthesis downregulation with
281 increasing $[CO_2]$ the unconstrained or potential GPP (for each time step and each PFT in a grid
282 cell) is multiplied by the global scalar $\xi(c)$

Deleted: Also, i

Moved (insertion) [1]

Deleted: of photosynthesis

Deleted: for emulating nutrient constraints,

$$283 \quad G = \xi(c) G_p \quad (1)$$

Deleted: 2

$$284 \quad \xi(c) = \frac{1 + \gamma_d \ln(c/c_0)}{1 + \gamma_p \ln(c/c_0)} \quad (2)$$

Deleted: 3

285 where c is $[CO_2]$ at time t and its initial value is c_0 , the parameter γ_p indicates the "potential" rate
286 of increase of GPP with $[CO_2]$ (indicated by the subscript p), the parameter γ_d represents the
287 downregulated rate of increase of GPP with $[CO_2]$ (indicated by the subscript d). When $\gamma_d < \gamma_p$
288 the modelled gross primary productivity (G) increases in response to $[CO_2]$ at a rate determined
289 by the value of γ_d . In the absence of the N cycle, the term $\xi(c)$ thus emulates down-regulation
290 of photosynthesis as CO_2 increases. For example, values of $\gamma_d=0.35$ and $\gamma_p=0.90$ yield a value of
291 $\xi(c) = 0.87$ (indicating a 13% downregulation) for $c=390$ ppm (corresponding to year 2010) and
292 $c_0=285$ ppm.

Deleted: where t is omitted for clarity and

Deleted: 42

Deleted: , from Arora et al. (2009)

Deleted: 94

Deleted: 6

304 Note that while the original model version does not include N cycle, it is capable of
 305 simulating realistic geographical distribution of GPP that partly comes from the specification of
 306 observation-based V_{cmax} values (which implicitly takes into account C and N interactions in a non-
 307 dynamic way) but more so the fact that the geographical distribution of GPP (and therefore net
 308 primary productivity, NPP), to the first order, depends on climate. The specified V_{cmax} values for
 309 the 9 PFTs in CLASSIC vary by about 2 times, from about 35 to 75 $\mu\text{-mol CO}_2 \text{ m}^{-2} \text{ s}^{-1}$. The simulated
 310 GPP in the model, however, varies from zero in the Sahara desert to about 3000 $\text{gC m}^{-2} \text{ year}^{-1}$ in
 311 the Amazonian rainforest indicating the overarching control of climate in determining the
 312 geographical distribution of GPP. This is further illustrated by the Miami NPP model, for instance,
 313 which is able to simulate the geographical distribution of NPP using only mean annual
 314 temperature and precipitation (Leith, 1975) since both the C and N cycles are governed primarily
 315 by climate. The current version of CLASSIC is also able to reasonably simulate the terrestrial C
 316 sink over the second half of the 20th century and early 21st century. CLASSIC (with its former
 317 CLASS-CTEM name) has regularly contributed to the annual Trends in Net Land–Atmosphere
 318 Carbon Exchange (TRENDY) model intercomparison since 2016 which contributes results to the
 319 Global Carbon Project’s annual assessments – the most recent one being Friedlingstein et al.
 320 (2019). What is then the purpose of coupling C and N cycles?

322 **3. Implementation of the N cycle in CLASSIC**

323 The primary objective of implementation of the N cycle is to model V_{cmax} as a function of
 324 leaf N content so as to make the use of multiplier $\xi(c)$ obsolete in the model, and allow to project

Moved up [1]: To parameterize downregulation of photosynthesis with increasing $[\text{CO}_2]$ for emulating nutrient constraints, the unconstrained or potential GPP (for each time step and each PFT in a grid cell) is multiplied by the global scalar $\xi(c)$ ¶

$$G = \xi(c) G_p \quad (2)$$

$$\xi(c) = \frac{1 + \gamma_d \ln(c/c_0)}{1 + \gamma_p \ln(c/c_0)} \quad (3) ¶$$

where t is omitted for clarity and the parameter γ_d represents the downregulated rate of increase of GPP with $[\text{CO}_2]$ (indicated by the subscript d). When $\gamma_d < \gamma_p$ the modelled gross primary productivity (G) increases in response to $[\text{CO}_2]$ at a rate determined by the value of γ_d . In the absence of the N cycle, the term $\xi(c)$ thus emulates down-regulation of photosynthesis as CO_2 increases. For example, values of $\gamma_d=0.42$ and $\gamma_p=0.90$, from Arora et al. (2009), yield a value of $\xi(c) = 0.94$ (indicating a 6% downregulation) for $c=390$ ppm (corresponding to year 2010) and $c_0=285$ ppm.

Deleted: ¶
 Following earlier simpler approaches (Cao et al., 2001; Alexandrov and Oikawa, 2002), GPP can be expressed as a logarithmic function of $[\text{CO}_2]$ ¶

$$G_p(t) = G_0 \left(1 + \gamma_p \ln \frac{c(t)}{c_0} \right) \quad (1) ¶$$

where the unconstrained or potential GPP at any given time, $G_p(t)$, is a function of its initial value G_0 , $[\text{CO}_2]$ at time t , $c(t)$, and its initial value c_0 . The rate of increase of GPP is determined by the parameter γ_p (where p indicates the “potential” rate of increase of GPP with $[\text{CO}_2]$). The parameter γ_p is calculated by fitting equation (1) to simulated GPP over the historical period. In the absence of any nutrient constraints, the rate of increase of carbon uptake per unit area of leaves is determined by the theoretical framework of Farquhar et al. (1980) and Collatz et al. (1992) for C_3 and C_4 photosynthetic pathways, respectively. The rate of increase of global GPP, however, also depends on how the model simulated LAI increases in response to increasing $[\text{CO}_2]$, which in turn depends on how photosynthate is allocated between leaves, stem, and root. Arora et al. (2009) compared the unconstrained simulated rate of increase of GPP per unit increase in $[\text{CO}_2]$ (their Figure 3) with that based on the theoretical framework to show that the model’s response to increasing $[\text{CO}_2]$ over the historical period is consistent with the theoretical framework, given specified time-independent V_{cmax} values for different PFTs. To parameterize downregulation of photosynthesis with increasing $[\text{CO}_2]$ for emulating nutrient constraints, the unconstrained or potential GPP (for each time step and each PFT in a grid cell) is multiplied by the global scalar $\xi(c)$ ¶

$$G = \xi(c) G_p \quad (2)$$

$$\xi(c) = \frac{1 + \gamma_d \ln(c/c_0)}{1 + \gamma_p \ln(c/c_0)} \quad (3) ¶$$

where t is omitted for clarity and the parameter γ_d represents the downregulated rate of increase of GPP with $[\text{CO}_2]$ (indic... [1])

Deleted: a

Deleted: rates

Deleted: T

Deleted: the

420 future carbon uptake that is constrained by available N. Modelling of leaf N content as a
421 prognostic variable, however, requires modelling the full N cycle over land. N enters the soil in
422 the inorganic mineral form through biological fixation of N, fertilizer application, and atmospheric
423 N deposition in the form of ammonium and nitrate. N cycling through plants implies uptake of
424 inorganic mineral N by plants, its return to soil through litter generation in the organic form, and
425 its conversion back to mineral form during decomposition of organic matter in litter and soil.
426 Finally, N leaves the coupled soil-vegetation system through leaching in runoff and through
427 various gaseous forms to the atmosphere. This section describes how these processes are
428 implemented and parameterized in the CLASSIC modelling framework. While the first order
429 interactions between C and N cycles are described well by the current climate, their temporal
430 dynamics over time require to explicitly model these processes.

431 Globally, terrestrial N cycle processes are even less constrained than the C cycle
432 processes. As a result, the model structure and parameterizations are based on conceptual
433 understanding and mostly empirical observations of N cycle related biological processes. We
434 attempt to achieve balance between a parsimonious and simple model structure and the ability
435 to represent the primary feedbacks and interactions between different model components.

436 3.1 Model structure, and N pools and fluxes

437 N is associated with each of the model's three live vegetation components and the two
438 dead carbon pools (shown in Figure A1). In addition, separate mineral pools of ammonium (NH_4^+)
439 and nitrate (NO_3^-) are considered. Figure 1 shows the C and N pools together in one graphic along
440 with the fluxes of N and C between various pools. The structural and non-structural N pools in

Deleted: five

Deleted: 2

443 root are written as $N_{R,S}$ and $N_{R,NS}$, respectively, and similarly for stem ($N_{S,S}$ and $N_{S,NS}$) and leaves
444 ($N_{L,S}$ and $N_{L,NS}$), and together the structural and non-structural pools make up the total N pools
445 in leaf ($N_L = N_{L,S} + N_{L,NS}$), root ($N_R = N_{R,S} + N_{R,NS}$), and stem ($N_S = N_{S,S} + N_{S,NS}$) components.

446 The fluxes between the pools in Figure 1 characterize the prognostic nature of the pools as
447 defined by the rate change equations summarized in section A1 in the appendix. The model
448 structure allows the C:N ratio of the live leaves ($C:N_L = C_L/N_L$), stem ($C:N_S = C_S/N_S$), and root
449 ($C:N_R = C_R/N_R$) components, and the dead litter (or debris) pool ($C:N_D = C_D/N_D$) to evolve
450 prognostically. The C:N ratio of soil organic matter ($C:N_H = C_H/N_H$), however, is assumed to be
451 constant at 13 following Wania et al. (2012) (see also references therein). The implications of this
452 assumption are discussed later.

Deleted: se

Deleted: below

Deleted:

453 The individual terms of the rate change equations of the 10 prognostic N pools (equations
454 A1 through A8, and equations A10 and A11 in the appendix), corresponding to Figure 1, are
455 specified or parameterized as explained in the following sections. These parameterizations are
456 divided into three groups and related to 1) N inputs, 2) N cycling in vegetation and soil, and 3) N
457 cycling in mineral pools and N outputs.

459 3.2 N inputs

460 3.2.1 Biological N fixation

461 Biological N fixation (BNF, B_{NH_4}) is caused by both free living bacteria in the soil and by
462 bacteria symbiotically living within nodules of host plants' roots. Here, the bacteria convert free
463 nitrogen from the atmosphere to ammonium, which is used by the host plants. Like any other

467 microbial activity, BNF is limited both by drier soil moisture conditions and cold temperatures.
 468 Cleveland et al. (1999) attempt to capture this by parameterizing BNF as a function of actual
 469 evapotranspiration (AET). AET is a function primarily of soil moisture (through precipitation and
 470 soil water balance) and available energy. In places where vegetation exists, AET is also affected
 471 by vegetation characteristics including LAI and rooting depth. Here, we parameterize BNF (B_{NH_4} ,
 472 $\text{gN m}^{-2} \text{day}^{-1}$) as a function of modelled soil moisture and temperature to depth of 0.5 m
 473 (following [the use of similar depth by Xu-Ri and Prentice \(2008\)](#)) which yields a very similar
 474 geographical distribution of BNF as the Cleveland et al. (1999) approach as seen later in Section
 475 4.

$$\begin{aligned}
 B_{NH_4} &= (\sum_c \alpha_c f_c + \sum_n \alpha_n f_n) f(T_{0.5}) f(\theta_{0.5}) \\
 f(T_{0.5}) &= 2^{(T_{0.5}-25)/10} \\
 f(\theta_{0.5}) &= \min\left(0, \max\left(1, \frac{\theta_{0.5}-\theta_w}{\theta_{fc}-\theta_w}\right)\right)
 \end{aligned}
 \tag{3}$$

477 where α_c and α_n ($\text{gN m}^{-2} \text{day}^{-1}$) are BNF coefficients for crop (c) and non-crop or natural (n) PFTs,
 478 which are area weighted using the fractional coverages f_c and f_n of crop and non-crop PFTs that
 479 are present in a grid cell, $f(T)$ is the dependence on soil temperature based on a Q_{10} formulation
 480 and $f(\theta)$ is the dependence on soil moisture which varies between 0 and 1. θ_{fc} and θ_w are the
 481 soil moisture at field capacity and wilting points, respectively. $T_{0.5}$ ($^{\circ}\text{C}$) and $\theta_{0.5}$ ($\text{m}^3 \text{m}^{-3}$) in
 482 equation (3) are averaged over the 0.5 m soil depth over which BNF is assumed to occur. We do
 483 not make the distinction between symbiotic and non-symbiotic BNF since this requires explicit
 484 knowledge of geographical distribution of N fixing PFTs which are not represented separately in
 485 our base set of nine PFTs. A higher value of α_c is used compared to α_n to account for the use of
 486 N fixing plants over agricultural areas. Biological nitrogen fixation has been an essential

Deleted: e

488 component of many farming systems for considerable periods, with evidence for the agricultural
489 use of legumes dating back more than 4,000 years (O'Hara, 1998). A higher α_c than α_n is also
490 consistent with Fowler et al. (2013) who report BNF of 58 and 60 Tg N yr⁻¹ for natural and
491 agricultural ecosystems for present day. Since the area of natural ecosystems is about five times
492 the current cropland area, ~~this implies BNF rate per unit land area is higher for crop ecosystems~~
493 than for natural ecosystems. Values of α_c than α_n and other model parameters are summarized
494 in Table A1.

Deleted: it

495 Similar to Cleveland et al. (1999), our approach does not lead to a significant change in
496 BNF with increasing atmospheric CO₂, other than through changes in soil moisture and
497 temperature. At least two meta-analyses, however, suggest that an increase in atmospheric CO₂
498 does lead to an increase in BNF through increased symbiotic activity associated with an increase
499 in both nodule mass and number (McGuire et al., 1995; Liang et al., 2016). Models have
500 attempted to capture this by simulating BNF as a function of NPP (Thornton et al., 2007; Wania
501 et al., 2012). The caveat with this approach and the implications of our BNF approach are
502 discussed in Section 6.

503 3.2.2 Atmospheric N deposition

504 Atmospheric N deposition is externally specified. The model reads in spatially- and
505 temporally-varying annual deposition rates from a file. Deposition is assumed to occur at the
506 same rate throughout the year so the same daily rate (gN m⁻² day⁻¹) is used for all days of a given
507 year. If separate information for ammonium (NH₄⁺) and nitrate (NO₃⁻) deposition rates is available

509 then it is used otherwise deposition is assumed to be split equally between NH_4^+ and NO_3^-
510 (indicated as P_{NH_4} and P_{NO_3} in equations A1 and A2).

511 3.2.3 Fertilizer application

512 Geographically and temporally varying annual fertilizer application rates (F_{NH_4}) are also
513 specified externally and read in from a file. Fertilizer application occurs over the C_3 and C_4 crop
514 fractions of grid cells. Agricultural management practices are difficult to model since they vary
515 widely between countries and even from farmer to farmer. For simplicity, we assume fertilizer is
516 applied at the same daily fertilizer application rate ($\text{gN m}^{-2} \text{day}^{-1}$) throughout the year in the
517 tropics (between 30°S and 30°N), given the possibility of multiple crop rotations in a given year.
518 Between the 30° and 90° latitudes in both northern and southern hemispheres, we assume that
519 fertilizer application starts on the spring equinox and ends on the fall equinox. The annual
520 fertilizer application rate is thus distributed over around 180 days. This provides somewhat more
521 realism, than using the same treatment as in tropical regions, since extra-tropical agricultural
522 areas typically do not experience multiple crop rotations in a given year. The prior knowledge of
523 start and end days for fertilizer application makes it easier to figure out how much fertilizer is to
524 be applied each day and helps ensure that the annual amount read from the externally specified
525 file is consistently applied.

526

527 3.3 N cycling in plants and soil

528 Plant roots take up mineral N from soil and then allocate it to leaves and stem to maintain
529 an optimal C:N ratio of each component. Both active and passive plant uptakes of N (from both

Moved down [4]: Litterfall from vegetation contributes to the litter pool and decomposition of litter transfers humified litter to the soil organic matter pool. Decomposition of litter and soil organic matter returns mineralized N back to the NH_4^+ pool, closing the soil-vegetation N cycle loop.

535 the NH_4^+ and NO_3^- pools; [explained in Sections 3.3.2 and 3.3.3](#)) are explicitly modelled. [The active](#)
536 [N uptake is modelled as a function of fine root biomass, and passive N uptake depends on the](#)
537 [transpiration flux](#). The modelled plant N uptake also depends on its N demand. Higher N demand
538 leads to higher mineral N uptake from soil as explained below. [Litterfall from vegetation](#)
539 [contributes to the litter pool and decomposition of litter transfers humified litter to the soil](#)
540 [organic matter pool. Decomposition of litter and soil organic matter returns mineralized N back](#)
541 [to the \$\text{NH}_4^+\$ pool, closing the soil-vegetation N cycle loop.](#)

Moved (insertion) [4]

542 3.3.1 Plant N demand

543 Plant N demand is calculated based on the fraction of NPP allocated to leaves, stem, and
544 root components and their specified minimum PFT-dependent C:N ratios, similar to other models
545 (Xu-Ri and Prentice, 2008; Jiang et al., 2019). The assumption is that plants always want to
546 achieve their desired minimum C:N ratios if enough N is available.

$$547 \quad \Delta_{WP} = \Delta_L + \Delta_R + \Delta_S$$
$$\Delta_i = \frac{\max(0, \text{NPP} \cdot a_{i,C})}{C:N_{i,\min}}, \quad i = L, S, R \quad (4)$$

548 where the whole plant N demand (Δ_{WP}) is the sum of N demand for the leaves (Δ_L), stem (Δ_S),
549 and root (Δ_R) components, $a_{i,C}$, $i = L, S, R$ is the fraction of NPP (i.e., carbon as indicated by
550 letter C in the subscript, $\text{gC m}^{-2} \text{day}^{-1}$) allocated to leaf, stem, and root components, and
551 $C:N_{i,\min}$, $i = L, S, R$ are their specified minimum C:N ratios (see Table A1 for these and all other
552 model parameters). A caveat with this approach when applied at the daily time step, for
553 biogeochemical processes in our model, is that during periods of time when NPP is negative due
554 to adverse climatic conditions (e.g., during winter or drought seasons), the calculated demand is

555 negative. If positive NPP implies there is demand for N, negative NPP cannot be taken to imply
556 that N must be lost from vegetation. As a result, from a plant's perspective, N demand is assumed
557 to be zero during periods of negative NPP. N demand is also set to zero when all leaves have been
558 shed (i.e., when GPP is zero). At the global scale, this leads to about 15% higher annual N demand
559 than would be the case if negative NPP values were taken into consideration.

560

561 3.3.2 Passive N uptake

562 N demand is weighed against passive and active N uptake. Passive N uptake depends on
563 the concentration of mineral N in the soil and the water taken up by the plants through their
564 roots as a result of transpiration. We assume that plants have no control over N that comes into
565 the plant through this passive uptake. This is consistent with existing empirical evidence that too
566 much N in soil will cause N toxicity (Goyal and Huffaker, 1984), although we do not model N
567 toxicity in our framework. If the N demand for the current time step cannot be met by passive N
568 uptake then a plant compensates for the deficit (i.e., the remaining demand) through active N
569 uptake.

570 The NH_4^+ concentration in the soil moisture within the rooting zone, referred to as $[\text{NH}_4]$
571 ($\text{gN gH}_2\text{O}^{-1}$), is calculated as

$$572 \quad [\text{NH}_4] = \frac{N_{\text{NH}_4}}{\sum_{i=1}^{i \leq r_d} 10^6 \theta_i z_i} \quad (5)$$

573 where N_{NH_4} is ammonium pool size (gN m^{-2}), θ_i is the volumetric soil moisture content for soil
574 layer i ($\text{m}^3 \text{m}^{-3}$), z_i is the thickness of soil layer i (m), r_d is the soil layer in which the 99% rooting
575 depth lies as dynamically simulated by the biogeochemical module of CLASSIC following Arora

576 and Boer (2003). The 10^6 term converts units of the denominator term to $\text{gH}_2\text{O m}^{-2}$. NO_3^-
577 concentration ($[\text{NO}_3]$, $\text{gN gH}_2\text{O}^{-1}$) in the rooting zone is found in a similar fashion. The
578 transpiration flux q_t ($\text{Kg H}_2\text{O m}^{-2} \text{s}^{-1}$) (calculated in the physics module of CLASSIC) is multiplied
579 by $[\text{NH}_4]$ and $[\text{NO}_3]$ ($\text{gN gH}_2\text{O}^{-1}$) to obtain passive uptake of NH_4^+ and NO_3^- ($\text{gN m}^{-2} \text{day}^{-1}$) as

$$\begin{aligned} U_{p,NH4} &= 86400 \times 10^3 \beta q_t [\text{NH}_4] \\ U_{p,NO3} &= 86400 \times 10^3 \beta q_t [\text{NO}_3] \end{aligned} \quad (6)$$

581 where the multiplier 86400×10^3 converts q_t to units of $\text{gH}_2\text{O m}^{-2} \text{day}^{-1}$, and β (see Table A1) is
582 the dimensionless mineral N distribution coefficient with β value less than 1 that accounts for the
583 fact that NH_4^+ and NO_3^- available in the soil are not well mixed in the soil moisture solution, and
584 not completely accessible to roots, to be taken up by plants.

Deleted:

Formatted: Superscript

585 3.3.3 Active N uptake

586 The active plant N uptake is parameterized as a function of fine root biomass and the size
587 of NH_4^+ and NO_3^- pools in a manner similar to Gerber et al. (2010) and Wania et al. (2012). The
588 distribution of fine roots across the soil layers is ignored. CLASSIC does not explicitly model fine
589 root biomass. We therefore calculate the fraction of fine root biomass using an empirical
590 relationship that is very similar to the relationship developed by Kurz et al. (1996) (their equation
591 5) but also works below total root biomass of 0.33 Kg C m^{-2} (the Kurz et al. (1996) relationship
592 yields a fraction of fine root more than 1.0 below this threshold). The fraction of fine root biomass
593 (f_r) is given by

Deleted: s

$$f_r = 1 - \frac{C_R}{C_R + 0.6} \quad (7)$$

597 where C_R is the root biomass (KgC m^{-2}) simulated by the biogeochemical module of CLASSIC.
 598 Equation (7) yields fine root fraction approaching 1.0 as C_R approaches 0, so at very low root
 599 biomass values all roots are considered fine roots. For grasses the fraction of fine root biomass is
 600 set to 1. The maximum or potential active N uptake for NH_4^+ and NO_3^- is given by

$$\begin{aligned}
 U_{a,pot,NH4} &= \frac{\varepsilon f_r C_R N_{NH4}}{k_{p,1/2} r_d + N_{NH4} + N_{NO3}} \\
 U_{a,pot,NO3} &= \frac{\varepsilon f_r C_R N_{NO3}}{k_{p,1/2} r_d + N_{NH4} + N_{NO3}}
 \end{aligned}
 \tag{8}$$

602 where ε (see Table A1) is the efficiency of fine roots to take up N per unit fine root mass per day
 603 ($\text{gN gC}^{-1} \text{day}^{-1}$), $k_{p,1/2}$ (see Table A1) is the half saturation constant (gN m^{-3}), and N_{NH4} and N_{NO3}
 604 are the ammonium and nitrate pool sizes (gN m^{-2}) as mentioned earlier. Depending on the
 605 geographical location and the time of the year, if passive uptake alone can satisfy plant N demand
 606 the actual active N uptake of NH_4^+ ($U_{a,actual,NH4}$) and NO_3^- ($U_{a,actual,NO3}$) is set to zero.
 607 Conversely, during other times both passive and potential active N uptakes may not be able to
 608 satisfy the demand and in this case actual active N uptake is equal to its potential rate. At times
 609 other than these, the actual active uptake is lower than its potential value. This adjustment of
 610 actual active uptake is illustrated in equation (9).

Formatted: Superscript

Deleted: the

$$\begin{aligned} \text{if } (\Delta_{WP} \leq U_{p,NH_4} + U_{p,NO_3}) \\ U_{a,actual,NH_4} &= 0 \\ U_{a,actual,NO_3} &= 0 \end{aligned}$$

$$\begin{aligned} \text{if } (\Delta_{WP} > U_{p,NH_4} + U_{p,NO_3}) \wedge (\Delta_{WP} < U_{p,NH_4} + U_{p,NO_3} + U_{a,pot,NH_4} + U_{a,pot,NO_3}) \\ U_{a,actual,NH_4} &= (\Delta_{WP} - U_{p,NH_4} - U_{p,NO_3}) \frac{U_{a,pot,NH_4}}{U_{a,pot,NH_4} + U_{a,pot,NO_3}} \\ U_{a,actual,NO_3} &= (\Delta_{WP} - U_{p,NH_4} - U_{p,NO_3}) \frac{U_{a,pot,NO_3}}{U_{a,pot,NH_4} + U_{a,pot,NO_3}} \end{aligned} \quad (9)$$

$$\begin{aligned} \text{if } (\Delta_{WP} \geq U_{p,NH_4} + U_{p,NO_3} + U_{a,pot,NH_4} + U_{a,pot,NO_3}) \\ U_{a,actual,NH_4} &= U_{a,pot,NH_4} \\ U_{a,actual,NO_3} &= U_{a,pot,NO_3} \end{aligned}$$

613 Finally, the total N uptake (U), uptake of NH_4^+ (U_{NH_4}) and NO_3^- (U_{NO_3}), are calculated as

$$\begin{aligned} U &= U_{p,NH_4} + U_{p,NO_3} + U_{a,actual,NH_4} + U_{a,actual,NO_3} \\ U_{NH_4} &= U_{p,NH_4} + U_{a,actual,NH_4} \\ U_{NO_3} &= U_{p,NO_3} + U_{a,actual,NO_3} \end{aligned} \quad (10)$$

615

616 3.3.4 Litterfall

617 Nitrogen litterfall from the vegetation components is directly tied to the carbon litterfall
618 calculated by the phenology module of CLASSIC through their current C:N ratios.

$$619 \quad LF_i = \frac{(1-r_L)LF_{i,C}}{C:N_i}, i = L, S, R \quad (11)$$

620 where $LF_{i,C}$ is the carbon litterfall rate ($gC \text{ day}^{-1}$) for component i , calculated by the phenology
621 module of CLASSIC, and division by its current C:N ratio yields the nitrogen litterfall rate, r_L (see
622 [Table A1](#)) is the leaf resorption coefficient that simulates the resorption of N from leaves of
623 deciduous tree PFTs before they are shed and $r_L = 0, i = R, S$. Litter from each vegetation

624 component is proportioned between structural and non-structural components according to
625 their pool sizes.

626 3.3.5 Allocation and reallocation

627 Plant N uptake by roots is allocated to leaves and stem to satisfy their N demand. When
628 plant N demand is greater than zero, total N uptake (U) is divided between leaves, stem, and root
629 components in proportion to their demands such that the allocation fractions for N ($a_i, i =$
630 L, S, R) are calculated as

$$\begin{aligned} a_i &= \frac{\Delta_i}{\Delta_{WP}}, i = L, S, R \\ A_{R2L} &= a_L (U_{NH4} + U_{NO3}) \\ A_{R2S} &= a_S (U_{NH4} + U_{NO3}) \end{aligned} \quad (12)$$

632 where A_{R2L} and A_{R2S} are the amounts of N allocated from root to leaves and stem components,
633 respectively, as shown in equations (A5) and (A7). During periods of negative NPP due to adverse
634 climatic conditions (e.g., during winter or drought seasons) the plant N demand is set to zero but
635 passive N uptake, associated with transpiration, may still be occurring if the leaves are still on.
636 Even though there is no N demand, passive N uptake still needs to be partitioned among the
637 vegetation components. During periods of negative NPP allocation fractions for N are, therefore,
638 calculated in proportion to the minimum PFT-dependent C:N ratios of the leaves, stem, and root
639 components as follows.

$$a_i = \frac{1/C:N_{i,\min}}{1/C:N_{L,\min} + 1/C:N_{S,\min} + 1/C:N_{R,\min}}, i = L, S, R \quad (13)$$

Deleted: A

641 For grasses, which do not have a stem component, equations (12) and (13) are modified
642 accordingly by removing the terms associated with the stem component.

644 Three additional rules override these general allocation rule specifically for deciduous
 645 tree PFTs (or deciduous PFTs in general). First, no N allocation is made to leaves once leaf fall is
 646 initiated for deciduous tree PFTs and plant N uptake is proportioned between stem and root
 647 components based on their demands in a manner similar to equation (12). Second, for deciduous
 648 tree PFTs, a fraction of leaf N is resorbed from leaves back into stem and root as follows

$$\begin{aligned}
 R_{L2R} &= r_L LF_L \frac{N_{R,NS}}{N_{R,NS} + N_{S,NS}} \\
 R_{L2S} &= r_L LF_L \frac{N_{S,NS}}{N_{R,NS} + N_{S,NS}}
 \end{aligned}
 \tag{14}$$

650
 651 where r_L is the leaf resorption coefficient, as mentioned earlier, and LF_L is the leaf litter fall rate.
 652 Third, and similar to resorption, at the time of leaf onset for deciduous tree PFTs, N is reallocated
 653 to leaves (in conjunction with reallocated carbon as explained in Asaadi et al. (2018)) from stem
 654 and root components.

$$\begin{aligned}
 R_{R2L} &= \frac{R_{R2L,C}}{C:N_L} \frac{N_{R,NS}}{N_{R,NS} + N_{S,NS}} \\
 R_{S2L} &= \frac{R_{S2L,C}}{C:N_L} \frac{N_{S,NS}}{N_{R,NS} + N_{S,NS}}
 \end{aligned}
 \tag{15}$$

656 where $R_{R2L,C}$ and $R_{S2L,C}$ represent reallocation of carbon from non-structural stem and root
 657 components to leaves and division by $C:N_L$ converts the flux into N units. This reallocated N, at
 658 the time of leaf onset, is proportioned between non-structural pools of stem and root according
 659 to their sizes.

660 3.3.6 N mineralization, immobilization, and humification

Deleted: e
 Deleted: ion
 Deleted: demand for

664 Decomposition of litter ($R_{h,D}$) and soil organic matter ($R_{h,H}$) releases C to the atmosphere
665 and this flux is calculated by the heterotrophic respiration module of CLASSIC. [The litter and soil](#)
666 [carbon decomposition rates used here are the same as in the standard model version \(Melton](#)
667 [and Arora, 2016; their Table A3\).](#) The amount of N mineralized is calculated straightforwardly by
668 division with the current C:N ratios of the respective pools and contributes to the NH_4^+ pool.

$$\begin{aligned} M_{D,NH_4} &= \frac{R_{h,D}}{C:N_D} \\ M_{H,NH_4} &= \frac{R_{h,H}}{C:N_H} \end{aligned} \quad (16)$$

670 An implication of mineralization contributing to the NH_4^+ pool, in addition to BNF and fertilizer
671 inputs that also contribute solely to the NH_4^+ pool, is that the simulated NH_4^+ pool is typically
672 larger than the NO_3^- pool. The exception is the dry and arid regions where the lack of
673 denitrification, as discussed below in Section 3.4.2., leads to a build-up of the NO_3^- pool.

Deleted:

674 Immobilization of mineral N from the NH_4^+ and NO_3^- pools into the soil organic matter
675 pool is meant to keep the soil organic matter C:N ratio ($C:N_H$) at its specified value of 13 for all
676 PFTs in a manner similar to Wania et al. (2012) and Zhang et al. (2018). A value of 13 is within the
677 range of observation-based estimates which vary from about 8 to 25 (Zinke et al., 1998; Tipping
678 et al., 2016). Although $C:N_H$ varies geographically, the driving factors behind this variability
679 remain unclear. It is even more difficult to establish if increasing atmospheric CO_2 is changing
680 $C:N_H$ given the large heterogeneity in soil organic C and N densities, and the difficulty in
681 measuring small trends for such large global pools. We therefore make the assumption that the
682 $C:N_H$ does not change with time. An implication of this assumption is that as GPP increases with
683 increasing atmospheric CO_2 rises, and plant litter becomes enriched in C with increasing C:N ratio

685 of litter, more and more N is locked up in the soil organic matter pool because its C:N ratio is
 686 fixed. As a result, mineral N pools of NH_4^+ and NO_3^- decrease in size and plant N content
 687 subsequently follows. This is consistent with studies of plants grown in elevated CO_2
 688 environment. For example, Cotrufo et al. (1998) summarize results from 75 studies and find an
 689 average 14% reduction in N concentration for above-ground tissues. Wang et al. (2019) find
 690 increased C concentration by 0.8–1.2% and a reduction in N concentration by 7.4–10.7% for rice
 691 and winter wheat crop rotation system under elevated CO_2 . Another implication of using
 692 specified fixed $C:N_H$ is that it does not matter if plant N uptake or immobilization is given
 693 preferred access to the mineral N pool since in the long term, by design, N will accumulate in the
 694 soil organic matter in response to atmospheric CO_2 increase.

695 Immobilization from both the NH_4^+ and NO_3^- pools ($\text{gN m}^{-2} \text{day}^{-1}$) is calculated in
 696 proportion to their pool sizes, employing the fixed $C:N_H$ ratio as

$$\begin{aligned} O_{\text{NH}_4} &= \max\left(0, \left(\frac{C_H}{C:N_H} - N_H\right) \frac{N_{\text{NH}_4}}{N_{\text{NH}_4} + N_{\text{NO}_3}}\right) k_O \\ O_{\text{NO}_3} &= \max\left(0, \left(\frac{C_H}{C:N_H} - N_H\right) \frac{N_{\text{NO}_3}}{N_{\text{NH}_4} + N_{\text{NO}_3}}\right) k_O \end{aligned} \quad (17)$$

698 where k_O is rate constant with a value of 1.0 day^{-1} . Finally, the carbon flux of humified litter from
 699 the litter to the soil organic matter pool ($H_{C,D2H}$) is also associated with a corresponding N flux
 700 that depends on the C:N ratio of the litter pool.

$$H_{N,D2H} = \frac{H_{C,D2H}}{C:N_D} \quad (18)$$

702 3.4 N cycling in mineral pools and N outputs

Deleted: ¶

704 This section presents the parameterizations of nitrification (which results in transfer of N
705 from the NH_4^+ to the NO_3^- pool) and the associated gaseous fluxes of N_2O and NO (referred to as
706 nitrifier denitrification), gaseous fluxes of N_2O , NO, and N_2 associated with denitrification,
707 volatilization of NH_4^+ into NH_3 , and leaching of NO_3^- in runoff.

708 3.4.1 Nitrification

709 Nitrification, the oxidative process converting ammonium to nitrate, is driven by microbial
710 activity and as such constrained both by high and low soil moisture (Porporato et al., 2003). At
711 high soil moisture content there is little aeration of soil and this constrains aerobic microbial
712 activity, while at low soil moisture content microbial activity is constrained by moisture
713 limitation. In CLASSIC, the heterotrophic respiration from soil carbon is constrained similarly but
714 rather than using soil moisture the parameterization is based on soil matric potential (Arora,
715 2003; Melton et al., 2015). Here, we use the exact same parameterization. In addition to soil
716 moisture, nitrification ($\text{gN m}^{-2} \text{day}^{-1}$) is modelled as a function of soil temperature and the size
717 of the NH_4^+ pool as follows

$$718 \quad I_{\text{NO}_3} = \eta f_i(T_{0.5}) f_i(\psi) N_{\text{NH}_4} \quad (19)$$

719 where η is the nitrification coefficient (day^{-1} , [see Table A1](#)), $f_i(\psi)$ is the dimensionless soil
720 moisture scalar that varies between 0 and 1 and depends on soil matric potential (ψ), $f_i(T_{0.5})$ is
721 the dimensionless soil temperature scalar that depends on soil temperature ($T_{0.5}$) averaged over
722 the top 0.5 m soil depth over which nitrification is assumed to occur (following Xu-Ri and Prentice,
723 2008), and N_{NH_4} is the ammonium pool size (gN m^{-2}), as mentioned earlier. Both $f_i(T_{0.5})$ and

Deleted: average

725 $f_I(\psi)$ are parameterized following Arora (2003) and Melton et al. (2015). $f_I(T_{0.5})$ is a Q_{10} type
 726 function with a temperature dependent Q_{10}

$$727 \quad f_I(T_{0.5}) = Q_{10,I}^{(T_{0.5}-20)/10}, Q_{10,I} = 1.44 + 0.56 (\tanh(0.075(46 - T_{0.5}))) \quad (20)$$

728 The reference temperature for nitrification is set to 20 °C following Lin et al. (2000). $f_I(\psi)$ is
 729 parameterized as a step function of soil matric potential (ψ) as

$$730 \quad f_I(\psi) = \begin{cases} 0.5 & \text{if } \psi \leq \psi_{sat} \\ 1 - 0.5 \frac{\log(0.4) - \log(\psi)}{\log(0.4) - \log(\psi_{sat})} & \text{if } 0.4 > \psi \geq \psi_{sat} \\ 1 & \text{if } 0.6 \geq \psi \geq 0.4 \\ 1 - 0.8 \frac{\log(\psi) - \log(0.6)}{\log(100) - \log(0.6)} & \text{if } 100 > \psi > 0.6 \\ 0.2 & \text{if } \psi > 100 \end{cases} \quad (21)$$

731 where the soil matric potential (ψ) is found, following Clapp and Hornberger (1978), as a function
 732 of soil moisture (θ)

$$733 \quad \psi(\theta) = \psi_{sat} \left(\frac{\theta}{\theta_{sat}} \right)^{-B} \quad (22)$$

734 Saturated matric potential (ψ_{sat}), soil moisture at saturation (i.e. porosity) (θ_{sat}), and the
 735 parameter B are calculated as functions of percent sand and clay in soil following Clapp and
 736 Hornberger (1978) as shown in Melton et al. (2015). The soil moisture scalar $f_I(\psi)$ is calculated
 737 individually for each soil layer and then averaged over the soil depth of 0.5 m over which
 738 nitrification is assumed to occur.

739 Gaseous fluxes of NO (I_{NO}) and N₂O (I_{N2O}) associated with nitrification, and generated
 740 through nitrifier denitrification, are assumed to be directly proportional to the nitrification flux
 741 (I_{NO3}) as

Deleted: (
 Deleted: ,
 Deleted: Lin et al. (2000)

745

$$\begin{aligned} I_{NO} &= \eta_{NO} I_{NO3} \\ I_{N2O} &= \eta_{N2O} I_{NO3} \end{aligned} \quad (23)$$

746 where η_{NO} and η_{N2O} are dimensionless fractions (see Table A1) which determine what fractions
747 of nitrification flux are emitted as NO and N₂O.

748 **3.4.2 Denitrification**

749 Denitrification is the stepwise microbiological reduction of nitrate to NO, N₂O, and ultimately to
750 N₂ in complete denitrification. Unlike nitrification, however, denitrification is primarily an
751 anaerobic process (Tomasek et al., 2017) and therefore occurs when soil is saturated. As a result,
752 we use a different soil moisture scalar than for nitrification. Similar to nitrification, denitrification
753 is modelled as a function of soil moisture, soil temperature and the size of the NO₃⁻ pool as follows
754 to calculate the gaseous fluxes of NO, N₂O, and N₂.

755

$$\begin{aligned} E_{NO} &= \mu_{NO} f_E(T_{0.5}) f_E(\theta) N_{NO3} \\ E_{N2O} &= \mu_{N2O} f_E(T_{0.5}) f_E(\theta) N_{NO3} \\ E_{N2} &= \mu_{N2} f_E(T_{0.5}) f_E(\theta) N_{NO3} \end{aligned} \quad (24)$$

756 where μ_{NO} , μ_{N2O} , and μ_{N2} are coefficients (day⁻¹, see Table A1) that determine daily rates of
757 emissions of NO, N₂O, and N₂. The temperature scalar $f_E(T_{0.5})$ is exactly the same as the one for
758 nitrification ($f_I(T_{0.5})$) since denitrification is also assumed to occur over the same 0.5 m soil
759 depth. The soil moisture scalar $f_E(\theta)$ is given by

760

$$\begin{aligned} f_E(\theta) &= 1 - \tanh\left(2.5 \left(\frac{1-w(\theta)}{1-w_d}\right)^2\right) \\ w(\theta) &= \max\left(0, \min\left(1, \frac{\theta - \theta_w}{\theta_f - \theta_w}\right)\right) \end{aligned} \quad (25)$$

Formatted: Font: (Default) +Body (Calibri)

Formatted: Font: (Default) +Body (Calibri)

761 where w is the soil wetness that varies between 0 and 1 as soil moisture varies between wilting
762 point (θ_w) and field capacity (θ_f), and w_d (see Table A1) is the threshold soil wetness for
763 denitrification below which very little denitrification occurs. Since arid regions are characterized
764 by low soil wetness values, typically below w_d , this leads to build up of the NO_3^- pool in arid
765 regions.

Deleted: Since very little denitrification occurs when soil wetness is below w_d

766 3.4.3 NO_3^- leaching

767 Leaching is the loss of water-soluble ions through runoff. In contrast to positively charged
768 NH_4^+ ions (i.e. cations), the NO_3^- ions do not bond to soil particles because of the limited exchange
769 capacity of soil for negatively charged ions (i.e. anions). As a result, leaching of N in the form of
770 NO_3^- ions is a common water quality problem, particularly over cropland regions. The leaching
771 flux (L_{NO_3} , $\text{gN m}^{-2} \text{day}^{-1}$) is parameterized to be directly proportional to baseflow (b_t , $\text{Kg m}^{-2} \text{s}^{-1}$)
772 calculated by the physics module of CLASSIC and the size of the NO_3^- pool (N_{NO_3} , gN m^{-2}).
773 Baseflow is the runoff rate from the bottommost soil layer.

$$774 \quad L_{\text{NO}_3} = 86400 \varphi b_t N_{\text{NO}_3} \quad (26)$$

775 where the multiplier 86400 converts units to per day, and φ is the leaching coefficient ($\text{m}^2 \text{Kg}^{-1}$)
776 see Table A1 that can be thought of as the soil particle surface area (m^2) that 1 Kg of water (or
777 about 0.001 m^3) can effectively wash to leach the nutrients.

Formatted: Font: (Default) +Body (Calibri)

Deleted:)

Formatted: Font: (Default) +Body (Calibri)

778 3.4.4 NH_3 volatilization

782 NH₃ volatilization (V_{NH_3} , gN m⁻² day⁻¹) is parametrized as a function of pool size of NH₄⁺,
 783 soil temperature, soil pH, aerodynamic and boundary layer resistances, and atmospheric NH₃
 784 concentration in a manner similar to Riddick et al. (2016) as

$$785 \quad V_{NH_4} = \vartheta \ 86400 \frac{1}{r_a+r_b} (\chi - [NH_{3,a}]) \quad (27)$$

786 where ϑ is the dimensionless NH₃ volatilization coefficient (see Table A1) which is set to less than
 787 1 to account for the fact that a fraction of ammonia released from the soil is captured by
 788 vegetation, r_a (s m⁻¹) is the aerodynamic resistance calculated by the physics module of CLASSIC,
 789 χ is the ammonia (NH₃) concentration at the interface of the top soil layer and the atmosphere
 790 (g m⁻³), $[NH_{3,a}]$ is the atmospheric NH₃ concentration specified at 0.3×10⁻⁶ g m⁻³ following
 791 Riddick et al. (2016), 86400 converts flux units from gN m⁻² s⁻¹ to gN m⁻² day⁻¹, and r_b (s m⁻¹) is
 792 the boundary layer resistance calculated following Thom (1975) as

$$793 \quad r_b = 6.2 \ u_*^{-0.67} \quad (28)$$

794 where u_* (m/s) is the friction velocity provided by the physics module of CLASSIC. The ammonia
 795 (NH₃) concentration at surface (χ), in a manner similar to Riddick et al. (2016), is calculated as

$$796 \quad \chi = 0.26 \frac{N_{NH_4}}{1+K_H+K_H[H^+]/K_{NH_4}} \quad (29)$$

797 where the coefficient 0.26 is the fraction of ammonium in the top 10 cm soil layer assuming
 798 exponential distribution of ammonium along the soil depth (given by $3e^{-3z}$, where z is the soil
 799 depth), K_H (dimensionless) is the Henry's law constant for NH₃, K_{NH_4} (mol L⁻¹) is the dissociation
 800 equilibrium constant for aqueous NH₃, and H^+ (mol L⁻¹) is the concentration of hydrogen ion

801 that depends on the soil pH ($H^+ = 10^{-pH}$). K_H and K_{NH_4} are modelled as functions of soil
 802 temperature of the top 10 cm soil layer ($T_{0.1}$) following Riddick et al. (2016) as

$$K_H = 4.59 T_{0.1} \exp\left(4092 \left(\frac{1}{T_{0.1}} - \frac{1}{T_{ref,v}}\right)\right) \quad (30)$$

$$K_{NH_4} = 5.67 \times 10^{-10} \exp\left(-6286 \left(\frac{1}{T_{0.1}} - \frac{1}{T_{ref,v}}\right)\right)$$

804 where $T_{ref,v}$ is the reference temperature of 298.15 K.

805 3.5 Coupling of C and N cycles

806 As mentioned earlier, the primary objective of coupling of C and N cycles is to be able to
 807 simulate V_{cmax} as a function of leaf N content (N_L) for each PFT. This coupling is represented
 808 through the following relationship

$$V_{cmax} = \Lambda (\Gamma_1 N_L + \Gamma_2) \quad (31)$$

811 where Γ_1 (13 $\mu\text{mol CO}_2 \text{ gN}^{-1} \text{ s}^{-1}$) and Γ_2 (8.5 $\mu\text{mol CO}_2 \text{ m}^{-2} \text{ s}^{-1}$) are global constants, except for
 812 the broadleaf evergreen tree PFT for which a lower value of Γ_1 (5.1 $\mu\text{mol CO}_2 \text{ gN}^{-1} \text{ s}^{-1}$) is used as
 813 discussed below. Λ (≤ 1) is a scalar that reduces calculated V_{cmax} when C:N ratio of any plant
 814 component (C: N_i , $i = L, S, R$) exceeds its specified maximum value (C: $N_{i,max}$, $i = L, S, R$) (see
 815 Table AA1).

$$\Lambda = \exp(-\omega k_\Lambda) \quad (32)$$

$$\omega = e_L b_L + e_S b_S + e_R b_R$$

Moved down [2]: The rates of change of N in the NH_4^+ and NO_3^- pools (in gN m^{-2}), N_{NH_4} and N_{NO_3} , respectively, are given by ¶

$$\frac{dN_{NH_4}}{dt} = B_{NH_4} + F_{NH_4} + P_{NH_4} + M_{D,NH_4} + M_{H,NH_4} - U_{NH_4} - (I_{NO_3} + I_{N_2O} + I_{NO}) - V_{NH_3} - O_{NH_4} \quad (4)¶$$

$\frac{dN_{NO_3}}{dt} = P_{NO_3} + I_{NO_3} - L_{NO_3} - U_{NO_3} - (E_{N_2} + E_{N_2O} + E_{NO}) - O_{NO_3} \quad (5)¶$

and all fluxes are represented in units of $\text{gN m}^{-2} \text{ day}^{-1}$. B_{NH_4} is the rate of biological N fixation which solely contributes to the NH_4^+ pool, F_{NH_4} is the fertilizer input which is assumed to contribute only to the NH_4^+ pool, and P_{NH_4} and P_{NO_3} are atmospheric deposition rates that contribute to the NH_4^+ and NO_3^- pools, respectively. Biological N fixation, fertilizer input, and atmospheric deposition are the three routes through which N enters the coupled soil-vegetation system. M_{D,NH_4} and M_{H,NH_4} are the mineralization flux from the litter and soil organic matter pools, respectively, associated with their decomposition. We assume mineralization of humus and litter pools only contributes to the NH_4^+ pool. O_{NH_4} and O_{NO_3} indicate immobilization of N from the NH_4^+ and NO_3^- pools, respectively, to the humus N pool which implies microbes (that are not represented explicitly) are part of the humus pool. Combined together the terms $(M_{D,NH_4} + M_{H,NH_4} - O_{NH_4} - O_{NO_3})$ yield the net mineralization rate. V_{NH_3} is the rate of ammonia (NH_3) volatilization and L_{NO_3} is the leaching of N that occurs only from the NO_3^- pool. The positively charged ammonium ions are attracted to the negatively charged soil particles and as a result it is primarily the negatively charged nitrate ions that leach through the soil (Porporato et al., 2003; Xu-Ri and Prentice, 2008). U_{NH_4} and U_{NO_3} are uptakes of NH_4^+ and NO_3^- by plants, respectively. The nitrification flux from NH_4^+ to NO_3^- pool is represented by I_{NO_3} which also results in the release of the nitrous oxide (N_2O), a greenhouse gas, and nitric oxide (NO) through nitrifier denitrification represented by the terms I_{N_2O} and I_{NO} , respectively. Finally, E_{N_2} , E_{N_2O} , and E_{NO} are the gaseous losses of N_2 (nitrogen gas), N_2O , and NO from the NO_3^- pool associated with denitrification. N is thus lost through the soil-vegetation system via leaching in runoff and through gaseous losses of I_{N_2O} , I_{NO} , E_{N_2} , E_{N_2O} , E_{NO} , and V_{NH_3} . ¶

The structural and non-structural N pools in root are written as $N_{R,S}$ and $N_{R,NS}$, respectively, and similarly for stem ($N_{S,S}$ and $N_{S,NS}$) and leaves ($N_{L,S}$ and $N_{L,NS}$), and together the structural and non-structural pools make the total N pool in leaf ($N_L = N_{L,S} + N_{L,NS}$), root ($N_R = N_{R,S} + N_{R,NS}$), and stem ($N_S = N_{S,S} +$

Deleted: $\frac{dN_{NH_4}}{dt} = B_{NH_4} + F_{NH_4} + P_{NH_4} + M_{D,NH_4} + M_{H,NH_4} - U_{NH_4} - (I_{NO_3} + I_{N_2O} + I_{NO}) - V_{NH_3} - O_{NH_4} \quad (4)¶$
 $\frac{dN_{NO_3}}{dt} = P_{NO_3} + I_{NO_3} - L_{NO_3} - U_{NO_3} - (E_{N_2} + E_{N_2O} + E_{NO}) - O_{NO_3} \quad (5)¶$

and all fluxes are represented in units of $\text{gN m}^{-2} \text{ day}^{-1}$. B_{NH_4} is the rate of biological N fixation which solely contributes to the NH_4^+ pool, F_{NH_4} is the fertilizer input which is assumed to contribute only to the NH_4^+ pool, and P_{NH_4} and P_{NO_3} are ... [2]

Deleted: 2

Deleted: in Section 2.1.2

Deleted: $\Gamma_1 N_L + \Gamma_2$

Deleted: 15

$$e_i = \max(0, C:N_i - C:N_{i,\max})$$

$$b_i = \frac{1/C:N_{i,\max}}{1/C:N_{L,\max} + 1/C:N_{S,\max} + 1/C:N_{R,\max}}, i = L, S, R \quad (33)$$

where k_{Λ} is a dimensionless parameter (see Table A1) and ω is dimensionless term that represents excess C:N ratios above specified maximum thresholds ($e_i, i = L, S, R$) weighted by $b_i, i = L, S, R$. When plant components do not exceed their specified maximum C:N ratio thresholds, e_i is zero and Λ is one. When plants components exceed their specified maximum C:N ratio thresholds, Λ starts reducing below one. This decreases $V_{c\max}$ and thus photosynthetic uptake which limits the rate of increase of C:N ratio of plant components, depending on the value of k_{Λ} .

The linear relationship between photosynthetic capacity and N_L (Evans, 1989; Field and Mooney, 1986; Garnier et al., 1999) (used in equation 31) and between photosynthetic capacity and leaf chlorophyll content (Croft et al., 2017) is empirically observed. We have avoided using PFT-dependent values of Γ_1 and Γ_2 for easy optimization of these parameter values but also because such an optimization can potentially hide other model deficiencies. More importantly, using PFT-independent values of Γ_1 and Γ_2 yields a more elegant framework whose successful evaluation will provide confidence in the overall model structure.

As shown later in the results section, using Γ_1 and Γ_2 as global constants yields GPP values that are higher in the tropical region than an observation-based estimate. This is not surprising since tropical and mid-latitude regions are known to be limited by P (Vitousek, 1984; Aragão et al., 2009; Vitousek et al., 2010; Du et al., 2020) and our framework currently doesn't model P cycle explicitly. An implication of productivity that is limited by P is that changes in N_L are less

Deleted: max A

Deleted: The modelled differences in PFT specific values of $V_{c\max}$ in our framework, come through differences in simulated N_L values that depend on BNF, given that BNF is the primary natural source of N input into the coupled soil-vegetation system. N_L values, however, also depend on leaf phenology, allocation of carbon and nitrogen, turnover rates, transpiration (which brings in N through passive uptake), and almost every aspect of plant biogeochemistry which affects a PFT's net primary productivity and therefore N demand.

Deleted:

Deleted: well

Field Code Changed

Deleted: (Vitousek, 1984; Aragão et al., 2009; Vitousek et al., 2010)

Deleted: a

1042 important. In the absence of explicit treatment of the P cycle, we therefore simply use a lower
1043 value of Γ_1 for the broadleaf evergreen tree PFT which, in our modelling framework, exclusively
1044 represents a tropical PFT. Although, a simple way to express P limitation, this approach yields the
1045 best comparison with observation-based GPP, as shown later, because the effect of P limitation
1046 is most pronounced in the high productivity tropical regions.

1047 The second pathway of coupling between the C and N cycles occurs through
1048 mineralization of litter and soil organic matter. During periods of higher temperature,
1049 heterotrophic C respiration fluxes increase from the litter and soil organic matter pools and this
1050 in turn implies an increased mineralization flux (via equation 16) leading to more mineral N
1051 available for plants to uptake.

Deleted: A14

Deleted: in the appendix

1052 **4.0 Methodology**

1053 **4.1 Model simulations and input data sets**

1054 We perform CLASSIC model simulations with the N cycle for the pre-industrial period
1055 followed by several simulations for the historical 1851-2017 period to evaluate the model's
1056 response to different forcings, as summarized below. The simulation for the pre-industrial period
1057 uses forcings that correspond to year 1850 and the model is run for thousands of years until its
1058 C and N pools come into equilibrium. Global thresholds of net atmosphere-land C flux of 0.05
1059 Pg/yr and net atmosphere-land N flux of 0.5 Tg N/yr are used to ensure the model pools have
1060 reached equilibrium. The pre-industrial simulation, therefore, yields the initial conditions from
1061 which the historical simulations for the period 1851-2017 are launched. To spin the mineral N
1062 pools to their initial values, the plant N uptake and other organic processes were turned off while

1065 the model used specified values of V_{cmax} and only the inorganic part of N cycle was operative.
1066 Once the inorganic mineral soil N pools reached near equilibrium, the organic processes were
1067 turned on. The model also uses an accelerated spin up procedure for the slow pools of soil organic
1068 matter and mineral N. The input and output terms are multiplied by a factor greater than one
1069 and this magnifies the change in pool size and therefore accelerates the spin up. Once the model
1070 pools reach near equilibrium, the factor is set back to one.

1071 To evaluate the model's response to various forcings over the historical period we
1072 perform several simulations turning on one forcing at a time as summarized in Table 1. The
1073 objective of these simulations is to see if the model response to individual forcings is consistent
1074 with expectations. For example, in the CO₂-only simulation only atmospheric CO₂ concentration
1075 increases over the historical period, while all other forcings stay at their 1850 levels. In the N-
1076 DEP-only simulation only N deposition increases over the historical period, and similarly for other
1077 runs in Table 1. A "FULL" simulations with all forcings turned on is then also performed which we
1078 compare to the original model without a N cycle which uses the photosynthesis downregulation
1079 parameterization (termed "ORIGINAL" in Table 1). Finally, a separate pre-industrial simulation is
1080 also performed that uses the same Γ_1 and Γ_2 globally (FULL-no-implicit-P-limitation). This
1081 simulation is used to illustrate the effect of neglecting P limitation for the broadleaf evergreen
1082 tree PFT in the tropics.

1083 For the historical period, the model is driven with time-varying forcings that include CO₂
1084 concentration, population density (used by the fire module of the model for calculating
1085 anthropogenic fire ignition and suppression), land cover, and meteorological data. In addition,
1086 for the N cycle module, the model requires time-varying atmospheric N deposition and fertilizer

Moved (insertion) [3]

Deleted: ¶

Deleted: ¶

1089 data. The atmospheric CO₂ and meteorological data (CRU-JRA) are same as those used for the
1090 TRENDY model intercomparison project for terrestrial ecosystem models for year 2018 (Le Quéré
1091 et al., 2018). The CRU-JRA meteorological data is based on 6-hourly Japanese Reanalysis (JRA).
1092 ~~However, since reanalysis data typically do match observations they are~~ adjusted for monthly
1093 values based on the Climate Research Unit (CRU) data. ~~This yields a blended product with sub-~~
1094 ~~daily temporal resolution that comes from the reanalysis and monthly means/sums that match~~
1095 ~~the CRU data to yield a meteorological product that can be used by models that require sub-daily~~
1096 ~~or daily meteorological forcing. These data are~~ available for the period 1901-2017. Since no
1097 meteorological data are available for the 1850-1900 period, we use 1901-1925 meteorological
1098 data repeatedly for this duration and also ~~for~~ the pre-industrial spin up. The assumption is that
1099 since there is no significant trend in the CRU-JRA data over this period, these data can be reliably
1100 used to spin up the model to equilibrium. The land cover data used to force the model are based
1101 on a geographical reconstruction of the historical land cover driven by the increase in crop area
1102 following Arora and Boer (2010) but using the crop area data prepared for the Global Carbon
1103 Project (GCP) 2018 following Hurtt et al. (2006). Since land cover is prescribed, the competition
1104 between PFTs for space for the simulations reported here is switched off. The population data
1105 for the period 1850-2017 are based on Klein Goldewijk et al. (2017) and obtained from
1106 <ftp://ftp.pbl.nl/./hyde/hyde3.2/baseline/zip/>. The time-independent forcings consist of soil
1107 texture and permeable depth data.

1108 Time-varying atmospheric N deposition and fertilizer data used over the historical period
1109 are also specified as per the TRENDY protocol. The fertilizer data are based on the N₂O model
1110 intercomparison project (NMIP) (Tian et al., 2018) and available for the period 1860-2014. For

Deleted:

Deleted: and

1113 the period before 1860, 1860 fertilizer application rates are used. For the period after 2014,
1114 fertilizer application rates for 2014 are used. Atmospheric N deposition data are from input4MIPs
1115 (<https://esgf-node.llnl.gov/search/input4mips/>) and are the same as used by models
1116 participating in CMIP6 for the historical period (1850-2014). For years 2015-2017 the N
1117 deposition data corresponding to those from representative concentration pathway (RCP) 8.5
1118 scenario are used. Figure 2 shows the time series of global annual values of externally specified
1119 fertilizer input, and deposition of ammonium and nitrate, based on the TRENDY protocol, for the
1120 six primary simulations. Geographical distribution of these inputs are also shown for the last 20
1121 years from the FULL simulation corresponding to the 1998-2017 period. In Figure 2 (panels a, c
1122 and e) ammonium and nitrate deposition, and fertilizer input stay at their pre-industrial level for
1123 simulations in which these forcings do not increase over the historical period. As mentioned
1124 earlier, N deposition is split evenly into ammonium and nitrate. The values in parenthesis in
1125 Figure 2a legend, and in subsequent time series plots, show average values over the 1850s, the
1126 last 20 years (1998-2017) of the simulations, and the change between these two periods. The
1127 present day values of fertilizer input and N deposition are consistent with other estimates
1128 available in the literature (Table 2). The fertilizer input rate in the simulation with all forcings
1129 except land use change (FULL-no-LUC, blue line), that is with no increase in crop area over its
1130 1850 value, is 50 Tg N yr⁻¹ compared to 91 Tg N yr⁻¹ in the FULL simulation, averaged over the
1131 1998-2017 period. The additional 41 Tg N yr⁻¹ of fertilizer input occurs in the FULL simulation due
1132 to the increase in crop area but also due to the increasing fertilizer application rates over the
1133 historical period. Geographical distribution of the fertilizer application rates in Figure 2b shows
1134 that they are concentrated in regions with crop area and with values as high as 16 gN m⁻² yr⁻¹

1135 especially in eastern China. The N deposition rates (Figure 2d, 2f) are more evenly distributed
1136 geographically than the fertilizer applications rates, as would be expected, since emissions are
1137 transported downstream from their point sources. Areas with high emissions like the eastern
1138 United States, India, eastern China, and Europe, however, still stand out as areas that receive
1139 higher N deposition.

1140 **4.2 Evaluation data sources**

1141 We compare globally-summed annual values of N pools and fluxes with observations and
1142 other models, and where available their geographical distribution and seasonality. In general,
1143 however, much less observation-based data are available to evaluate simulated terrestrial N
1144 cycle components than for C cycle components. As a result, N pools and fluxes are primarily
1145 compared to results from both observation-based studies and other modelling studies
1146 (Bouwman et al., 2013; Fowler et al., 2013; Galloway et al., 2004; Vitousek et al., 2013; Zaehle,
1147 2013). Since the primary purpose of the N cycle in our framework is to constrain the C cycle, we
1148 also compare globally-summed annual values of GPP and net atmosphere-land CO₂ flux, and their
1149 zonal distribution with available observation-based and other estimates. The observation-based
1150 estimate of GPP is from Beer et al. (2010), who apply diagnostic models to extrapolate ground-
1151 based carbon flux tower observations from about 250 stations to the global scale. Observation-
1152 based net atmosphere-land CO₂ flux is from Global Carbon Project's 2019 assessment
1153 (Friedlingstein et al., 2019).

1154 **5.0 Results**

1155 **5.1 N inputs**

Deleted: ¶

Moved up [3]: To evaluate the model's response to various forcings over the historical period we perform several simulations turning on one forcing at a time as summarized in Table 1. The objective of these simulations is to see if the model response to individual forcings is consistent with expectations. For example, in the CO₂-only simulation only atmospheric CO₂ concentration increases over the historical period, while all other forcings stay at their 1850 levels. In the N-DEP-only simulation only N deposition increases over the historical period, and similarly for other runs in Table 1. A "FULL" simulations with all forcings turned on is then also performed which we compare to the original model without a N cycle which uses the photosynthesis downregulation parameterization (termed "ORIGINAL" in Table 1). ¶

Finally, a separate pre-industrial simulation is also performed that uses the same Γ_1 and Γ_2 globally (FULL-no-implicit-P-limitation). This simulation is used to illustrate the effect of neglecting P limitation for the broadleaf evergreen tree PFT in the tropics.¶

1175 Figure 3 (panels a, c, e) shows the time series of annual values BNF and its natural and
 1176 anthropogenic components from the six primary simulations summarized in Table 1. BNF stays
 1177 at its pre-industrial value of around 80 Tg N yr⁻¹ in the CO₂-only and N-DEP-only simulations. In
 1178 the CLIM-only (indicated by magenta coloured line) and the FULL-no-LUC (blue line) simulations
 1179 the change in climate, associated with increases in temperature and precipitation over the 1901-
 1180 2017 period (see Figure A2 in the appendix), increases BNF to about 85 Tg N yr⁻¹. In our
 1181 formulation (equation 3) BNF is positively impacted by increases in temperature and
 1182 precipitation. In the LUC+FERT-only simulation (dark green line) the increase in crop area
 1183 contributes to an increase in global BNF with a value around 110 Tg N yr⁻¹ for the present day,
 1184 since a higher BNF per unit crop area is assumed than for natural vegetation. Finally, in the FULL
 1185 simulation (red line) the 1998-2017 average value is around 117 Tg N yr⁻¹ due both to changes in
 1186 climate over the historical period and the increase in crop area. Our present day value of global
 1187 BNF is broadly consistent with other modelling and data-based studies as summarized in Table 2.
 1188 Panels c and e in Figure 3 show the decomposition of the total terrestrial BNF into its natural
 1189 (over non-crop PFTs) and anthropogenic (over C₃ and C₄ crop PFTs) components. The increase in
 1190 crop area over the historical period decreases natural BNF from its pre-industrial value of 59 to
 1191 54 Tg N yr⁻¹ for the present day as seen for the LUC+FERT-only simulation (green line) in Figure
 1192 3c, while anthropogenic BNF over agricultural area increases from 21 to 56 Tg N yr⁻¹ (Figure 3e).
 1193 Figure 3c and 3e show that the increase in BNF (Figure 3a) in the FULL simulation is caused
 1194 primarily by an increase in crop area. Our present day values of natural and anthropogenic BNF
 1195 are also broadly consistent with other modelling and data-based studies as summarized in Table
 1196 2.

Deleted: 3
 Deleted: ,
 Deleted: panel a, shows the global values of simulated BNF

Deleted: ,
 Deleted: FIRE-only,

Deleted: 1

Deleted: A1

Deleted: The values in parenthesis in Figure 3a legend, and in subsequent panels of this and other figures, show average values over the 1850s, the last 20 years (1998-2017) of the simulations, and the change between these two periods.

Deleted: 3

Deleted: 3
 Deleted: 3
 Deleted: 3
 Deleted: 3

1213 Figure 3 (panels b, d, and f) shows the geographical distribution of simulated BNF and its
1214 natural and anthropogenic components. The geographical distribution of BNF (Figure 3a) looks
1215 very similar to the current distribution of vegetation (not shown) with warm and wet regions
1216 showing higher values than cold and dry regions since BNF is parameterized as a function of
1217 temperature and soil moisture. Anthropogenic BNF only occurs in regions where crop area exists
1218 according to the specified land cover and it exhibits higher values than natural BNF in some
1219 regions because of its higher value per unit area (see section 3.2.1).

1220 At the global scale, and for the present day, natural BNF (59 Tg N yr⁻¹) is overwhelmed by
1221 anthropogenic sources: anthropogenic BNF (60 Tg N yr⁻¹), fertilizer input (91.7 Tg N yr⁻¹), and
1222 atmospheric N deposition increase since the pre-industrial era (~45 Tg N yr⁻¹). Currently humanity
1223 fixes more N than the natural processes (Vitousek, 1994).

1224 5.2 C and N pools, fluxes response to historical changes in forcings

1225 To understand the model response to changes in various forcings over the historical
1226 period we first look at the evolution of global values of primary C and N pools, and fluxes, shown
1227 in Figures 4 through 8. Figure 4a shows the time evolution of global annual GPP values, the
1228 primary flux of C into the land surface, for the six primary simulations, the ORIGINAL simulation
1229 performed with the model version with no N cycle, and the ORIG-UNCONST simulation with no
1230 photosynthesis downregulation (see Table 1). The unconstrained increase in GPP (35.6 Pg C yr⁻¹
1231 over the historical period) in the ORIG-UNCONST simulation (dark cyan line) is governed by the
1232 standard photosynthesis model equations following Farquhar et al. (1980) and Collatz et al.
1233 (1992) for C₃ and C₄ plants, respectively. Downregulation of photosynthesis in the ORIGINAL

Deleted: Figure 3, panels b, d, and f, show the global values of externally specified fertilizer input, and deposition of ammonium and nitrate, based on the TRENDY protocol, for the six primary simulations. Ammonium and nitrate deposition, and fertilizer input stay at their pre-industrial level for simulations in which these forcings do not increase over the historical period. As mentioned earlier, N deposition is split evenly into ammonium and nitrate. The present day values of fertilizer input and N deposition are consistent with other estimates available in the literature (Table 2). The fertilizer input rate in the simulation with all forcings except land use change (FULL-no-LUC, blue line), that is with no increase in crop area over its 1850 value, is 50 Tg N yr⁻¹ compared to 91 Tg N yr⁻¹ in the FULL simulation, averaged over the 1998-2017 period. The additional 41 Tg N yr⁻¹ of fertilizer input occurs in the FULL simulation due to the increase in crop area but also due to the increasing fertilizer application rates over the historical period. ¶

Deleted: 4

Deleted: , and specified fertilizer application and N deposition rates

Deleted: 4

Deleted: Figures 4c and 4e show the split of BNF into its natural and anthropogenic components.

Deleted: A

Deleted: 1

Deleted: in the appendix

Deleted: In Figure 4b, the fertilizer application rates are concentrated in regions with crop area and with values as high as 16 gN m⁻² especially in eastern China. The N deposition rates are more evenly distributed than fertilizer applications rates, as would be expected, since emissions are transported downstream from their point sources. Areas with high emissions like the eastern United States, India, eastern China, and Europe, however, still stand out as areas that receive higher N deposition.

Deleted:

Deleted: 5

Deleted: 9

Deleted: 5

Deleted: rate of

1273 simulation (purple line) is modelled on the basis of equation (1), while in the FULL simulation (red
1274 line) photosynthesis downregulation results from a decrease in V_{cmax} values (Figure 5d) due to a
1275 decrease in leaf N content (Figure 5b). We will compare the FULL and ORIGINAL simulations in
1276 more detail later. The simulations with individual forcings, discussed below, provide insight into
1277 the combined response of GPP to all forcings in the FULL simulation.

1278 5.2.1 Response to increasing CO₂

1279 The response of C and N cycles to increasing CO₂ in the CO₂-only simulation (orange lines
1280 in Figure 4) is the most straightforward to interpret. A CO₂ increase causes GPP to increase by 7.5
1281 Pg C yr⁻¹ above its pre-industrial value (Figure 4a), which in turn causes vegetation (Figure 4b),
1282 leaf (Figure 4c), and soil (Figure 4d) carbon mass to increase as well. The vegetation and leaf N
1283 amounts (orange line, Figures 5a and 5b), in contrast, decrease in response to increasing CO₂.
1284 This is because N gets locked up in the soil organic matter pool (Figure 5c) in response to an
1285 increase in the soil C mass (due to the increasing GPP), litter inputs which are now rich in C (due
1286 to CO₂ fertilization) but poor in N (since N inputs are still at their pre-industrial level), and the fact
1287 that the C:N ratio of the soil organic matter is fixed at 13. This response to elevated CO₂ which
1288 leads to increased C and decreased N in vegetation is consistent with meta-analysis of 75 field
1289 experiments of elevated CO₂ (Cotrufo et al., 1998). A decrease in N in leaves (orange line, Figure
1290 5b) leads to a concomitant decrease in maximum carboxylation capacity (V_{cmax}) (orange line,
1291 Figure 5d) and as a result GPP increases at a much slower rate in the CO₂-only simulation than in
1292 the ORIG-UNCONST simulation (Figure 4a). Due to the N accumulation in the soil organic matter
1293 pool, the NH₄⁺ and NO₃⁻ (Figures 5e and 5f) pools also decrease in size in the CO₂-only simulation.

Deleted: 6

Deleted: 6

Deleted: 5

Deleted: over

Deleted: 5

Deleted: 5

Deleted: 5

Deleted: 5

Deleted: 6

Deleted: 6

Deleted: 6

Deleted: 6

Deleted: 6

Deleted: 5

Deleted: 6

Deleted: 6

1310 Figure 6 shows the time series of N demand, plant N uptake and its split between passive
1311 and active N uptakes. The plant N demand in the CO₂-only simulation (Figure 6a, orange line)
1312 increases from its pre-industrial value of 1512 Tg N/yr to 1639 Tg N/yr for the present day since
1313 the increasing C input from increasing GPP requires higher N input to maintain preferred
1314 minimum C:N ratio of plant tissues. However, since mineral N pools decrease in size over the
1315 historical period in this simulation (Figures 5e and 5f), the total plant N uptake (Figure 6b)
1316 reduces. Passive plant N uptake is directly proportional to pool sizes of NH₄⁺ and NO₃⁻ and
1317 therefore it reduces in response to increasing CO₂. Active plant N uptake, which compensates for
1318 insufficient passive N uptake compared to the N demand, also eventually starts to decline as it
1319 also depends on mineral N pool sizes. The eventual result of increased C supply and reduced N
1320 supply is an increase in the C:N ratio of all plant components and litter (Figure 7). The
1321 preindustrial total N uptake of around 960 Tg N/yr (Figure 6b) is lower than the preindustrial N
1322 demand (1512 Tg N/yr, Figure 6a) despite the sum of global NH₄ and NO₃ pool sizes being around
1323 4000 Tg N (Figures 5e and 5f). This is because of the mismatch between where the pools are high
1324 and where the vegetation actually grows and the fact that plant N uptake is limited by its rate.
1325 As a result, in our model, even in the preindustrial era vegetation is N limited.

Deleted: 7

Deleted:

Deleted: 7

Deleted: 6

Deleted: 6

Deleted: 7

Deleted: 8

1326 Figure 8 shows the net mineralization flux (the net transfer of mineralized N from litter
1327 and humus pools to the mineral N pools as a result of the decomposition of organic matter),
1328 nitrification (N flux from NH₄⁺ to the NO₃⁻ pool), and the gaseous and leaching losses from the
1329 mineral pools. The net mineralization flux reduces in the CO₂-only simulation (Figure 8a, orange
1330 line) as N gets locked up in the soil organic matter. A reduction in the NH₄⁺ pool size in response
1331 to increasing CO₂ also yields a reduction in the nitrification flux over the historical period (Figure

Deleted: 9

Deleted: 9

Deleted: implies

1342 8b, orange line) since nitrification depends on the NH_4^+ pool size (equation 19). Finally, leaching
1343 from the NO_3^- pool (Figure 8c), NH_3 volatilization (Figure 8d), and the gaseous losses associated
1344 with nitrification from the NH_4^+ pool (Figure 8e) and denitrification from the NO_3^- pool (Figure 8f)
1345 all reduce in response to reduction in pool sizes of NH_4^+ and NO_3^- in the CO_2 -only simulation.

Deleted: 9

Deleted: 9

Deleted: 9

Deleted: 9

Deleted: 9

1346 5.2.2 Response to changing climate

1347 The perturbation due to climate change alone over the historical period in the CLIM-only

1348 simulation (magenta coloured lines in Figures 4 to 8) is smaller than that due to increasing CO_2 .

Deleted: 5

Deleted: -9

1349 In Figure 4a, changes in climate over the historical period increase GPP slightly by $3.60 \text{ Pg C yr}^{-1}$

Deleted: simulation

Deleted: 5

1350 which in turn slightly increases vegetation (including leaf) C mass (Figure 4b,c). The litter and soil

Deleted: 5

1351 carbon mass (Figure 4d), however, decrease slightly due to increased decomposition rates

Deleted: 5

1352 associated with increasing temperature (see Figure A2b). Both the increase in BNF due to

Deleted: 1

1353 increasing temperature (magenta line in Figure 2a), and the reduction in litter and soil N mass

Deleted: 3

1354 (Figure 5c) due to increasing decomposition and higher net N mineralization (Figure 8a, magenta

Deleted: 6

Deleted: 9

1355 line), make more N available. This results in a slight increase in vegetation and leaf N mass

1356 (Figures 5a and 5b) and the NH_4^+ (Figure 5e) pool which is the primary mineral pool in soils under

Deleted: 6

Deleted: 6

1357 vegetated regions. The global NO_3^- pool, in contrast, decreases in the CLIM-only simulation

Deleted: 6

1358 (Figure 5f) with the reduction primarily occurring in arid regions where the NO_3^- amounts are very

Deleted: 6

1359 large (see Figure 9 that shows the geographical distribution of the primary C and N pools). The

Deleted: 10

Deleted: b

1360 geographical distribution of NH_4^+ (Figure 9a) generally follows the geographical distribution of

Deleted: 10

1361 BNF, but with higher values in areas where cropland exists and where N deposition is high. The

1362 geographical distribution of NO_3^- (Figure 9b) generally shows lower values than NH_4^+ except in

Deleted: 10

1363 the desert regions where lack of denitrification leads to a large buildup of the NO_3^- pool (as

Deleted: see

1388 explained earlier in section 3.4.2). Although Figure 9 shows the geographical distribution of
1389 mineral N pools from the FULL simulation, the geographical distribution of pools are broadly
1390 similar between different simulations with obvious differences such as lack of hot spots of N
1391 deposition and fertilizer input in simulations in which these forcings stay at their pre-industrial
1392 levels. Figure 9 also shows the simulated geographical distribution of C and N pools in the
1393 vegetation and soil organic matter. The increase in GPP due to changing climate increases the N
1394 demand (Figure 6a, magenta line) but unlike the CO₂-only simulation, the plant N uptake
1395 increases since the NH₄⁺ and NO₃⁻ pools increase in size over the vegetated area in response to
1396 increased mineralization (Figure 8a, magenta line) and increased BNF (Figure 3a, magenta line).
1397 The increase in plant N uptake comes from the increase in passive plant N uptake (Figure 6c)
1398 while the active plant N uptake reduces (Figure 6d). Active and passive plant N uptakes are
1399 inversely correlated. This is by design since active plant N uptake increases when passive plant N
1400 uptake reduces and vice-versa, although eventually both depend on the size of available mineral
1401 N pools. Enhancement of plant N uptake due to changes in climate, despite increases in GPP
1402 associated with a small increase in V_{cmax} (Figure 5d), leads to a small reduction in the C:N ratio of
1403 all plant tissues (Figure 7). The litter C:N, in contrast, shows a small increase since not all N makes
1404 its way to the litter as a specified fraction of 0.54 (Table A1) leaf N is resorbed from deciduous
1405 trees leaves prior to leaf fall (Figure 7e). Although the leaf C:N ratio decreases in the CLIM only
1406 simulation, in response to increased BNF and increased mineralization, this decrease is not large
1407 enough to overcome the effect of resorption and as a result the C:N litter increases.

Deleted: A

Deleted: 3

Deleted: in the appendix

Deleted: 10

Deleted: 10

Deleted: 7

Deleted: increased BNF (Figure 3a, magenta line)

Deleted: 7

Deleted: 7

Deleted: 6

Deleted: 8

Deleted: 8

1420 Finally, the small increase in pool sizes of NH_4^+ and NO_3^- leads to a small increase in
1421 leaching, volatilization, and gaseous losses associated with nitrification and denitrification (Figure
1422 [8](#)).

Deleted: 9

1423 5.2.3 Response to N deposition

1424 The simulated response of GPP to changes in N deposition (brown line) over the historical
1425 period is smaller than that for CO_2 and climate (Figure [4a](#)). The small increase in GPP of 2.0 Pg C
1426 yr^{-1} leads to commensurately small increases in vegetation (Figure [4b](#)) and litter plus soil (Figure
1427 [4d](#)) C mass. Vegetation and leaf N mass (Figure [5a,b](#)) also increase in response to N deposition
1428 and so do mineral pools of NH_4^+ and NO_3^- (Figure [5e,f](#)). The increase in GPP in the simulation with
1429 N deposition results from an increase in V_{cmax} rates (Figure [5d](#)) associated with an increase in leaf
1430 N content (Figure [5b](#)). N demand increases marginally and so does plant N uptake in response to
1431 N deposition (Figure [6](#)). As would be intuitively expected, the C:N ratio of the whole plant, its
1432 components of leaves, stem, and root, and litter decreases slightly in response to N deposition
1433 (Figure [7](#)). Net N mineralization, nitrification, leaching, volatilization, and gaseous losses
1434 associated with nitrification and denitrification all increase in response to N deposition (Figure
1435 [8](#)).

Deleted: 5

Deleted: 5

Deleted: 5

Deleted: 6

Deleted: 6

Deleted: 6

Deleted: 6

Deleted: 7

Deleted: 8

Deleted: 9

1436 5.2.4 Response to LUC and fertilizer input

1437 The simulated response to LUC, which reflects an increase in crop area, and increased
1438 fertilizer deposition rates over the historical period is shown by dark green lines in Figures [4](#)
1439 through [8](#). The increase in fertilizer input is a much bigger perturbation to the N cycle system
1440 than N deposition. Figure [2](#) shows that at the global scale the fertilizer inputs increase from 0 to

Deleted: 5

Deleted: 9

Deleted: 3

1455 ~92 Tg N/yr over the historical period, while the combined NH_4^+ and NO_3^- N deposition rate
1456 increases from around 20 to 65 Tg N/yr. In addition, because of higher per unit area BNF rates
1457 over crop area than natural vegetation, the increase in crop area in this simulation leads to an
1458 increase in anthropogenic BNF from about 20 to 56 Tg N/yr over the historical period. All together
1459 increasing crop area and fertilizer inputs imply an additional ~130 Tg N/yr being input into the
1460 terrestrial N cycle at the present day since the pre-industrial period, compared to an increase of
1461 only 45 Tg N/yr for the N deposition forcing.

1462 The global increase in fertilizer input over the historical period leads to higher NH_4^+ and
1463 NO_3^- pools (Figures 5e and 5f). Although both fertilizer and BNF contribute to the NH_4^+ pool, the
1464 NO_3^- pool also increases through the nitrification flux (Figure 8b). An increase in crop area over
1465 the historical period results in deforestation of natural vegetation that reduces vegetation
1466 biomass (Figure 4b). However, soil carbon mass also decreases (Figure 4d) despite higher litter
1467 inputs. This is because a higher soil decomposition rate is assumed over cropland areas to
1468 simulate soil carbon loss as empirical measurements of soil carbon show over deforested areas
1469 which are converted to croplands (Wei et al., 2014). Fertilizer application only occurs over crop
1470 areas which increases the V_{cmax} rates for crops and, as expected, this yields an increase in globally-
1471 averaged V_{cmax} (Figure 5d). A corresponding large increase in leaf N content (Figure 5b) is,
1472 however, not seen because vegetation (and therefore leaf) N (Figure 5a,b) is also lost through
1473 deforestation. In addition, V_{cmax} is essentially a flux (expressed per unit leaf area) that is averaged
1474 over the whole year while leaf and vegetation N pools are sampled at the end of each year and
1475 all crops in the northern hemisphere above 30° N are harvested before the year end. Vegetation
1476 N mass, in fact, decreases in conjunction with vegetation C mass (Figure 4b). Plant N demand

Deleted: 6

Deleted: 6

Deleted: 9

Deleted: but also

Deleted: ,

Deleted: since

Deleted: (Figures 5b and 5d),

Deleted: consistent with

Deleted: 6

Deleted: 6

Deleted: 6

Deleted: rate

Deleted: 5

1490 reduces (Figure 6a) and plant N uptake increases (Figure 6b) driven by crop PFTs in response to
1491 fertilizer input, as would be intuitively expected. The increase in plant N uptake comes from the
1492 increase in passive N uptake, in response to increases in pool sizes of NH_4^+ and NO_3^- over crop
1493 areas, while active plant N uptake decreases since passive uptake can more than keep up with
1494 the demand over cropland area. While the C:N ratio of vegetation biomass decreases over
1495 cropland area in response to fertilizer input (not shown) this is not seen in the globally-averaged
1496 C:N ratio of vegetation (Figure 7a) and its components because C and N are also lost through
1497 deforestation and the fact that crop biomass is harvested. The C:N of the global litter pool,
1498 however, decreases in response to litter from crops which gets rich in N as fertilizer application
1499 rates increase. Finally, in Figure 8, global net N mineralization, nitrification, leaching,
1500 volatilization, and gaseous losses associated with nitrification and denitrification all increase by
1501 a large amount in response to an increase in fertilizer input.

Deleted: 7

Deleted: 7

Deleted: 8

Deleted: 9

1502 5.2.5 Response to all forcings

1503 We can now evaluate and understand the simulated response of the FULL simulation to
1504 all forcings (red line in Figures 4 through 8). The increase in GPP in the FULL simulation (14.5 Pg
1505 C/yr) in Figure 4a over the historical period is driven by GPP increase associated with increase in
1506 CO_2 (7.5 Pg C/yr), changing climate (3.6 Pg C/yr), and N deposition (2.0 Pg C/yr). The increases
1507 associated with these individual forcings add up to 13.1 Pg C/yr indicating that synergistic effects
1508 between forcings contribute to the additional 1.4 Pg C/yr increase in GPP. The changes in
1509 vegetation and soil plus litter carbon mass (Figures 4b and 4d) in the FULL simulation are similarly
1510 driven by these three factors but, in addition, LUC contributes to decreases in vegetation and soil
1511 carbon mass as natural vegetation is deforested to accommodate for increases in crop area.

Deleted: 5

Deleted: 9

Deleted: 5

Deleted:

Deleted: 5

Deleted: 5

1522 Vegetation and leaf N mass (Figures 5a and 5b) decrease in the FULL simulation driven primarily
 1523 by the response to increasing CO₂ (orange line compared to the red line) while changes in litter
 1524 and soil N mass are affected variably by all forcings (Figure 5c). Changes in V_{cmax} (Figure 5d) are
 1525 similarly affected by all forcings: increasing CO₂ leads to a decrease in globally-averaged V_{cmax}
 1526 values while changes in climate, N deposition, and fertilizer inputs lead to increases in V_{cmax}
 1527 values with the net result being a small decrease over the historical period. The increase in global
 1528 NH₄⁺ mass in the FULL simulation is driven primarily by the increase in fertilizer input (Figure 5e,
 1529 red versus green line) while the changes in NO₃⁻ mass are primarily the result of changes in
 1530 climate (Figure 5f, magenta line) which causes a decrease in NO₃⁻ mass from about 1940 to 1970
 1531 and N deposition and fertilizer input (Figure 5f, green and brown lines) which contribute to the
 1532 increase in NO₃⁻ mass later on in the historical period. The increase in N demand (Figure 6a) over
 1533 the historical period is also driven primarily by the increase in atmospheric CO₂. Plant N uptake
 1534 (Figure 6b) decreases in response to increasing CO₂ but increases in response to changes in
 1535 climate, N deposition, and fertilizer inputs such that the net change over the historical is a small
 1536 decrease. The increase in the C:N ratio of vegetation and its components (leaves, stem, and root)
 1537 is driven primarily by an increase in atmospheric CO₂ (Figure 7a, red versus orange line). Litter
 1538 C:N in the FULL simulation, in contrast, does not change substantially over the historical period
 1539 in a globally-averaged sense as the increase in the C:N ratio of litter associated with an increase
 1540 in atmospheric CO₂ is mostly compensated by the decrease associated with an increase in N
 1541 deposition and fertilizer application. The simulated change in global net N mineralization (Figure
 1542 8a) in the FULL simulation, over the historical period, is small since the decrease in net N
 1543 mineralization due to increasing CO₂ (orange line) is compensated by the increase caused by

Deleted: 6

Deleted: 6

Deleted: 6

Deleted: 6

Deleted: (Figure 6e)

Deleted: net

Deleted: all forcings with no single forcing dominating the response

Deleted: 7

Deleted: 7

Deleted: (Figure 8a)

Deleted: Changes in l

Deleted: experience

Deleted: dominant influence from any one of the forcings

Deleted: 9

1559 changes in climate, N deposition, and fertilizer inputs (magenta, brown, and green lines
1560 respectively). The remaining fluxes of nitrification, NO₃⁻ leaching, NH₃ volatilization, and gaseous
1561 losses associated with nitrification and denitrification in the FULL simulation (Figure 8) are all
1562 strongly influenced by fertilizer input (green line compared to red line).

Deleted: 9

1563 Table 2 compares simulated values of all primary N pools and fluxes from the FULL
1564 simulation with other modelling and quasi observation-based studies. Simulated values are
1565 averaged over the 1998-2017 period. Where available, time-periods for other modelling and
1566 quasi observation-based studies to which estimates correspond are also noted. For the most part
1567 simulated pools and fluxes lie within the range of existing studies with the exception of N₂ and
1568 NO emissions that are somewhat higher.

1569 5.2.6 Response to all forcings except LUC

1570 The FULL-no-LUC simulation includes all forcings except LUC (blue line in Figures 4
1571 through 8) and corroborates several of the points mentioned above. In this simulation crop area
1572 stays at its 1850 value. Figure 2b (blue line) shows increasing global fertilizer input in this
1573 simulation despite crop area staying at its 1850 value since fertilizer application rates per unit
1574 area increase over the historical period. In the absence of the LUC, vegetation C mass (Figure 4b)
1575 and soil plus litter C (Figure 4d) and N (Figure 5c) are higher in the FULL-no-LUC compared to the
1576 FULL simulation. N demand (Figure 6a) is slightly higher in FULL-no LUC than in FULL simulation
1577 because there is more standing vegetation biomass that is responding to increasing CO₂. The
1578 increase in volatilization, leaching, and gaseous losses associated with nitrification and
1579 denitrification (Figures 8c-8f) are all primarily caused by increased fertilizer input over the

Deleted: 5

Deleted: 9

Deleted: 3

Deleted: 5

Deleted: 5

Deleted: 6

Deleted: 7

Deleted: 9

Deleted: 9

1590 specified 1850 crop area. The increase in N losses associated with these processes, over the
1591 historical period, is much lower in the FULL-no-LUC simulation than in the FULL simulation since
1592 crop area stays at its 1850 values.

1593 5.3 Comparison of FULL and ORIGINAL simulations

1594 We now compare the results from the FULL simulation that includes the N cycle with that
1595 from the ORIGINAL simulation that does not include the N cycle. Both simulations are driven with
1596 all forcings over the historical period. Figure 4a shows that the global GPP values in the FULL (red
1597 line) and ORIGINAL (purple line) simulations are quite similar although the rate of increase of GPP
1598 in the FULL simulation is slightly higher than in the ORIGINAL simulation. As a result, simulated
1599 global vegetation biomass is somewhat higher in the FULL simulation (Figure 4b). The simulated
1600 global litter and soil carbon mass (Figure 4d) is, however, lower in the FULL simulation (1073 Pg
1601 C) compared to the ORIGINAL simulation (1142 Pg C) and this decrease mainly comes from a
1602 decrease at higher latitudes (not shown) due to a decrease in GPP (Figure 10a). The lower GPP in
1603 the FULL simulation, combined with the slow decomposition at cold high latitudes, results in a
1604 lower equilibrium for litter and soil carbon compared with the ORIGINAL simulation. Litter mass
1605 contributes about 80 Pg C to the total dead carbon mass. Overall both estimates of 1073 Pg C
1606 and 1142 Pg C are somewhat lower than the bulk density corrected estimate of 1230 Pg C based
1607 on the Harmonized World Soil Database (HWSD) v.1.2 (Köchy et al., 2015). One reason for this is
1608 that CLASSIC does not yet represent permafrost related soil C processes.

1609 Figure 10a shows that the zonal distribution of GPP from the FULL and ORIGINAL
1610 simulations, for the 1998-2017 period, compares reasonably well to the observation-based

Deleted: 5

Deleted: 5

Deleted: 5

Deleted: 1

Deleted: these

Deleted: 1

1617 estimate from Beer et al. (2010). The FULL simulation has slightly lower productivity at high-
1618 latitudes than the ORIGINAL simulation, as mentioned above. Overall, however, the inclusion of
1619 the N cycle does not change the zonal distribution of GPP in the model substantially, which is
1620 determined primarily by the geographical distribution of climate. Figure 10b compares the zonal
1621 distribution of GPP from the pre-industrial simulation (corresponding to 1850s) from the FULL
1622 and FULL-with-no-implicit-P-limitation simulations to illustrate the high GPP in the tropics where
1623 P and not N limitation affects GPP and the reason for choosing a lower value of Γ_1 in equation
1624 (31) for the broadleaf evergreen tree PFT.

Deleted: 1

Deleted: .

1625 The global GPP in the ORIGINAL and FULL simulations averaged over the period 1998-
1626 2017 (120.0 and 120.4 PgC/yr, respectively) are around 15% lower compared to that in the ORIG-
1627 UNCONST simulation (142 PgC/yr), as shown in Figure 4a, yielding a global downregulation factor
1628 of about 0.85. Figure 10c shows how downregulation works in the ORIGINAL and FULL
1629 simulations in a zonally-averaged sense. Ratios of annual GPP averaged over the 1998-2017
1630 period from the ORIGINAL versus ORIG-UNCONST simulations, and FULL versus ORIG-UNCONST
1631 simulations were first calculated for each grid cell and then zonally-averaged over the land grid
1632 cells. Ratios can be misleading especially for grid cells with low values, for example, in the desert
1633 regions. In addition, these ratios also depend on the specified V_{cmax} values in the ORIG-UNCONST
1634 simulation. In Figure 10c, the purple line for the ORIGINAL simulation exhibits values around 0.8
1635 consistent with the global downregulation of around 0.85 and the fact that the same scalar
1636 downregulation multiplier is used everywhere on the globe (equation 1). The red line for the FULL
1637 simulation, however, indicates a pattern of higher downregulation at high-latitudes. The peaks
1638 in red line, especially the one around 23°N (Sahara desert), are due to higher values in selected

1641 grid cells in dry and arid regions where the build-up of NO_3^- in the soil (due to reduced
1642 denitrification) increases V_{cmax} and thus GPP in the run with N cycle leading to higher ratios
1643 although the absolute GPP values still remain low.

1644 Figure 11a compares globally-summed net atmosphere-land CO_2 flux from the FULL,
1645 FULL-no-LUC, and ORIGINAL simulations with quasi observation-based estimates from the 2019
1646 Global Carbon Project (Friedlingstein et al., 2019). There are two kinds of estimates in Figure 11a
1647 from Friedlingstein et al. (2019): the first is the net atmosphere-land CO_2 flux for the decades
1648 spanning the 1960s to the 2000s which are shown as rectangular boxes with their corresponding
1649 mean values and ranges, and the second is the terrestrial sink from 1959 to 2018 (dark yellow
1650 line). Positive values indicate a sink of carbon over land and negative values a source. The
1651 difference between the net atmosphere-land CO_2 flux and the terrestrial sink is that the
1652 terrestrial sink minus the LUC emissions yields the net atmosphere-land CO_2 flux. The
1653 atmosphere-land CO_2 flux from the FULL-no-LUC simulation (blue line) is directly comparable to
1654 the terrestrial sink since 1959, since the FULL-no-LUC simulation includes no LUC, and shows that
1655 the simulated terrestrial sink compares fairly well to the estimates from Friedlingstein et al.
1656 (2019). Averaged over the period 1959-2017, the modelled and Global Carbon Project values are
1657 2.0 and 2.1 Pg C/yr, respectively. The net atmosphere-land CO_2 flux from the FULL simulation
1658 mostly lies within the uncertainty range for the five decades considered, although it is on the
1659 higher side compared to estimates from Friedlingstein et al. (2019). The reason for this is that
1660 LUC emissions in CLASSIC are much lower than observation-based estimates, as discussed below
1661 in context of Figure 11c. CLASSIC simulates LUC emissions only in response to changes in crop
1662 area whereas changes in pasture area and wood harvesting also contribute to LUC emissions. The

Deleted: ¶

Deleted: 2

Deleted: 2

Deleted: two

Deleted: 2

1668 net-atmosphere land CO₂ flux from the ORIGINAL simulation compares better with the estimates
1669 from Friedlingstein et al. (2019), than the FULL simulation, because the photosynthesis down-
1670 regulation parameter in the ORIGINAL simulation has been adjusted despite discrepancies in
1671 simulated LUC processes.

1672 Figure 11b compares the zonal distribution of simulated net atmosphere-land CO₂ flux
1673 from the FULL and ORIGINAL simulations with the model-mean and range from the terrestrial
1674 ecosystem models that participated in the 2019 TRENDY model intercomparison and contributed
1675 results to 2019 Global Carbon Project (Friedlingstein et al., 2019). The carbon sink simulated by
1676 CLASSIC in the northern hemisphere is broadly comparable to the model-mean estimate from
1677 the TRENDY models. However, in the tropics CLASSIC simulates a much stronger sink than the
1678 model-mean, likely because of its lower LUC emissions.

1679 5.4 Contribution of forcings to land C sink and sources

1680 Figure 11c shows cumulative net atmosphere-land CO₂ flux for the 1850-2017 period from
1681 the six primary simulations with N cycle. These simulations facilitate the attribution of carbon
1682 uptake and release over the historical period to various forcings. The cumulative terrestrial sink
1683 in the FULL-no-LUC simulation for the period 1850-2017 is simulated to be ~153 Pg C and this
1684 compares reasonably well with the estimate of 185 ± 50 Pg C for the period 1850-2014 from Le
1685 Quéré et al. (2018). Increase in CO₂ (~115 Pg C), change in climate (~3 Pg C), and N deposition
1686 (~19 Pg C) all contribute to this terrestrial sink. These three contributions add up to 137 Pg C so
1687 the additional 16 Pg C is contributed by the synergistic effects between the three forcings.
1688 Quantified in this way, the contribution of increasing CO₂ (115 out of 137 Pg C), climate change

Deleted: 2

Deleted: 2

1691 (3 out of 137 Pg C), and N deposition (19 out of 137 Pg C) to carbon uptake by land over the
1692 historical period (1850-2017) is calculated to be 84%, 2%, and 14%, respectively. Cumulative LUC
1693 emissions simulated for the period 1850-2017 by CLASSIC can be estimated using a negative
1694 cumulative net-atmosphere-land CO₂ flux of ~66 Pg C from the LUC+FERT-only simulation or by
1695 the differencing the FULL and FULL-no-LUC simulations (~71 Pg C). While LUC emissions are highly
1696 uncertain, both of these estimates are much lower than the 195 ± 75 Pg C estimate from Le Quéré
1697 et al. (2018).

1698 **6.0 Discussion and conclusions**

1699 The interactions between terrestrial C and N cycles are complex and our understanding
1700 of these interactions, and their representation in models, is based on empirical observations of
1701 various terrestrial ecosystem processes. In this paper, we have evaluated the response of these
1702 interactions by perturbing the coupled C and N cycle processes in the CLASSIC model with one
1703 forcing at a time over the historical period: 1) increase in CO₂, 2) change in climate, 3) increase in
1704 N deposition, and 4) LUC with increasing fertilizer input. These simulations are easier to interpret
1705 and the model response can be evaluated against both our conceptual knowledge as well as
1706 empirical observation-based data. Our assumption is that, if the model response to individual
1707 forcings is realistic and consistent with expectations based on empirical observations then the
1708 response of the model to all forcings combined will also be realistic and easier to interpret,
1709 although we do expect and see synergistic effects between forcings.

1710 The simulated response of coupled C and N cycles in CLASSIC to increasing atmospheric
1711 CO₂ is an increase in the C:N ratio of vegetation components due to an increase in their C content

Deleted: .

1713 but also a decrease in their N content. This model response is conceptually consistent with a
1714 meta-analysis of 75 field experiments of elevated CO₂ as reported in Cotrufo et al. (1998) who
1715 find an average reduction in tissue N concentration of 14%. Most studies analyzed in the Cotrufo
1716 et al. (1998) meta-analysis used ambient CO₂ of around 350 ppm and elevated CO₂ of around
1717 650-700 ppm. In comparison, the plant N concentration in CLASSIC reduces by ~26% in response
1718 to a gradual increase in atmospheric CO₂ from 285 ppm to 407 ppm (an increase of 122 ppm)
1719 over the 1850-2017 period (whole plant C:N ratio increases from 142.6 to 194.1 in the CO₂-only
1720 simulation, Figure 7a). These two estimates cannot be compared directly - the majority (59%) of
1721 Free-Air Carbon dioxide Enrichment (FACE) experiments last less than 3 years (Jones et al., 2014)
1722 and the vegetation experiences a large CO₂ change of around 300-350 ppm while the duration of
1723 our historical simulation is 167 years and the gradual increase in CO₂ of 122 ppm over the
1724 historical period is much smaller.

Deleted: vegetation

Deleted: content

Deleted: 18

1725 The response of our model to CO₂ increase over the historical period is also consistent
1726 with the meta-analysis of McGuire et al. (1995) who report an average decrease in leaf N
1727 concentration of 21% in response to elevated CO₂ based on 77 studies, which is the primary
1728 reason for downregulation of photosynthetic capacity. The simulated decrease in leaf N
1729 concentration in our study for the CO₂-only experiment is around 27% (leaf C:N ratio increases
1730 from 42.8 to 58.6 in the CO₂-only simulation, Figure 7b). Although, the same caveats that apply
1731 to the comparison with the Cotrufo et al. (1998) study also apply to this comparison. The
1732 decrease in whole plant and leaf N concentrations in our results is conceptually consistent with
1733 the meta-analyses of McGuire et al. (1995) and Cotrufo et al. (1998). The decrease in whole plant
1734 N concentration in our CO₂-only and FULL simulations is the result of an increase in both tissue

Deleted: elevated

Deleted: mass

Deleted: also

Deleted: 1

Deleted: 6

1743 ~~C amount and a decrease in N amount. The decrease in tissue N amount is,~~ in fact, necessary in
1744 our modelling framework to induce the required downregulation of photosynthesis to simulate
1745 the land carbon sink realistically over the historical period.

Deleted: is

Deleted: s

1746 ~~The meta-analysis of Liang et al. (2016) reports an increase in above and belowground~~
1747 ~~plant N pools in response to elevated CO₂ associated with increase in BNF but since their results~~
1748 ~~are based on pool sizes they cannot be compared directly to the N concentration based results~~
1749 ~~from~~ McGuire et al. (1995) and Cotrufo et al. (1998). Liang et al. (2016) also report results from
1750 short-term (≤ 3 years) and long-term (between 3 to 15 years) studies separately (their Figure 3).
1751 They show that the increase in total plant and litter N pools become smaller for long-term studies.
1752 ~~Regardless,~~ the difference in time scales of empirical studies and the real world is a caveat that
1753 will always make it difficult to evaluate model results over long time scales.

Deleted: However, the decrease in plant N in response to elevated CO₂, found by

Deleted: , is inconsistent with the meta-analysis of Liang et al. (2016) who, in contrast, report an increase in above and belowground plant N pools in response to elevated CO₂ associated with increase in BNF. We are unable to reconcile this difference between the meta-analysis of Liang et al. (2016) and those from McGuire et al. (1995) and Cotrufo et al. (1998).

Deleted: T

1754 The response of C and N cycles to changes in climate in our model ~~(in the CLIM-only~~
1755 ~~simulation)~~ is also conceptually realistic. Globally, GPP increases in response to climate that
1756 gradually gets warmer and wetter ~~(see Figure A2)~~ and as a result vegetation biomass increases.
1757 Soil carbon mass, however, decreases (despite increase in NPP inputs) since warmer
1758 temperatures also increase heterotrophic respiration (not shown). As a result of increased
1759 decomposition of soil organic matter, net N mineralization increases and together with increased
1760 BNF the overall C:N ratio of vegetation and leaves decreases, which leads to a V_{cmax} increase. The
1761 small increase in V_{cmax} , due to ~~increased mineralization,~~ thus also contributes to an increase in
1762 GPP over and above that due to ~~a change in climate alone,~~ and therefore compensates for the
1763 amount of carbon lost due to increased soil organic matter decomposition associated with
1764 warmer temperatures. This behaviour is consistent with land C cycle models showing a reduction

Deleted: the change in climate

Deleted: n

Deleted: increase

Deleted: temperature

Deleted: solely

1781 in the absolute value of the strength of the carbon-climate feedback when they include coupling
1782 of C and N cycles (Arora et al., 2020).

1783 The modelled differences in PFT specific values of V_{cmax} , in our framework, come through
1784 differences in simulated values of leaf N content (N_l) that depend on BNF (given that BNF is the
1785 primary natural source of N input into the coupled soil-vegetation system) but also differences
1786 in mineralization that are governed by climate. N_l values, however, also depend on leaf
1787 phenology, allocation of carbon and nitrogen, turnover rates, transpiration (which brings in N
1788 through passive uptake), and almost every aspect of plant biogeochemistry which affects a PFT's
1789 net primary productivity and therefore N demand. Modelled increases in GPP in response to N
1790 deposition come through an increase in leaf N content and therefore V_{cmax} values.

Deleted: increases

1791 Finally, changes in land use associated with an increase in crop area, and the associated
1792 increase in fertilizer application rates lead to the largest increase in NO_3^- leaching, NH_3
1793 volatilization, and gaseous losses associated with nitrification and denitrification among all
1794 forcings. Overall, the model response to perturbation by all individual forcings is realistic,
1795 conceptually expected, and of the right sign (positive or negative) although it is difficult to
1796 evaluate the magnitude of these responses in the absence of directly comparable observation-
1797 based estimates.

1798 Despite the model responses to individual forcings that appears consistent with our
1799 conceptual understanding of coupled C and N cycles, our modelling framework misses an
1800 important feedback process that has been observed in the FACE and other experiments related
1801 to changes in natural BNF. FACE sites and other empirical studies report an increase in natural

1803 BNF rates at elevated CO₂ (McGuire et al., 1995; Liang et al., 2016) and a decrease in natural BNF
1804 rates when additional N is applied to soils (Salvagiotti et al., 2008; Ochoa-Hueso et al., 2013). On
1805 a broad scale this is intuitively expected but the biological processes behind changes in BNF rates
1806 remain largely unclear. A response can still be parameterized even if the underlying physical and
1807 biological processes are not well understood. For instance, Goll et al. (2012) parameterize BNF as
1808 an increasing and saturating function of NPP, $BNF = 1.8 (1.0 - \exp(-0.003 NPP))$. This
1809 approach, however, does not account for the driver behind the increase in NPP - increasing
1810 atmospheric CO₂, change in environmental conditions (e.g., wetter and warmer conditions), or
1811 increased N deposition. Clearly, increasing BNF if the NPP increase is due to N deposition is
1812 inconsistent with empirical observations. Over the historical period an increase in atmospheric
1813 CO₂ has been associated with an increase in N deposition so to some extent changes in BNF due
1814 to both forcings will cancel each other. We realize the importance of changes in BNF, given it is
1815 the single largest natural flux of N into the coupled soil-vegetation system yet highly uncertain,
1816 and aim to address these issues in a future version of the model by exploring existing BNF
1817 formulations. Meyerholt et al. (2016), for example, demonstrate the uncertainty arising from the
1818 use of five different BNF parameterizations in the context of the O-CN model. They use
1819 formulations that parameterize BNF as a function of 1) evapotranspiration, 2) NPP, 3) leaf C:N
1820 ratio, that takes into account energy cost for N fixation (Fisher et al., 2010), 4) plant N demand,
1821 and 5) an optimality-based approach that follows Rastetter et al. (2001) in which BNF only occurs
1822 when the carbon cost of N fixation is lower than the carbon cost of root N uptake. The approach
1823 used in our study is closest to the one that is based on evapotranspiration but makes the
1824 distinction in BNF rates over natural and agricultural areas.

Deleted: i

Deleted: .

Deleted: (

Deleted: .,

Deleted: (

Deleted: .,

1831 The reduction of photosynthesis rates in response to N limitation is the most important
1832 linkage between C and N cycles and yet it too is parameterized differently across models. Given
1833 that leaf N content and photosynthetic capacity are strongly correlated (Evans, 1989; Field and
1834 Mooney, 1986; Garnier et al., 1999), photosynthesis downregulation due to N limitation reduces
1835 photosynthetic capacity, and thus the GPP flux. Yet models reduce both NPP (Wiltshire et al.,
1836 2020) and V_{cmax} rates, and thus GPP. (Zaehle and Friend, 2010; Wania et al., 2012; von Bloh et al.,
1837 2018) in reponse to N limitation. V_{cmax} rates may themselves be parameterized as a function leaf
1838 N content directly (von Bloh et al., 2018; Zaehle and Friend, 2010) or leaf C:N ratio (Wania et al.,
1839 2012). In this study, we have parameterized V_{cmax} rates as a function of leaf N content (equation
1840 31) since the use of leaf C:N ratio leads to an incorrect seasonal variation of V_{cmax} . If an increase
1841 in leaf C:N ratio, as a result of increase in atmospheric CO_2 , leads to a decrease in V_{cmax} rates over
1842 the historical period then it implies that V_{cmax} is inversely related to leaf C:N ratios. Since leaf C:N
1843 ratio peak during the growing season (Li et al., 2017) this also implies V_{cmax} rates are lower during
1844 the growing season than at its start and this is in contrast to observations that show an increase
1845 in V_{cmax} during the growing season (e.g., see Fig. 1a of Bauerle et al. (2012)).

1846 Our framework assumes a constant C:N ratio of 13 for soil organic matter ($C:N_H$), an
1847 assumption also made in other models (e.g., Wania et al., 2012; Zhang et al., 2018). This
1848 assumption is also broadly consistent with Zhao et al. (2019) who attempt to model C:N of soil
1849 organic matter, among other soil properties, as a function of mean annual temperature and
1850 precipitation using machine learning algorithms (their Figure 2h). It is difficult to currently
1851 establish if increasing atmospheric CO_2 is changing $C:N_H$ given the large heterogeneity in soil
1852 organic C and N densities, and the difficulty in measuring small trends for such large global pools.

Deleted: (

Deleted: ,

Deleted: ¶

Deleted: (

Field Code Changed

1857 A choice of a somewhat different value for all PFTs or had we chosen specified constant PFT-
1858 dependent values of $C:N_H$ is of relatively less importance in this context since the model is spun
1859 to equilibrium for 1850 conditions anyway. It is the change in $C:N_H$ over time that is of
1860 importance. The assumption of constant $C:N_H$ is the key to yielding a decrease in vegetation N
1861 mass, and therefore leaf N mass and V_{cmax} , as CO_2 increases, in our framework. Without a
1862 decrease in V_{cmax} in our modelling framework, in response to elevated CO_2 , we cannot achieve
1863 the downregulation noted by McGuire et al. (1995) in their meta-analysis, and the simulated
1864 carbon sink over the historical period would be greater than observed as noted above. It is
1865 possible that we are simulating the reduction in leaf N mass, in response to elevated CO_2 , for a
1866 wrong reason in which case our model processes need to be revisited based on additional
1867 empirical data. If our assumption of constant or extremely slowly changing $C:N_H$ is indeed
1868 severely unrealistic, this necessitates a point of caution that a realistic land carbon sink can be
1869 simulated over the historical period with such an assumption.

Deleted:

1870 Related to this assumption is also the fact that we cannot make decomposition rates of
1871 soil organic matter a function of its C:N ratio since it is assumed to be a constant. It is well known
1872 that after climate, litter and soil organic matter decomposition rates are controlled by their C:N
1873 ratio (Manzoni et al., 2008). Litter decomposition rates can still be made a function of its C:N ratio
1874 and we aim to do this for a future model version.

Deleted: Since the C:N ratio of litter increases over the historical period, one implication of inclusion of this model feature will be an enhanced land carbon sink over the historical period due to decreasing litter decomposition rates.

1875 The work presented in this study of coupling C and N cycles in CLASSIC yields a framework
1876 that we can build upon to make model processes more realistic, test the effect of various model
1877 assumptions, parameterize existing processes in other ways, include additional processes, and
1878 evaluate model response at FluxNet sites to constrain model parameters.

Appendix

A1. Budget equations for N pools

The rates of change of N in the NH_4^+ and NO_3^- pools (in gN m^{-2}), N_{NH_4} and N_{NO_3} respectively, are given by

$$\frac{d N_{\text{NH}_4}}{dt} = B_{\text{NH}_4} + F_{\text{NH}_4} + P_{\text{NH}_4} + M_{D,\text{NH}_4} + M_{H,\text{NH}_4}$$

$$-U_{\text{NH}_4} - (I_{\text{NO}_3} + I_{\text{N}_2\text{O}} + I_{\text{NO}}) - V_{\text{NH}_3} - O_{\text{NH}_4} \quad (\text{A1})$$

$$\frac{d N_{\text{NO}_3}}{dt} = P_{\text{NO}_3} + I_{\text{NO}_3} - L_{\text{NO}_3} - U_{\text{NO}_3} - (E_{\text{N}_2} + E_{\text{N}_2\text{O}} + E_{\text{NO}}) - O_{\text{NO}_3} \quad (\text{A2})$$

and all fluxes are represented in units of $\text{gN m}^{-2} \text{day}^{-1}$. B_{NH_4} is the rate of biological N fixation which solely contributes to the NH_4^+ pool, F_{NH_4} is the fertilizer input which is assumed to contribute only to the NH_4^+ pool, and P_{NH_4} and P_{NO_3} are atmospheric deposition rates that contribute to the NH_4^+ and NO_3^- pools, respectively. Biological N fixation, fertilizer input, and atmospheric deposition are the three routes through which N enters the coupled soil-vegetation system. M_{D,NH_4} and M_{H,NH_4} are the mineralization flux from the litter and soil organic matter pools, respectively, associated with their decomposition. We assume mineralization of humus and litter pools only contributes to the NH_4^+ pool. O_{NH_4} and O_{NO_3} indicate immobilization of N from the NH_4^+ and NO_3^- pools, respectively, to the humus N pool which implies microbes (that are not represented explicitly) are part of the humus pool. Combined together the terms $(M_{D,\text{NH}_4} + M_{H,\text{NH}_4} - O_{\text{NH}_4} - O_{\text{NO}_3})$ yield the net mineralization rate. V_{NH_3} is the rate of ammonia (NH_3) volatilization and L_{NO_3} is the leaching of N that occurs only from the NO_3^- pool.

Deleted: ¶

Page Break

¶

Deleted: ¶

Moved (insertion) [2]

Deleted: 4

Deleted:

Deleted: 5

1911 The positively charged ammonium ions are attracted to the negatively charged soil particles and
 1912 as a result it is primarily the negatively charged nitrate ions that leach through the soil (Porporato
 1913 et al., 2003; Xu-Ri and Prentice, 2008). U_{NH_4} and U_{NO_3} are uptakes of NH_4^+ and NO_3^- by plants,
 1914 respectively. The nitrification flux from NH_4^+ to NO_3^- pool is represented by I_{NO_3} which also results
 1915 in the release of the nitrous oxide (N_2O), a greenhouse gas, and nitric oxide (NO) through nitrifier
 1916 denitrification represented by the terms I_{N_2O} and I_{NO} , respectively. Finally, E_{N_2} , E_{N_2O} and E_{NO}
 1917 are the gaseous losses of N_2 (nitrogen gas), N_2O , and NO from the NO_3^- pool associated with
 1918 denitrification. N is thus lost through the soil-vegetation system via leaching in runoff and
 1919 through gaseous losses of I_{N_2O} , I_{NO} , E_{N_2} , E_{N_2O} , E_{NO} and V_{NH_3} .

1920 The structural and non-structural N pools in root are written as $N_{R,S}$ and $N_{R,NS}$
 1921 respectively, and similarly for stem ($N_{S,S}$ and $N_{S,NS}$) and leaves ($N_{L,S}$ and $N_{L,NS}$), and together the
 1922 structural and non-structural pools make the total N pool in leaf ($N_L = N_{L,S} + N_{L,NS}$), root ($N_R =$
 1923 $N_{R,S} + N_{R,NS}$), and stem ($N_S = N_{S,S} + N_{S,NS}$) components. The rate change equation for
 1924 structural and non-structural N pools in root are given by

1925
$$\frac{dN_{R,NS}}{dt} = U_{NH_4} + U_{NO_3} + R_{L2R} - R_{R2L} - A_{R2L} - A_{R2S} - LF_{R,NS} - T_{R,NS2S} \quad (A3)$$

Deleted:
Deleted: 6

1926
$$\frac{dN_{R,S}}{dt} = T_{R,NS2S} - LF_{R,S} \quad (A4)$$

Deleted:
Deleted: 7

1927 Similar to the uptake of carbon by leaves and its subsequent allocation to root and stem
 1928 components, N is taken up by roots and then allocated to leaves and stem. A_{R2L} and A_{R2S}
 1929 represent the allocation of N from roots to leaves and stem, respectively. The terms R_{L2R} and
 1930 R_{R2L} represent the reallocation of N between the non-structural components of root and leaves.
 1931 R_{L2R} is the N reallocated from leaves to root representing resorption of a fraction of leaf N during

1936 leaf fall for deciduous tree PFTs. R_{R2L} indicates reallocation of N from roots to leaves (termed
 1937 reallocation in Figure 2) at the time of leaf-out for deciduous tree PFTs. At times other than leaf-
 1938 out and leaf-fall and for other PFTs these two terms are zero. $T_{R,NS2S}$ is the one way transfer of
 1939 N from the non-structural to the structural root pool, and similar to the carbon pools, once N is
 1940 converted to its structural form it cannot be converted back to its non-structural form. Finally,
 1941 the litterfall due to turnover of roots occurs from both the structural ($LF_{R,S}$) and non-structural
 1942 ($LF_{R,NS}$) N pools.

1943 The rate change equations for non-structural and structural components of leaves are
 1944 written as

1945
$$\frac{d N_{L,NS}}{dt} = A_{R2L} - R_{L2R} - R_{L2S} + R_{R2L} + R_{S2L} - LF_{L,NS} - T_{L,NS2S} \quad (A5)$$

Deleted: 8

1946
$$\frac{d N_{L,S}}{dt} = T_{L,NS2S} - LF_{L,S} \quad (A6)$$

Deleted: 9

1947 where $T_{L,NS2S}$ is the one way transfer of N from the non-structural leaf component to its
 1948 structural N pool and R_{S2L} indicates reallocation of N from stem to leaves (similar to R_{R2L}) at the
 1949 time of leaf out for deciduous tree PFTs. Litterfall occurs from both the structural ($LF_{L,S}$) and non-
 1950 structural ($LF_{L,NS}$) N pools of leaves, and all other terms have been previously defined.

1951 Finally, the rate change equations for non-structural and structural components of stem
 1952 are written as

1953
$$\frac{d N_{S,NS}}{dt} = A_{R2S} + R_{L2S} - R_{S2L} - LF_{S,NS} - T_{S,NS2S} \quad (A7)$$

Deleted: 10

1954
$$\frac{d N_{S,S}}{dt} = T_{S,NS2S} - LF_{S,S} \quad (A8)$$

Deleted: 11

1959 where $LF_{S,NS}$ and $LF_{S,S}$ represent stem litter from the non-structural and structural components,
 1960 $T_{S,NS2S}$ is the one way transfer of N from the non-structural stem component to its structural N
 1961 pool. All other terms have been previously defined.

1962 Adding equations (6) through (11) yields rate of change of N in the entire vegetation pool
 1963 (N_V) as

$$\frac{dN_V}{dt} = \frac{dN_{R,NS}}{dt} + \frac{dN_{R,S}}{dt} + \frac{dN_{L,NS}}{dt} + \frac{dN_{L,S}}{dt} + \frac{dN_{S,NS}}{dt} + \frac{dN_{S,S}}{dt} = \frac{dN_R}{dt} + \frac{dN_L}{dt} + \frac{dN_S}{dt}$$

$$\frac{dN_V}{dt} = U_{NH_4} + U_{NO_3} - LF_{R,NS} - LF_{R,S} - LF_{L,NS} - LF_{L,S} - LF_{S,NS} - LF_{S,S} \quad \text{(A9)}$$

$$= U_{NH_4} + U_{NO_3} - LF_R \quad \quad \quad - LF_L \quad \quad \quad - LF_S$$

Deleted: 12

1965 which indicates how the dynamically varying vegetation N pool is governed by mineral N uptake
 1966 from the NH_4^+ and NO_3^- pools and litterfall from the structural and non-structural components of
 1967 the leaves, stem, and root pools. LF_R is the total N litter generation from the root pool and sum
 1968 of litter generation from its structural and non-structural components ($LF_R = LF_{R,S} + LF_{R,NS}$),
 1969 and similarly for the leaves (LF_L) and the stem (LF_S) pools.

1970 The rate change equations for the organic N pools in the litter (N_D) and soil (N_H) pools
 1971 are written as follows.

$$\frac{dN_D}{dt} = LF_R + LF_L + LF_S - H_{N,D2H} - M_{D,NH_4} \quad \text{(A10)}$$

Deleted: 13

$$\frac{dN_H}{dt} = H_{N,D2H} + O_{NH_4} + O_{NO_3} - M_{H,NH_4} \quad \text{(A11)}$$

Deleted: 4

1974 where $H_{N,D2H}$ is the transfer of humidified organic matter from litter to the soil organic matter
 1975 pool, and all other terms have been previously defined.

1976

1980

1981 **Acknowledgments**

1982 We are grateful and thank Joe Melton and Paul Bartlett for their comments on an earlier version
1983 of this manuscript.

1984

1985 **Code/Data availability**

1986 Model code for the operational CLASSIC model can be obtained from
1987 <https://gitlab.com/ccma/classic>. Changes made to the operational version to include N cycle
1988 and the results shown here can be obtained from the second author.

1989

1990 **Author contributions**

1991 A.A. implemented the N cycle in the CLASSIC code, put together all the N cycle related input
1992 data, and performed all the simulations. V.A. and A.A. wrote the manuscript.

1993

1994 **Competing interests**

1995 There are no competing interests.

1996

Deleted: A1. N inputs ¶

A1.1 Biological N fixation ¶

Biological N fixation (BNF, B_{NH_4}) is caused by both free living bacteria in the soil and by bacteria symbiotically living within nodules of host plants' roots. Here, the bacteria convert free nitrogen from the atmosphere to ammonium, which is used by the host plants. Like any other microbial activity, BNF is limited both by drier soil moisture conditions and cold temperatures. Cleveland et al. (1999) attempt to capture this by parameterizing BNF as a function of actual evapotranspiration (AET). AET is a function primarily of soil moisture (through precipitation and soil water balance) and available energy. In places where vegetation exists, AET is also affected by vegetation characteristics including LAI and rooting depth. Here, we parameterize BNF (B_{NH_4} , $gN\ m^{-2}\ day^{-1}$) as a function of modelled soil moisture and temperature to depth of 0.5 m following Xu-Ri and Prentice (2008) which yields a very similar geographical distribution of BNF as the Cleveland et al. (1999) approach as seen in Figure 4c. ¶

$$B_{NH_4} = (\sum_c \alpha_c f_c + \sum_n \alpha_n f_n) f(T_{0.5}) f(\theta_{0.5})$$

$$f(T_{0.5}) = 2^{(T_{0.5}-25)/10}$$

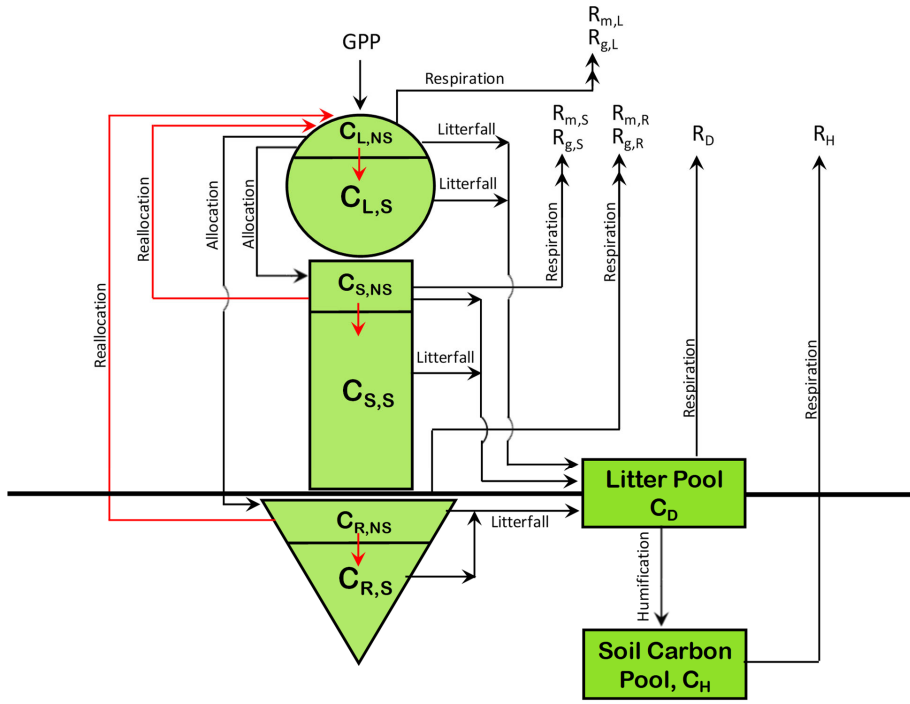
$$f(\theta_{0.5}) = \min\left(0, \max\left(1, \frac{\theta_{0.5}-\theta_w}{\theta_{fc}-\theta_w}\right)\right)$$

(A1) ¶

where α_c and α_n ($gN\ m^{-2}\ day^{-1}$) are BNF coefficients for crop (c) and non-crop or natural (n) PFTs, which are area weighted using the fractional coverages f_c and f_n of crop and non-crop PFTs that are present in a grid cell, $f(T)$ is the dependence on soil temperature based on a Q_{10} formulation and $f(\theta)$ is the dependence on soil moisture which varies between 0 and 1. θ_{fc} and θ_w are the soil moisture at field capacity and wilting points, respectively. $T_{0.5}$ ($^{\circ}C$) and $\theta_{0.5}$ ($m^3\ m^{-3}$) in equation (A1) are averaged over the 0.5 m soil depth over which BNF is assumed to occur. We do not make the distinction between symbiotic and non-symbiotic BNF since this requires explicit knowledge of geographical distribution of N fixing PFTs which are not represented separately in our base set of nine PFTs. A higher value of α_c is used compared to α_n to account for the use of N fixing plants over agriculture areas. Biological nitrogen fixation has been an essential component of many farming systems for considerable periods, with evidence for the agricultural use of legumes dating back more than 4,000 years (O'Hara, 1998). A higher α_c than α_n is also consistent with Fowler et al. (2013) who report BNF of 58 and 60 $Tg\ N\ yr^{-1}$ for natural and agricultural ecosystems for present day. Since the area of natural ecosystems is about five times the current cropland area it implies BNF rate per unit land area is higher for crop ecosystems than for natural ecosystems. Values of α_c than α_n and other model parameters are summarized in Table A1. ¶

Similar to Cleveland et al. (1999), our approach does not lead to a significant change in BNF with increasing atmospheric CO_2 , other than through changes in soil moisture and temperature. At least two meta-analyses, however, suggest that an increase in atmospheric CO_2 does lead to an increase in BNF through increased symbiotic activity associated with an increase in both nodule mass and number (McGuire et al., 1995; Liang et al., 2016). Models have attempted to capture this by simulating BNF as a function of NPP (Thornton et al., 2007; Wania et al., 20... [3]

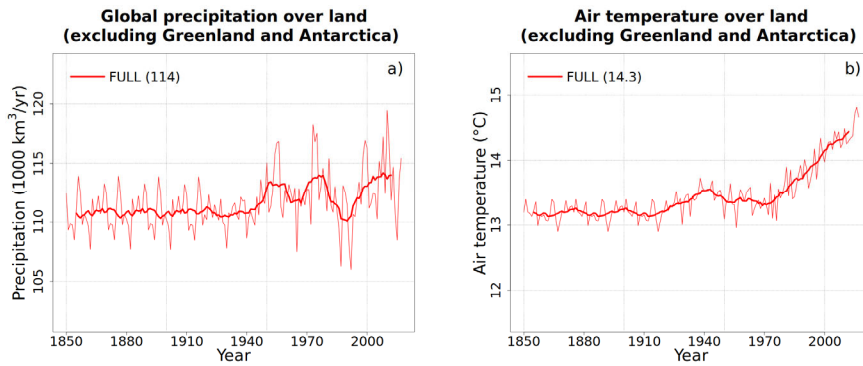
2119
2120



2121
2122
2123
2124
2125
2126
2127
2128

Figure A1: The structure of CLASSIC model used in this study, upon which the N cycle is implemented, with its carbon pools and fluxes. The fluxes of non-structural carbon are shown in red colour.

2129
2130
2131



2132
2133

2134 Figure A2: Annual values of global precipitation (a) and air temperature (b) over land in the
2135 CRU-JRA reanalysis data that are used to drive the model. The data are available for the period
2136 1901-2017. In the absence of meteorological data, the period 1851-1900 uses the data from the
2137 period 1901-1925 twice. The thin lines are the annual values and the thick line their 10 year
2138 running mean.

2139

Deleted: 1

2141 **Table A1:** Model parameters for various model parameterizations. Corresponding equation in which the
 2142 parameter appears in the main text is also noted. Model parameters may be scalar or an array (if they
 2143 are PFT dependent) in which case they are written according to the following structure in the table
 2144 below.

Needleleaf evergreen	Needleleaf deciduous	
Broadleaf evergreen	Broadleaf deciduous cold	Broadleaf deciduous drought
C ₃ crop	C ₄ crop	
C ₃ grass	C ₄ grass	

2145

Model parameter	Eqn	Description	Units	Value(s)
<i>Biological N fixation</i>				
α_c	3	BNF rate for crop PFTs	gN m ⁻² day ⁻¹	0.00217
α_n	3	BNF rate for natural PFTs	gN m ⁻² day ⁻¹	0.00037
<i>Plant N demand</i>				
$C: N_{L,min}$	4	Minimum C:N ratio for leaves	dimensionless	25 22 20 18 16 20 13 18
$C: N_{S,min}$	4	Minimum C:N ratio for stem	dimensionless	450 450 430 430 285 285 - -
$C: N_{R,min}$	4	Minimum C:N ratio for root	dimensionless	45 45 35 35 30 35 30 35
<i>Plant uptake</i>				
β	6	Mineral N distribution coefficient	dimensionless	0.5
ε	8	Fine root efficiency	gN gC ⁻¹ day ⁻¹	4.92E-5
$k_{p,1/2}$	8	Half saturation constant	gN m ⁻³	3
<i>Litterfall</i>				
r_L	11	Leaf resorption coefficient	dimensionless	0.54
<i>Nitrification</i>				
η	19	Nitrification coefficient	day ⁻¹	7.33E-4

Deleted: A

Deleted: are follow

Deleted: .

Deleted: ¶

Deleted: Corresponding equation in which the parameter appears in the main text is also noted.¶

Deleted: A1

Deleted: A1

Deleted: A2

Deleted: A2

Deleted: A2

Deleted: A4

Deleted: A6

Deleted: A6

Deleted: A9

Deleted: A1

Deleted: 7

η_{NO}	<u>23</u>	Fraction of nitrification flux emitted as NO	dimensionless	7.03E-5
η_{N2O}	<u>23</u>	Fraction of nitrification flux emitted as N ₂ O	dimensionless	2.57E-5
<i>Denitrification</i>				
μ_{NO}	<u>24</u>	Fraction of denitrification flux emitted as NO	day ⁻¹	3.872E-4
μ_{N2O}	<u>24</u>	Fraction of denitrification flux emitted as N ₂ O	day ⁻¹	1.408E-4
μ_{N2}	<u>24</u>	Fraction of denitrification flux emitted as N ₂	day ⁻¹	3.872E-3
w_d	<u>24</u>	Soil wetness threshold below which very little denitrification occurs	dimensionless	0.3
<i>Leaching</i>				
φ	<u>26</u>	Leaching coefficient	m ² Kg ⁻¹	1.15E-3
<i>NH₃ volatilization</i>				
ϑ	<u>27</u>	NH ₃ volatilization coefficient	dimensionless	<u>0.54</u>
<i>Coupling of C and N cycles</i>				
Γ_1	<u>31</u>	Parameter for calculating V_{cmax} from leaf N content	$\mu\text{mol CO}_2 \text{ gN}^{-1} \text{ s}^{-1}$	13 (all PFTs except broadleaf evergreen tree) 5.1 (for broadleaf evergreen tree)
Γ_2	<u>31</u>	Parameter for calculating V_{cmax} from leaf N content	$\mu\text{mol CO}_2 \text{ m}^{-2} \text{ s}^{-1}$	8.5
k_A	<u>32</u>	Parameter for constraining V_{cmax} increase when C:N ratios exceed their maximum limit	dimensionless	<u>0.05</u>
$C:N_{L,max}$	<u>33</u>	Maximum C:N ratio for leaves	dimensionless	<u>60</u> <u>50</u> <u>55</u> <u>40</u> <u>40</u> <u>40</u> <u>50</u> <u>35</u> <u>50</u>
$C:N_{S,max}$	<u>33</u>	Maximum C:N ratio for stem	dimensionless	<u>800</u> <u>800</u> <u>670</u> <u>670</u> <u>670</u> <u>500</u> <u>500</u>

Deleted: A

Deleted: 1

Deleted: A

Deleted: 1

Deleted: A22

Deleted: A22

Deleted: A22

Deleted: A23

Deleted: A24

Deleted: A25

Deleted: 1.8

Deleted: 15

Deleted: 15

2178

				=	=	
$C: N_{R,max}$	<u>33</u>	<u>Maximum C:N ratio for root</u>	<u>dimensionless</u>	<u>90</u> <u>70</u> <u>60</u> <u>60</u>	<u>90</u> <u>70</u> <u>70</u> <u>70</u>	<u>70</u>

Deleted: ¶

2180

2181 **Table 1:** Historical simulations performed over the period 1851-2017 to evaluate the model’s
 2182 response to various forcings. All forcings are time varying. All forcings are also spatially explicit
 2183 except atmospheric CO₂ for which a globally constant value is specified.

2184

Simulation name	Forcing that varies over the historical period	N cycle
<i>Primary simulations performed to evaluate N cycle response to various forcings</i>		
1. CO2-only	Atmospheric CO ₂ concentration	Runs with N cycle
2. CLIM-only	1901-1925 meteorological data are used twice over the 1850-1900 period. For the 1901-2017 period, meteorological data for the correct year is used.	
3. LUC+FERT-only	Land cover with increasing crop area, and fertilizer application rates over the crop area	
4. N-DEP-only	N deposition of ammonia and nitrate	
5. FULL	All forcings	
6. FULL-no-LUC	All forcings except increasing crop area	
<i>Other simulations</i>		
7. ORIGINAL	All forcings	Runs without N cycle using the original model configuration.
8. ORIG-UNCONST	All forcings but with downregulation turned off	
9. FULL-no-implicit-P-limitation	All forcings but using same Γ_1 and Γ_2 globally	Run with N cycle

2185

2186

2187

2188 **Table 2:** Comparison of simulated global N pools and fluxes, from the FULL simulation, with other
 2189 modelling and quasi observation-based studies (references for which are noted as superscripts
 2190 and listed below the table). The time-periods to which the other modelling and quasi
 2191 observation-based estimates correspond are also noted, where available. The estimates are for
 2192 land. Simulated fluxes and pool corresponds to the period 1997-2018.

2193

N pool and fluxes	This study (1998-2017)	Other model and quasi observation-based estimates
<i>N inputs (Tg N yr⁻¹)</i>		
BNF	119	118 ^a 99 ^b (2001-2010) 138.5 ^c (early 1990s) 128.9 ^d (2000-2009) 104-118 ^e 92 ^f (year 2000)
Natural BNF	59	58 ^a 107 ^c (early 1990s) 30-130 ^e 39 ^f (year 2000)
Anthropogenic BNF	60	60 ^a 31.5 ^c (early 1990s) 14-89 ^e 53 ^f (year 2000)
Fertilizer input	91 (based on TRENDY protocol)	100 ^a 100 ^b (2001-2010) 100 ^c (early 1990s) 83 ^f (year 2000)
N deposition	66 (based on TRENDY protocol)	70 ^a 56-62 ^b 63.5 ^c (early 1990s) 69 ^f (year 2000)
<i>N pools (Tg N yr⁻¹)</i>		
Vegetation	3034	1,780 ^d (2000s) 3,800 ^e (1990s) 5,300 ^h 2,940 ⁱ (1990s)
Litter and soil	77161	106,000 ^d (2000s) 100,000 ^e (1990s) 56,800 ^h 113,000 ⁱ (1990s)
Ammonia	1924	163.7 ^d (2000s) 361 ^h 1200 ⁱ (1990s)
Nitrate	2974	2,778 ^d (2000s) 580 ^h 14,800 ⁱ (1990s)
<i>N fluxes related to N cycling (Tg N yr⁻¹)</i>		
Plant uptake	940	618 ^d (2000s) 1,127 ^e (1990s) 1,084 ^h 873 ⁱ (1990s)
Net mineralization	947	
Mineralization	2045	1,678 ^d (2000s)
Immobilization	1097	1,177 ^d (2000s)
Nitrification	239	

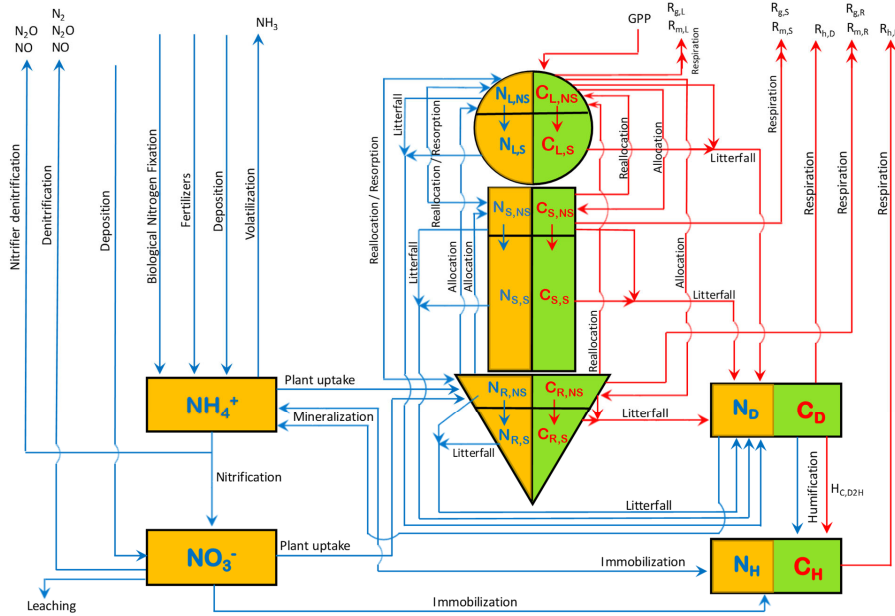
<i>N</i> losses (Tg N yr ⁻¹)			
NO ₃ - Leaching	53.5		97.1 ^b (2001-2010) 62.8 ^d (2000s) 77.0 ^e (1990s)
NH ₃ Volatilization	53.9		124.9 ^b (2001-2010) 52.6 ^c (early 1990s) 20.4 ^d (2000s)
N ₂ from denitrification	114.2		105.8 ^b (2001-2010) 68 ^f (year 2000)
N ₂ O from denitrification	4.2	12.6	8.7 ^b (2001-2010)
N ₂ O from nitrification	8.4		10.9 ^c (early 1990s) 13.0 ^a
NO from denitrification	11.4	34.3	24.8 ^c (early 1990s)
NO from nitrification	22.9		26.8 ^e (1990s)

2194

2195 ^aFowler et al. (2013), ^bZaehle (2013), ^cGalloway et al. (2004), ^dvon Bloh et al. (2018), ^eGalloway et al.

2196 (2013), ^fBouwman et al. (2013), ^gZaehle et al. (2010), ^hXu-Ri and Prentice (2008), ⁱWania et al. (2012)

2197



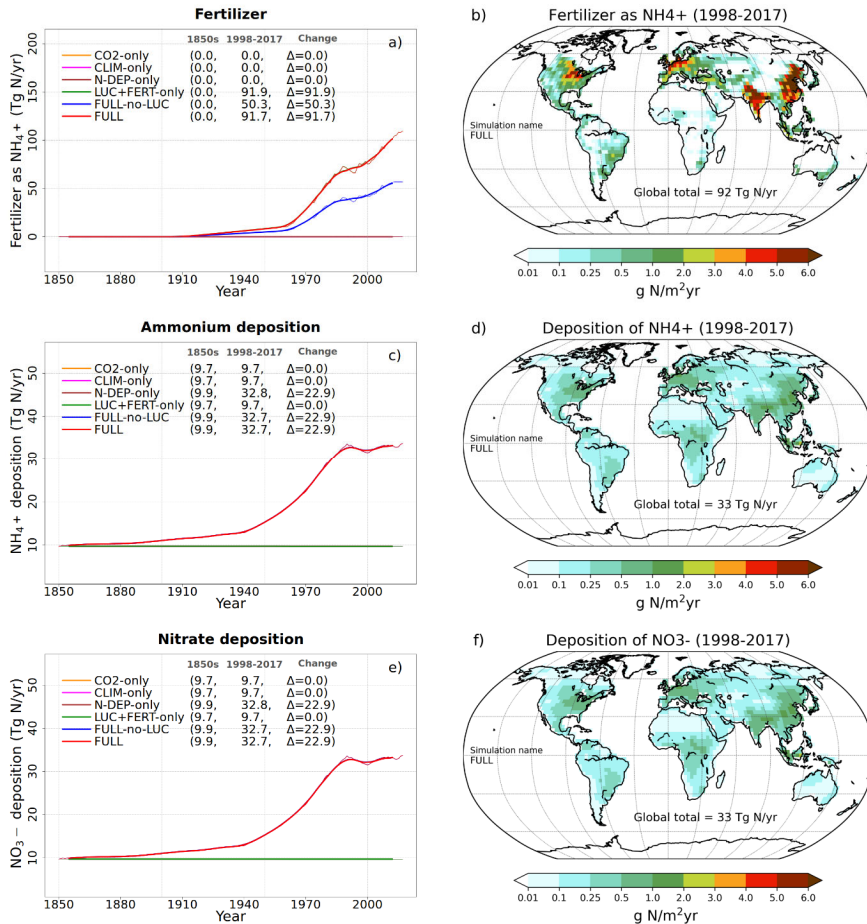
Deleted: 1

Figure 1: The structure of CLASSIC model used in this study, upon which the N cycle is implemented, with its carbon pools and fluxes. The fluxes of non-structural carbon are shown in red colour.

Page Break

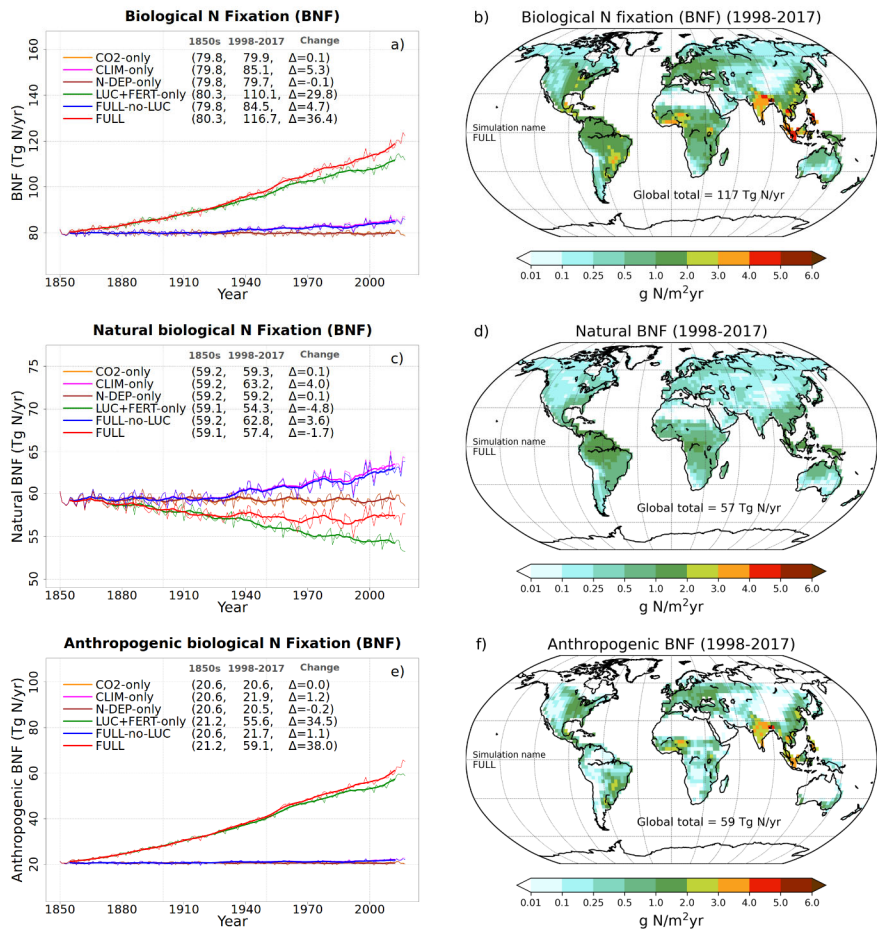
2201 Figure 1: The structure of CLASSIC model used in this study. The eight prognostic carbon pools
 2202 are shown in green colour and carbon fluxes in red colour. The ten prognostic nitrogen pools are
 2203 shown in orange colour and nitrogen fluxes are shown in blue colour.

Deleted: 2



2217 Figure 2: Time series and geographical distribution of global annual values of externally specified
 2218 N inputs. Fertilizer input (a, b), atmospheric deposition of ammonium (c, d) and atmospheric
 2219 deposition of nitrate (e, f). The values in the parenthesis for legend entries in the time series plots
 2220 show averages for the 1850s, the 1998-2017 period, and the change between these two periods.
 2221 The thin lines in the time series plots show the annual values and the thick lines their 10-year
 2222 moving average. The geographical plots show the average values over the last 20-years of the
 2223 FULL simulation corresponding to the 1998-2017 period. Note that in the time series plots lines
 2224 from some simulations are hidden behind lines from other simulations and this can be inferred
 2225 from the legend entries which shows averages for the 1850s, the 1998-2017 period.

- Deleted: 3
- Deleted: Global annual values
- Deleted: Biological N fixation
- Deleted: and its break down into natural (c) and anthropogenic components (e). Fertilizer input (b) and
- Deleted: 1850s and 1998-2017



2232

2233 **Figure 3: Time series and geographical distribution of annual values biological N fixation (BNF)**
 2234 **(a,b) and its natural (c, d) and anthropogenic (e, f) components. The values in the parenthesis for**
 2235 **legend entries in the time series plots show averages for the 1850s, the 1998-2017 period, and**
 2236 **the change between these two periods. The thin lines in the time series plots show the annual**
 2237 **values and the thick lines their 10-year moving average. The geographical plots show the average**
 2238 **values over the last 20-years of the FULL simulation corresponding to the 1998-2017 period. Note**
 2239 **that in the time series plots lines from some simulations are hidden behind lines from other**
 2240 **simulations and this can be inferred from the legend entries which shows averages for the 1850s,**
 2241 **the 1998-2017 period.**

Deleted: <object>

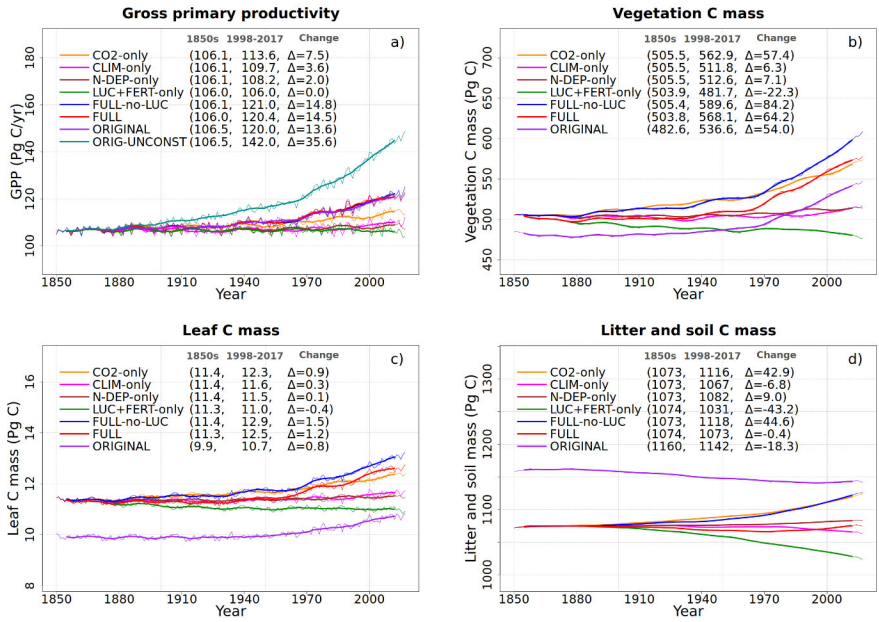
Deleted: 4

Deleted: G

Deleted: of N inputs

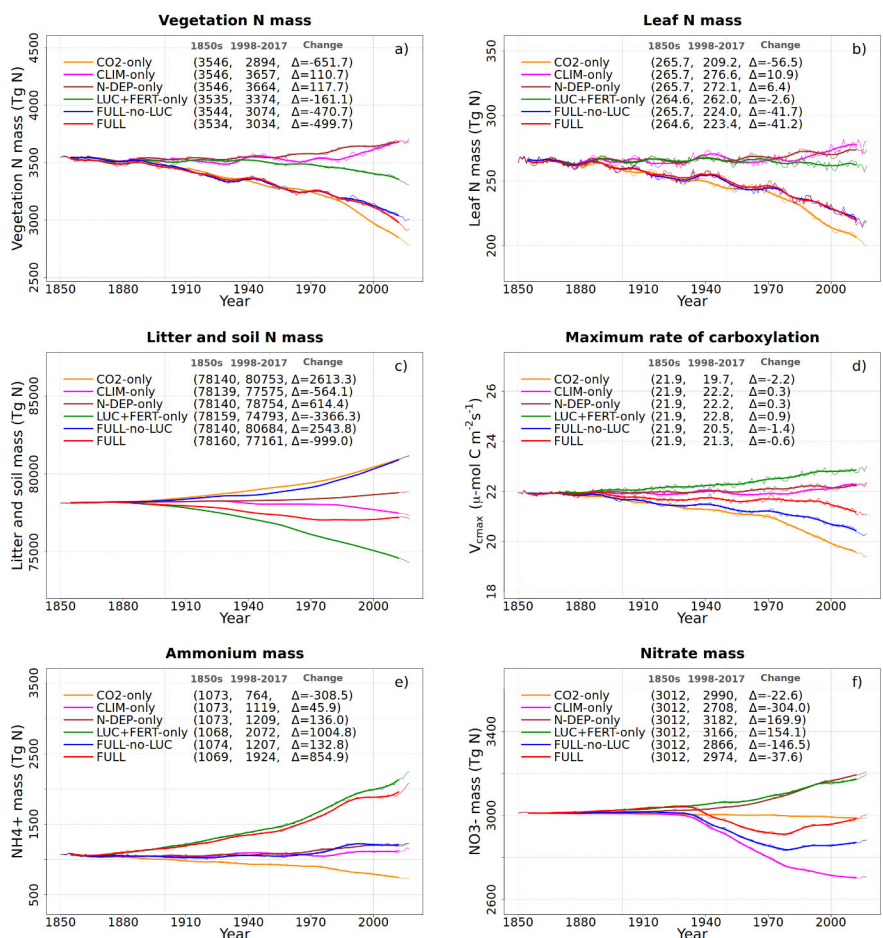
Deleted: Biological N fixation (a) and its break down into natural (c) and anthropogenic components (e). Fertilizer input (b) and atmospheric deposition of ammonium (d) and nitrate (f). The global total values shown are averaged over the 1998-2017 period. The thin lines show the annual values and the thick lines their 10-year moving average.

Deleted: ¶



2254 Figure 4: Global annual values of gross primary productivity (a), vegetation carbon (b), leaf
 2255 carbon (c), and litter and soil carbon (d) for the primary simulations performed. The values in
 2256 the parenthesis for legend entries show averages for the 1850s, the 1998-2017 period, and the
 2257 change between 1850s and 1998-2017 periods. The thin lines show the annual values and the
 2258 thick lines their 10-year moving average.

Deleted: 5

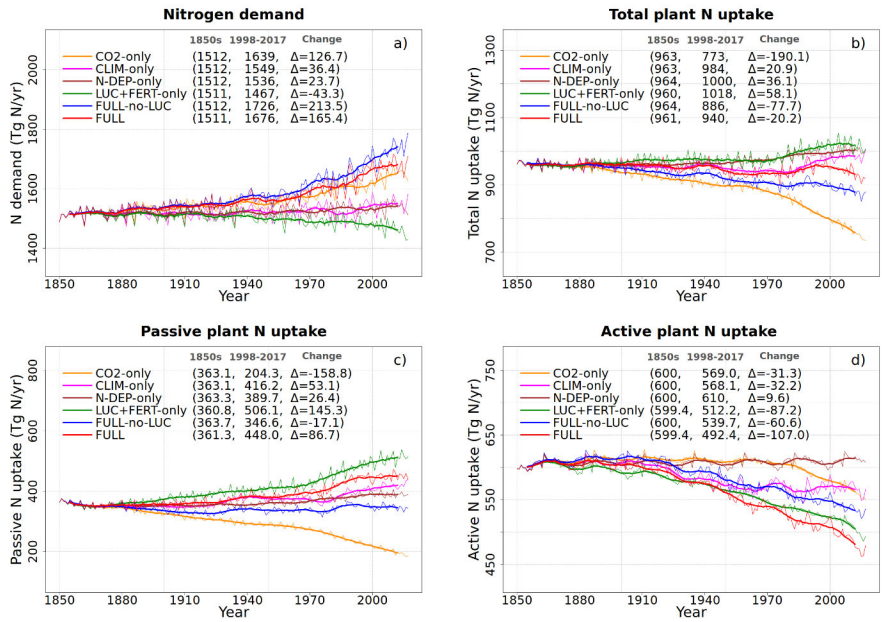


2262

2263 Figure 5: Global annual values of N in vegetation (a), leaves (b), litter and soil organic matter (c)
 2264 pools, V_{cmax} (d), and ammonium (e), and nitrate (f) pools for the primary simulations performed.
 2265 The values in the parenthesis for legend entries show averages for the 1850s, the 1998-2017
 2266 period, and the change between 1850s and 1998-2017 periods. The thin lines show the annual
 2267 values and the thick lines their 10-year moving average.

2268

Deleted: 6



2270

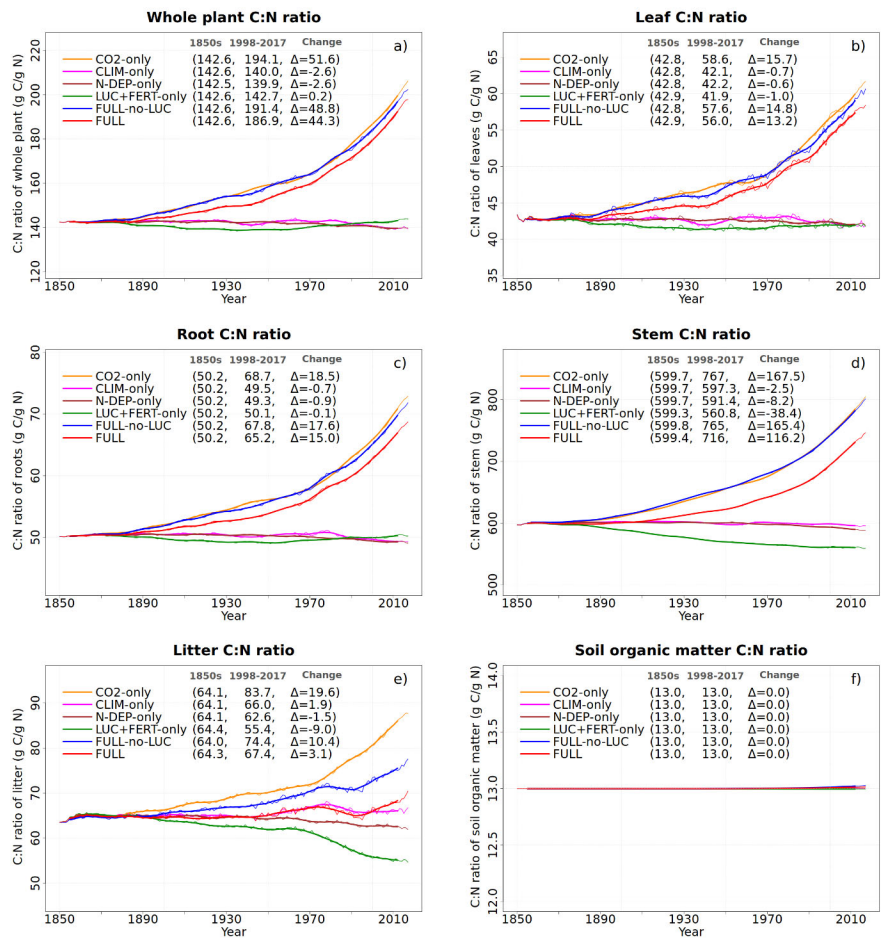
2271

2272 Figure 6: Global annual values of N demand (a), total plant N uptake (b) and its split into passive
 2273 (c) and active (d) components for the primary simulations performed. The values in the
 2274 parenthesis for legend entries show averages for the 1850s, the 1998-2017 period, and the
 2275 change between 1850s and 1998-2017 periods. The thin lines show the annual values and the
 2276 thick lines their 10-year moving average.

2277

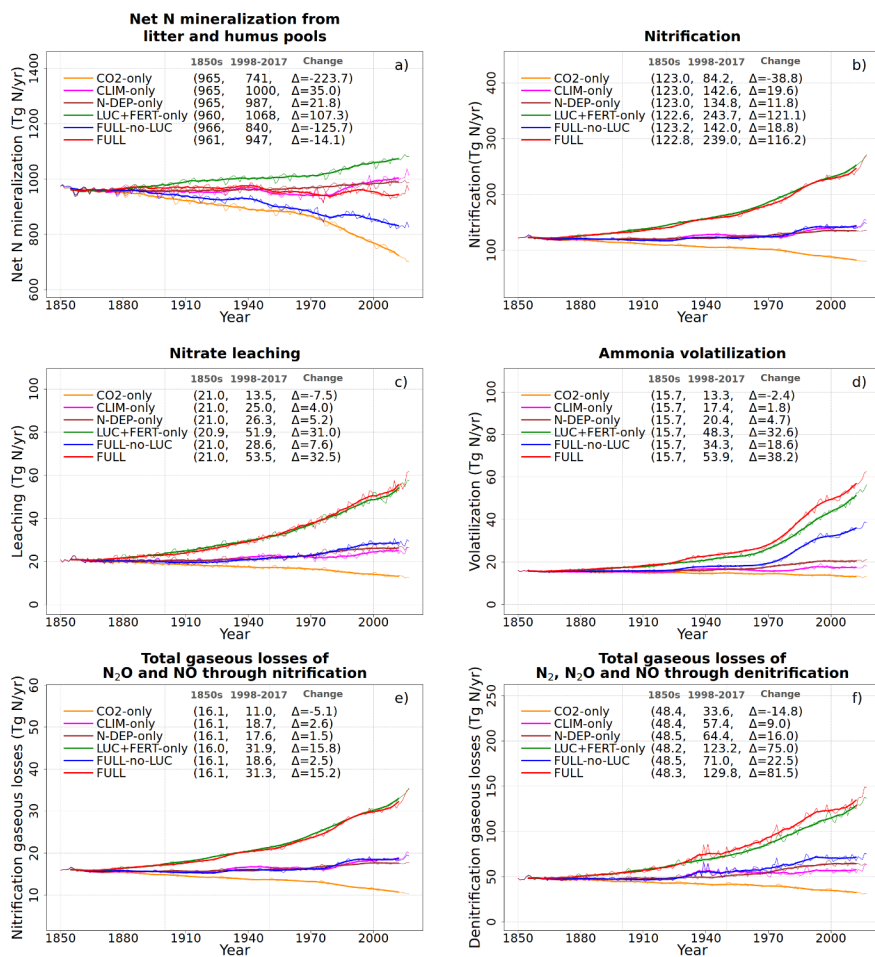
2278

Deleted: 7



2282 Figure 7: Global annual values of C:N ratios for whole plant (a), leaves (b), root (c), stem (d),
 2283 litter (e) and soil organic matter (f) pools from the primary six simulations. The values in the
 2284 parenthesis for legend entries show averages for the 1850s, the 1998-2017 period, and the
 2285 change between 1850s and 1998-2017 periods. The thin lines show the annual values and the
 2286 thick lines their 10-year moving average.

Deleted: 8

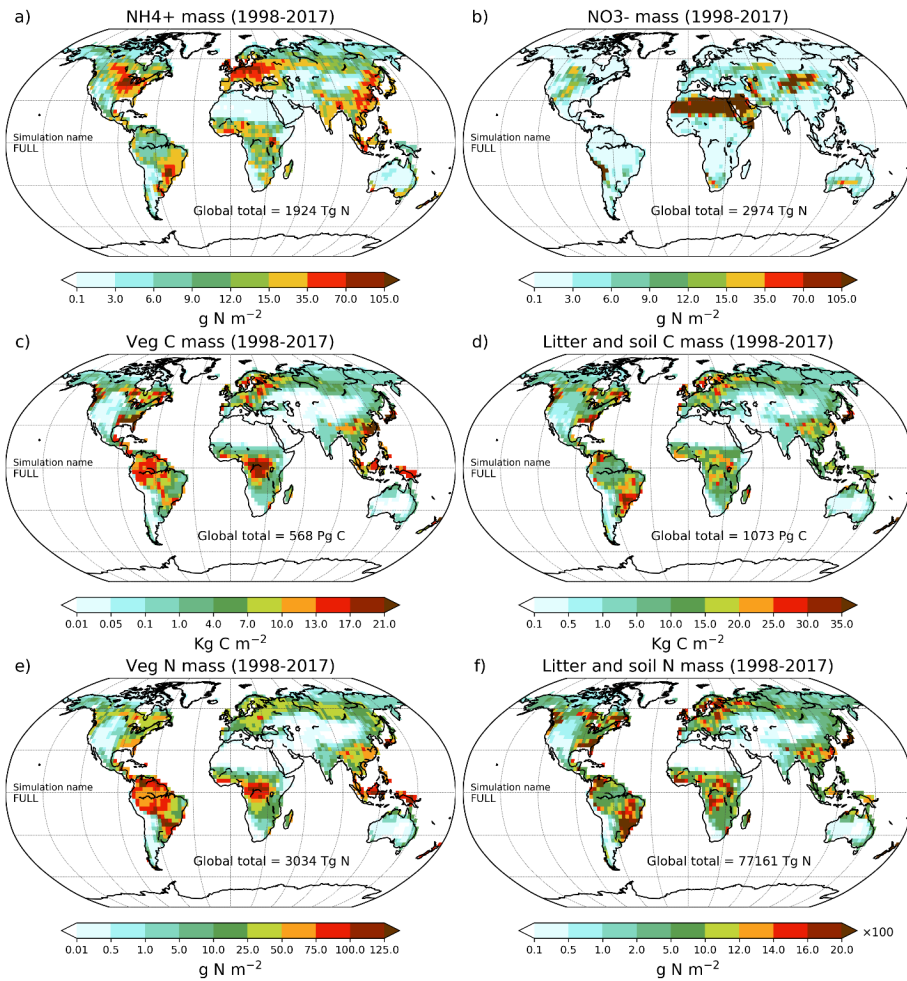


2290

2291 Figure 8: Global annual values of net mineralization (a), nitrification (b), NO₃- leaching (c), NH₃
 2292 volatilization (d), and gaseous losses associated with nitrification (e) and denitrification (f) from
 2293 the primary six simulations. The values in the parenthesis for legend entries show averages for
 2294 the 1850s, the 1998-2017 period, and the change between 1850s and 1998-2017 periods. The
 2295 thin lines show the annual values and the thick lines their 10-year moving average.

2296

Deleted: 9



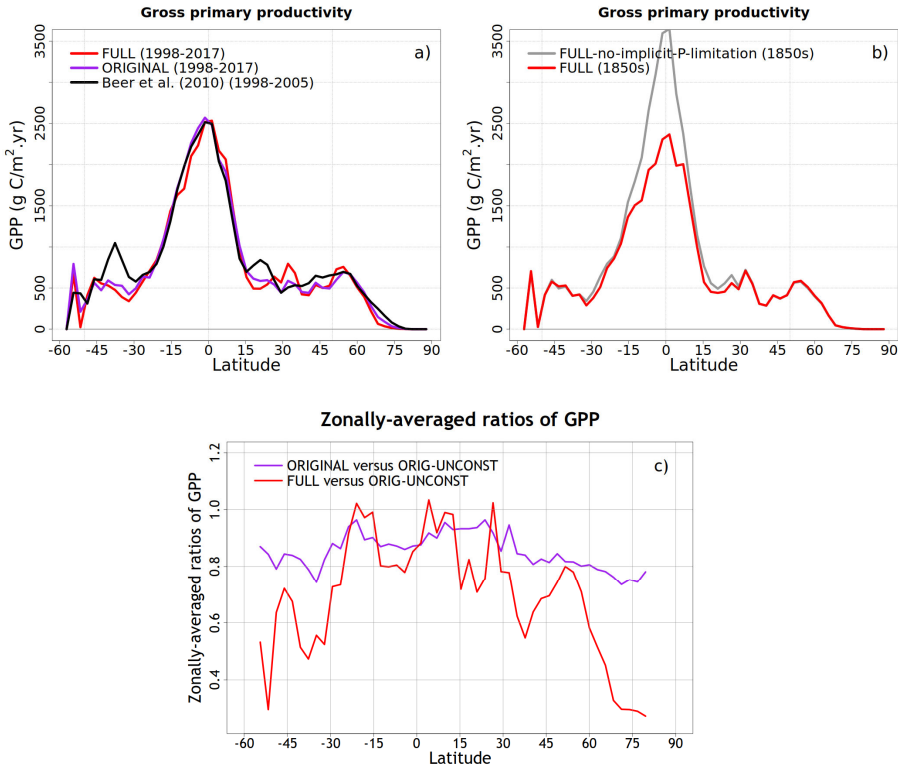
2298

2299 **Figure 9:** Geographical distribution of primary C and N pools. Ammonium (a), nitrate (b),
 2300 vegetation C mass (c), litter and soil C mass (d), vegetation N mass (e), and litter and soil N mass
 2301 (f). The global total values shown are averaged over the 1998-2017 period.

Deleted: 10

2302

2304

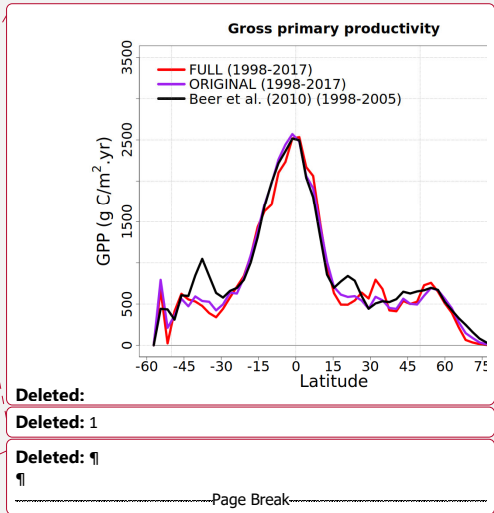


Deleted: ¶
¶

2305

2306 **Figure 10:** Comparison of zonal distribution of gross primary productivity (GPP) and the effect of
 2307 GPP downregulation compared to the ORIG-UNCONST simulation. Panel (a) compares zonal
 2308 distribution of GPP from FULL and ORIGINAL simulations with observation-based estimate from
 2309 Beer et al. (2010) for the present day. Panel (b) compares the zonal distribution of GPP from the
 2310 pre-industrial simulation, corresponding to 1850 conditions, from the FULL and FULL-no-
 2311 implicit-P-limitation simulations to illustrate the effect of not reducing the Γ_1 parameter for
 2312 calculating V_{cmax} for the broadleaf evergreen tree PFT that implicitly accounts for phosphorus
 2313 limitation. Panel (c) shows the zonally-averaged ratios of GPP from the ORIGINAL and FULL
 2314 simulations versus those from the ORIG-UNCONST simulations to illustrate how downregulation
 2315 acts in the ORIGINAL and FULL simulations.

2316



Deleted:

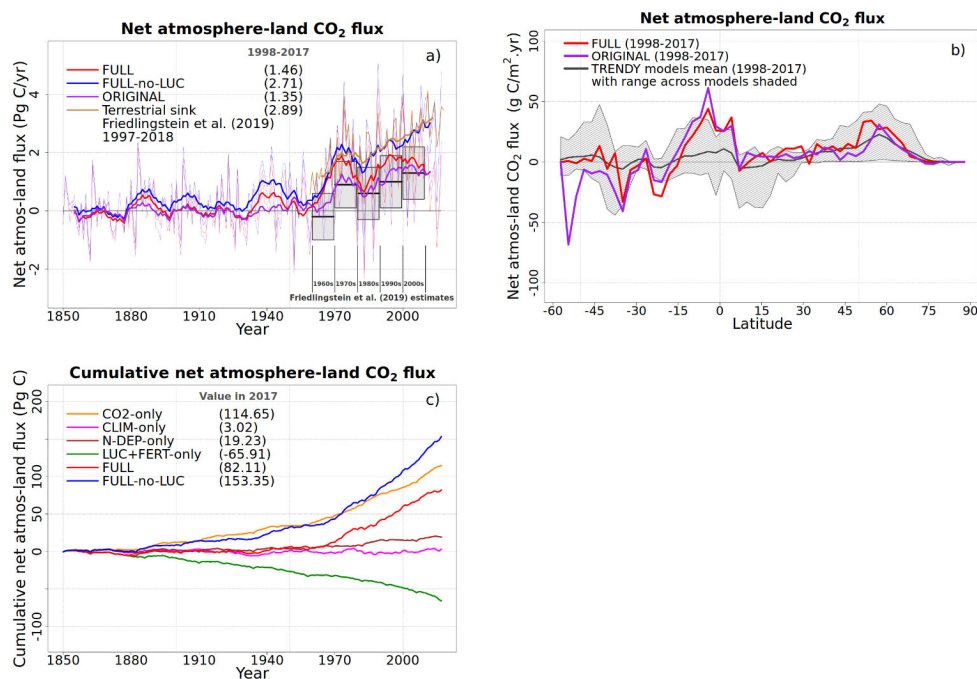
Deleted: 1

Deleted: ¶

¶

Page Break

2324



2325

2326 Figure 11: Comparison of simulated net atmosphere-land CO₂ flux from various simulations.
2327 Panel (a) compares globally-summed values of net atmosphere-land CO₂ flux from FULL, FULL-
2328 no-LUC simulation, and ORIGINAL simulations with estimate of terrestrial sink (dark yellow line)
2329 and net atmosphere-land CO₂ flux (grey bars) from Friedlingstein et al. (2019). The thin lines
2330 show the annual values and the thick lines their 10-year moving average. Panel (b) compares
2331 zonal distribution of net atmosphere-land CO₂ flux from FULL and ORIGINAL simulations with
2332 the range from TRENDY models that contributed to the Friedlingstein et al. (2019) study. Panel
2333 (c) shows cumulative values of net atmosphere-land CO₂ flux from the six primary simulations
2334 to investigate the contribution of each forcing to the cumulative land carbon sink over the
2335 historical period.

2336

Deleted: 2

2338 **References**

- 2339 Alexandrov, G. and Oikawa, T.: TsuBiMo: a biosphere model of the CO₂-fertilization effect, *Clim. Res.*,
2340 19(3), 265–270, 2002.
- 2341 Aragão, L. E. O. C., Malhi, Y., Metcalfe, D. B., Silva-Espejo, J. E., Jiménez, E., Navarrete, D., Almeida, S.,
2342 Costa, A. C. L., Salinas, N., Phillips, O. L., Anderson, L. O., Alvarez, E., Baker, T. R., Goncalvez, P. H.,
2343 Huamán-Ovalle, J., Mamani-Solórzano, M., Meir, P., Monteagudo, A., Patiño, S., Peñuela, M. C., Prieto,
2344 A., Quesada, C. A., Rozas-Dávila, A., Rudas, A., Silva Jr., J. A. and Vásquez, R.: Above- and below-ground
2345 net primary productivity across ten Amazonian forests on contrasting soils, *Biogeosciences*, 6(12), 2759–
2346 2778, doi:10.5194/bg-6-2759-2009, 2009.
- 2347 Arneeth, A., Harrison, S. P., Zaehle, S., Tsigaridis, K., Menon, S., Bartlein, P. J., Feichter, J., Korhola, A.,
2348 Kulmala, M., O'Donnell, D., Schurgers, G., Sorvari, S. and Vesala, T.: Terrestrial biogeochemical feedbacks
2349 in the climate system, *Nat. Geosci.*, 3(8), 525–532, doi:10.1038/ngeo905, 2010.
- 2350 Arora, V. K.: Simulating energy and carbon fluxes over winter wheat using coupled land surface and
2351 terrestrial ecosystem models, *Agric. For. Meteorol.*, 118(1), 21–47, doi:https://doi.org/10.1016/S0168-
2352 1923(03)00073-X, 2003.
- 2353 Arora, V. K. and Boer, G. J.: A Representation of Variable Root Distribution in Dynamic Vegetation
2354 Models, *Earth Interact.*, 7(6), 1–19, doi:10.1175/1087-3562(2003)007<0001:AROVRD>2.0.CO;2, 2003.
- 2355 Arora, V. K. and Boer, G. J.: A parameterization of leaf phenology for the terrestrial ecosystem
2356 component of climate models, *Glob. Change Biol.*, 11(1), 39–59, doi:10.1111/j.1365-2486.2004.00890.x,
2357 2005.
- 2358 Arora, V. K. and Boer, G. J.: Uncertainties in the 20th century carbon budget associated with land use
2359 change, *Glob. Change Biol.*, 16(12), 3327–3348, doi:10.1111/j.1365-2486.2010.02202.x, 2010.
- 2360 Arora, V. K. and Melton, J. R.: Reduction in global area burned and wildfire emissions since 1930s
2361 enhances carbon uptake by land, *Nat. Commun.*, 9(1), 1326, doi:10.1038/s41467-018-03838-0, 2018.
- 2362 Arora, V. K., Boer, G. J., Christian, J. R., Curry, C. L., Denman, K. L., Zahariev, K., Flato, G. M., Scinocca, J.
2363 F., Merryfield, W. J. and Lee, W. G.: The Effect of Terrestrial Photosynthesis Down Regulation on the
2364 Twentieth-Century Carbon Budget Simulated with the CCCma Earth System Model, *J. Clim.*, 22(22),
2365 6066–6088, doi:10.1175/2009JCLI3037.1, 2009.
- 2366 Arora, V. K., Scinocca, J. F., Boer, G. J., Christian, J. R., Denman, K. L., Flato, G. M., Kharin, V. V., Lee, W. G.
2367 and Merryfield, W. J.: Carbon emission limits required to satisfy future representative concentration
2368 pathways of greenhouse gases, *Geophys. Res. Lett.*, 38(5), doi:10.1029/2010GL046270, 2011.
- 2369 Arora, V. K., Boer, G. J., Friedlingstein, P., Eby, M., Jones, C. D., Christian, J. R., Bonan, G., Bopp, L.,
2370 Brovkin, V., Cadule, P., Hajima, T., Ilyina, T., Lindsay, K., Tjiputra, J. F. and Wu, T.: Carbon–Concentration
2371 and Carbon–Climate Feedbacks in CMIP5 Earth System Models, *J. Clim.*, 26(15), 5289–5314,
2372 doi:10.1175/JCLI-D-12-00494.1, 2013.
- 2373 Arora, V. K., Katavouta, A., Williams, R. G., Jones, C. D., Brovkin, V., Friedlingstein, P., Schwinger, J., Bopp,
2374 L., Boucher, O., Cadule, P., Chamberlain, M. A., Christian, J. R., Delire, C., Fisher, R. A., Hajima, T., Ilyina,

2375 T., Joetzjer, E., Kawamiya, M., Koven, C. D., Krasting, J. P., Law, R. M., Lawrence, D. M., Lenton, A.,
2376 Lindsay, K., Pongratz, J., Raddatz, T., Séférian, R., Tachiiri, K., Tjiputra, J. F., Wiltshire, A., Wu, T. and
2377 Ziehn, T.: Carbon-concentration and carbon-climate feedbacks in CMIP6 models and their comparison
2378 to CMIP5 models, *Biogeosciences*, 17(16), 4173–4222, doi:10.5194/bg-17-4173-2020, 2020.

2379 Asaadi, A., Arora, V. K., Melton, J. R. and Bartlett, P.: An improved parameterization of leaf area index
2380 (LAI) seasonality in the Canadian Land Surface Scheme (CLASS) and Canadian Terrestrial Ecosystem
2381 Model (CTEM) modelling framework, *Biogeosciences*, 15(22), 6885–6907, doi:10.5194/bg-15-6885-2018,
2382 2018.

2383 Bauerle, W. L., Oren, R., Way, D. A., Qian, S. S., Stoy, P. C., Thornton, P. E., Bowden, J. D., Hoffman, F. M.
2384 and Reynolds, R. F.: Photoperiodic regulation of the seasonal pattern of photosynthetic capacity and the
2385 implications for carbon cycling, *Proc. Natl. Acad. Sci.*, 109(22), 8612–8617,
2386 doi:10.1073/pnas.1119131109, 2012.

2387 Beer, C., Reichstein, M., Tomelleri, E., Ciais, P., Jung, M., Carvalhais, N., Rödenbeck, C., Arain, M. A.,
2388 Baldocchi, D., Bonan, G. B., Bondeau, A., Cescatti, A., Lasslop, G., Lindroth, A., Lomas, M., Luysaert, S.,
2389 Margolis, H., Oleson, K. W., Rouspard, O., Veenendaal, E., Viovy, N., Williams, C., Woodward, F. I. and
2390 Papale, D.: Terrestrial Gross Carbon Dioxide Uptake: Global Distribution and Covariation with Climate,
2391 *Science*, 329(5993), 834–838, 2010.

2392 von Bloh, W., Schaphoff, S., Müller, C., Rolinski, S., Waha, K. and Zaehle, S.: Implementing the nitrogen
2393 cycle into the dynamic global vegetation, hydrology, and crop growth model LPJmL (version 5.0), *Geosci.*
2394 *Model Dev.*, 11(7), 2789–2812, doi:10.5194/gmd-11-2789-2018, 2018.

2395 Bouwman, A. F., Beusen, A. H. W., Griffioen, J., Van Groenigen, J. W., Hefting, M. M., Oenema, O., Van
2396 Puijenbroek, P. J. T. M., Seitzinger, S., Slomp, C. P. and Stehfest, E.: Global trends and uncertainties in
2397 terrestrial denitrification and N₂O emissions, *Philos. Trans. R. Soc. B Biol. Sci.*, 368(1621), 20130112,
2398 doi:10.1098/rstb.2013.0112, 2013.

2399 Cao, M., Zhang, Q. and Shugart, H. H.: Dynamic responses of African ecosystem carbon cycling to climate
2400 change, *Clim. Res.*, 17(2), 183–193, 2001.

2401 Clapp, R. B. and Hornberger, G. M.: Empirical equations for some soil hydraulic properties, *Water*
2402 *Resour. Res.*, 14(4), 601–604, doi:10.1029/WR014i004p00601, 1978.

2403 Cleveland, C. C., Townsend, A. R., Schimel, D. S., Fisher, H., Howarth, R. W., Hedin, L. O., Perakis, S. S.,
2404 Latty, E. F., Von Fischer, J. C., Elseroad, A. and Wasson, M. F.: Global patterns of terrestrial biological
2405 nitrogen (N₂) fixation in natural ecosystems, *Glob. Biogeochem. Cycles*, 13(2), 623–645,
2406 doi:10.1029/1999GB900014, 1999.

2407 Collatz, G., Ribas-Carbo, M. and Berry, J.: Coupled Photosynthesis-Stomatal Conductance Model for
2408 Leaves of C₄ Plants, *Funct. Plant Biol.*, 19(5), 519–538, 1992.

2409 Cotrufo, M. F., Ineson, P. and Scott, A.: Elevated CO₂ reduces the nitrogen concentration of plant
2410 tissues, *Glob. Change Biol.*, 4(1), 43–54, doi:10.1046/j.1365-2486.1998.00101.x, 1998.

2411 Croft, H., Chen, J. M., Luo, X., Bartlett, P., Chen, B. and Staebler, R. M.: Leaf chlorophyll content as a
2412 proxy for leaf photosynthetic capacity, *Glob. Change Biol.*, 23(9), 3513–3524, doi:10.1111/gcb.13599,
2413 2017.

2414 Du, E., Terrer, C., Pellegrini, A. F. A., Ahlström, A., van Lissa, C. J., Zhao, X., Xia, N., Wu, X. and Jackson, R.
2415 B.: Global patterns of terrestrial nitrogen and phosphorus limitation, *Nat. Geosci.*, 13(3), 221–226,
2416 doi:10.1038/s41561-019-0530-4, 2020.

2417 Evans, J. R.: Photosynthesis and nitrogen relationships in leaves of C3 plants, *Oecologia*, 78(1), 9–19,
2418 doi:10.1007/BF00377192, 1989.

2419 Eyring, V., Bony, S., Meehl, G. A., Senior, C. A., Stevens, B., Stouffer, R. J. and Taylor, K. E.: Overview of
2420 the Coupled Model Intercomparison Project Phase 6 (CMIP6) experimental design and organization,
2421 *Geosci. Model Dev.*, 9(5), 1937–1958, doi:10.5194/gmd-9-1937-2016, 2016.

2422 Faria, T., Wilkins, D., Besford, R. T., Vaz, M., Pereira, J. S. and Chaves, M. M.: Growth at elevated CO2
2423 leads to down-regulation of photosynthesis and altered response to high temperature in *Quercus suber*
2424 L. seedlings, *J. Exp. Bot.*, 47(11), 1755–1761, doi:10.1093/jxb/47.11.1755, 1996.

2425 Farquhar, G. D., von Caemmerer, S. and Berry, J. A.: A biochemical model of photosynthetic CO2
2426 assimilation in leaves of C3 species, *Planta*, 149(1), 78–90, doi:10.1007/BF00386231, 1980.

2427 Field, C. and Mooney, H.: The Photosynthesis-Nitrogen Relationship in Wild Plants, *Biol. Int.*, 13, 25–56,
2428 1986.

2429 Fisher, J. B., Sitch, S., Malhi, Y., Fisher, R. A., Huntingford, C. and Tan, S.-Y.: Carbon cost of plant nitrogen
2430 acquisition: A mechanistic, globally applicable model of plant nitrogen uptake, retranslocation, and
2431 fixation: CARBON COST OF PLANT N ACQUISITION, *Glob. Biogeochem. Cycles*, 24(1), n/a-n/a,
2432 doi:10.1029/2009GB003621, 2010.

2433 Fowler, D., Coyle, M., Skiba, U., Sutton, M. A., Cape, J. N., Reis, S., Sheppard, L. J., Jenkins, A., Grizzetti,
2434 B., Galloway, J. N., Vitousek, P., Leach, A., Bouwman, A. F., Butterbach-Bahl, K., Dentener, F., Stevenson,
2435 D., Amann, M. and Voss, M.: The global nitrogen cycle in the twenty-first century, *Philos. Trans. R. Soc. B*
2436 *Biol. Sci.*, 368(1621), 20130164, doi:10.1098/rstb.2013.0164, 2013.

2437 Friedlingstein, P., Cox, P., Betts, R., Bopp, L., von Bloh, W., Brovkin, V., Cadule, P., Doney, S., Eby, M.,
2438 Fung, I., Bala, G., John, J., Jones, C., Joos, F., Kato, T., Kawamiya, M., Knorr, W., Lindsay, K., Matthews, H.
2439 D., Raddatz, T., Rayner, P., Reick, C., Roeckner, E., Schnitzler, K.-G., Schnur, R., Strassmann, K., Weaver,
2440 A. J., Yoshikawa, C. and Zeng, N.: Climate–Carbon Cycle Feedback Analysis: Results from the C4MIP
2441 Model Intercomparison, *J. Clim.*, 19(14), 3337–3353, doi:10.1175/JCLI3800.1, 2006.

2442 Friedlingstein, P., Jones, M. W., O’Sullivan, M., Andrew, R. M., Hauck, J., Peters, G. P., Peters, W.,
2443 Pongratz, J., Sitch, S., Le Quéré, C., Bakker, D. C. E., Canadell, J. G., Ciais, P., Jackson, R. B., Anthoni, P.,
2444 Barbero, L., Bastos, A., Bastrikov, V., Becker, M., Bopp, L., Buitenhuis, E., Chandra, N., Chevallier, F.,
2445 Chini, L. P., Currie, K. I., Feely, R. A., Gehlen, M., Gilfillan, D., Gkritzalis, T., Goll, D. S., Gruber, N.,
2446 Gutekunst, S., Harris, I., Haverd, V., Houghton, R. A., Hurtt, G., Ilyina, T., Jain, A. K., Joetzjer, E., Kaplan, J.
2447 O., Kato, E., Klein Goldewijk, K., Korsbakken, J. I., Landschützer, P., Lauvset, S. K., Lefèvre, N., Lenton, A.,
2448 Lienert, S., Lombardozi, D., Marland, G., McGuire, P. C., Melton, J. R., Metzl, N., Munro, D. R., Nabel, J.
2449 E. M. S., Nakaoka, S.-I., Neill, C., Omar, A. M., Ono, T., Pregon, A., Pierrot, D., Poulter, B., Rehder, G.,

- 2450 Resplandy, L., Robertson, E., Rödenbeck, C., Séférian, R., Schwinger, J., Smith, N., Tans, P. P., Tian, H.,
 2451 Tilbrook, B., Tubiello, F. N., van der Werf, G. R., Wiltshire, A. J. and Zaehle, S.: Global Carbon Budget
 2452 2019, *Earth Syst. Sci. Data*, 11(4), 1783–1838, doi:10.5194/essd-11-1783-2019, 2019.
- 2453 Galloway, J. N., Dentener, F. J., Capone, D. G., Boyer, E. W., Howarth, R. W., Seitzinger, S. P., Asner, G. P.,
 2454 Cleveland, C. C., Green, P. A., Holland, E. A., Karl, D. M., Michaels, A. F., Porter, J. H., Townsend, A. R. and
 2455 Vöosmarty, C. J.: Nitrogen Cycles: Past, Present, and Future, *Biogeochemistry*, 70(2), 153–226,
 2456 doi:10.1007/s10533-004-0370-0, 2004.
- 2457 Galloway, J. N., Leach, A. M., Bleeker, A. and Erisman, J. W.: A chronology of human understanding of
 2458 the nitrogen cycle^{8#x2020}, *Philos. Trans. R. Soc. B Biol. Sci.*, 368(1621), 20130120,
 2459 doi:10.1098/rstb.2013.0120, 2013.
- 2460 Garnier, E., Salager, J.-L., Laurent, G. and Sonie, L.: Relationships between photosynthesis, nitrogen and
 2461 leaf structure in 14 grass species and their dependence on the basis of expression, *New Phytol.*, 143(1),
 2462 119–129, doi:10.1046/j.1469-8137.1999.00426.x, 1999.
- 2463 Gerber, S., Hedin, L. O., Oppenheimer, M., Pacala, S. W. and Shevliakova, E.: Nitrogen cycling and
 2464 feedbacks in a global dynamic land model, *Glob. Biogeochem. Cycles*, 24(1),
 2465 doi:10.1029/2008GB003336, 2010.
- 2466 Goll, D. S., Brovkin, V., Parida, B. R., Reick, C. H., Kattge, J., Reich, P. B., van Bodegom, P. M. and
 2467 Niinemets, Ü.: Nutrient limitation reduces land carbon uptake in simulations with a model of combined
 2468 carbon, nitrogen and phosphorus cycling, *Biogeosciences*, 9(9), 3547–3569, doi:10.5194/bg-9-3547-
 2469 2012, 2012.
- 2470 Goyal, S. S. and Huffaker, R. C.: Nitrogen toxicity in plants, in *Nitrogen in Crop Production*, pp. 97–118,
 2471 American Society of Agronomy, Madison, WI., 1984.
- 2472 Hungate, B. A., Dukes, J. S., Shaw, M. R., Luo, Y. and Field, C. B.: Nitrogen and Climate Change, *Science*,
 2473 302(5650), 1512–1513, doi:10.1126/science.1091390, 2003.
- 2474 Hurtt, G. C., Frolking, S., Fearon, M. G., Moore, B., Shevliakova, E., Malyshev, S., Pacala, S. W. and
 2475 Houghton, R. A.: The underpinnings of land-use history: three centuries of global gridded land-use
 2476 transitions, wood-harvest activity, and resulting secondary lands, *Glob. Change Biol.*, 12(7), 1208–1229,
 2477 doi:10.1111/j.1365-2486.2006.01150.x, 2006.
- 2478 Jiang, M., Zaehle, S., De Kauwe, M. G., Walker, A. P., Caldararu, S., Ellsworth, D. S. and Medlyn, B. E.: The
 2479 quasi-equilibrium framework revisited: analyzing long-term CO₂ enrichment responses in plant–soil
 2480 models, *Geosci. Model Dev.*, 12(5), 2069–2089, doi:10.5194/gmd-12-2069-2019, 2019.
- 2481 Jones, A. G., Scullion, J., Ostle, N., Levy, P. E. and Gwynn-Jones, D.: Completing the FACE of elevated CO₂
 2482 research, *Environ. Int.*, 73, 252–258, doi:https://doi.org/10.1016/j.envint.2014.07.021, 2014.
- 2483 Jones, C. D., Arora, V., Friedlingstein, P., Bopp, L., Brovkin, V., Dunne, J., Graven, H., Hoffman, F., Ilyina,
 2484 T., John, J. G., Jung, M., Kawamiya, M., Koven, C., Pongratz, J., Raddatz, T., Randerson, J. T. and Zaehle,
 2485 S.: C4MIP – The Coupled Climate–Carbon Cycle Model Intercomparison Project: experimental protocol
 2486 for CMIIP6, *Geosci. Model Dev.*, 9(8), 2853–2880, doi:10.5194/gmd-9-2853-2016, 2016.

- 2487 Kattge, J., Knorr, W., Raddatz, T. and Wirth, C.: Quantifying photosynthetic capacity and its relationship
2488 to leaf nitrogen content for global-scale terrestrial biosphere models, *Glob. Change Biol.*, 15(4), 976–
2489 991, doi:10.1111/j.1365-2486.2008.01744.x, 2009.
- 2490 Klein Goldewijk, K., Beusen, A., Doelman, J. and Stehfest, E.: Anthropogenic land use estimates for the
2491 Holocene – HYDE 3.2, *Earth Syst. Sci. Data*, 9(2), 927–953, doi:10.5194/essd-9-927-2017, 2017.
- 2492 Köchy, M., Hiederer, R. and Freibauer, A.: Global distribution of soil organic carbon – Part 1: Masses and
2493 frequency distributions of SOC stocks for the tropics, permafrost regions, wetlands, and the world, *SOIL*,
2494 1(1), 351–365, doi:10.5194/soil-1-351-2015, 2015.
- 2495 Kurz, W. A., Beukema, S. J. and Apps, M. J.: Estimation of root biomass and dynamics for the carbon
2496 budget model of the Canadian forest sector, *Can. J. For. Res.*, 26(11), 1973–1979, doi:10.1139/x26-223,
2497 1996.
- 2498 Le Quéré, C., Andrew, R. M., Friedlingstein, P., Sitch, S., Hauck, J., Pongratz, J., Pickers, P. A., Korsbakken,
2499 J. I., Peters, G. P., Canadell, J. G., Arneeth, A., Arora, V. K., Barbero, L., Bastos, A., Bopp, L., Chevallier, F.,
2500 Chini, L. P., Ciais, P., Doney, S. C., Gkritzalis, T., Goll, D. S., Harris, I., Haverd, V., Hoffman, F. M.,
2501 Hoppema, M., Houghton, R. A., Hurtt, G., Ilyina, T., Jain, A. K., Johannessen, T., Jones, C. D., Kato, E.,
2502 Keeling, R. F., Goldewijk, K. K., Landschützer, P., Lefèvre, N., Lienert, S., Liu, Z., Lombardozi, D., Metzl,
2503 N., Munro, D. R., Nabel, J. E. M. S., Nakaoka, S., Neill, C., Olsen, A., Ono, T., Patra, P., Peregon, A., Peters,
2504 W., Peylin, P., Pfeil, B., Pierrot, D., Poulter, B., Rehder, G., Resplandy, L., Robertson, E., Rocher, M.,
2505 Rödenbeck, C., Schuster, U., Schwinger, J., Séférian, R., Skjelvan, I., Steinhoff, T., Sutton, A., Tans, P. P.,
2506 Tian, H., Tilbrook, B., Tubiello, F. N., van der Laan-Luijkx, I. T., van der Werf, G. R., Viovy, N., Walker, A.
2507 P., Wiltshire, A. J., Wright, R., Zaehle, S. and Zheng, B.: Global Carbon Budget 2018, *Earth Syst. Sci. Data*,
2508 10(4), 2141–2194, doi:10.5194/essd-10-2141-2018, 2018.
- 2509 Leith, H.: Modeling the primary productivity of the world, in *Primary Productivity of the Biosphere* (H.
2510 Leith and R. H. Whittaker, Eds.), pp. 237–263, Springer-Verlag, Berlin and New York., 1975.
- 2511 Li, H., Crabbe, M., Xu, F., Wang, W., Niu, R., Gao, X., Zhang, P. and Chen, H.: Seasonal Variations in
2512 Carbon, Nitrogen and Phosphorus Concentrations and C:N:P Stoichiometry in the Leaves of Differently
2513 Aged *Larix principis-rupprechtii* Mayr. Plantations, *Forests*, 8(10), 373, doi:10.3390/f8100373, 2017.
- 2514 Liang, J., Qi, X., Souza, L. and Luo, Y.: Processes regulating progressive nitrogen limitation under elevated
2515 carbon dioxide: a meta-analysis, *Biogeosciences*, 13(9), 2689–2699, doi:10.5194/bg-13-2689-2016, 2016.
- 2516 Lin, B.-L., Sakoda, A., Shibasaki, R., Goto, N. and Suzuki, M.: Modelling a global biogeochemical nitrogen
2517 cycle in terrestrial ecosystems, *Ecol. Model.*, 135(1), 89–110, doi:https://doi.org/10.1016/S0304-
2518 3800(00)00372-0, 2000.
- 2519 Manzoni, S., Jackson, R. B., Trofymow, J. A. and Porporato, A.: The Global Stoichiometry of Litter
2520 Nitrogen Mineralization, *Science*, 321(5889), 684–686, doi:10.1126/science.1159792, 2008.
- 2521 McGuire, A. D., Melillo, J. M. and Joyce, L. A.: The role of nitrogen in the response of forests net primary
2522 production to elevated atmospheric carbon dioxide, *Annu. Rev. Ecol. Syst.*, 26(1), 473–503,
2523 doi:10.1146/annurev.es.26.110195.002353, 1995.

- 2524 Melton, J. R. and Arora, V. K.: Competition between plant functional types in the Canadian Terrestrial
2525 Ecosystem Model (CTEM) v. 2.0, *Geosci Model Dev*, 9(1), 323–361, doi:10.5194/gmd-9-323-2016, 2016.
- 2526 Melton, J. R., Shrestha, R. K. and Arora, V. K.: The influence of soils on heterotrophic respiration exerts a
2527 strong control on net ecosystem productivity in seasonally dry Amazonian forests, *Biogeosciences*, 12(4),
2528 1151–1168, doi:10.5194/bg-12-1151-2015, 2015.
- 2529 Melton, J. R., Arora, V. K., Wisernig-Cojoc, E., Seiler, C., Fortier, M., Chan, E. and Teckentrup, L.: CLASSIC
2530 v1.0: the open-source community successor to the Canadian Land Surface Scheme (CLASS) and the
2531 Canadian Terrestrial Ecosystem Model (CTEM) – Part 1: Model framework and site-level performance,
2532 *Geosci. Model Dev. Discuss.*, 2019, 1–40, doi:10.5194/gmd-2019-329, 2019.
- 2533 Meyerholt, J., Zaehle, S. and Smith, M. J.: Variability of projected terrestrial biosphere responses to
2534 elevated levels of atmospheric CO₂ due to uncertainty in biological nitrogen fixation, *Biogeosciences*,
2535 13(5), 1491–1518, doi:10.5194/bg-13-1491-2016, 2016.
- 2536 Ochoa-Hueso, R., Maestre, F. T., Ríos, A. [de los, Valea, S., Theobald, M. R., Vivanco, M. G., Manrique, E.
2537 and Bowker, M. A.: Nitrogen deposition alters nitrogen cycling and reduces soil carbon content in low-
2538 productivity semiarid Mediterranean ecosystems, *Environ. Pollut.*, 179, 185–193,
2539 doi:https://doi.org/10.1016/j.envpol.2013.03.060, 2013.
- 2540 O’Hara, G. W.: The Role of Nitrogen Fixation in Crop Production, *J. Crop Prod.*, 1(2), 115–138,
2541 doi:10.1300/J144v01n02_05, 1998.
- 2542 Porporato, A., D’Odorico, P., Laio, F. and Rodriguez-Iturbe, I.: Hydrologic controls on soil carbon and
2543 nitrogen cycles. I. Modeling scheme, *Adv. Water Resour.*, 26(1), 45–58,
2544 doi:https://doi.org/10.1016/S0309-1708(02)00094-5, 2003.
- 2545 Rastetter, E. B., Vitousek, P. M., Field, C., Shaver, G. R., Herbert, D. and gren, G. I.: Resource Optimization
2546 and Symbiotic Nitrogen Fixation, *Ecosystems*, 4(4), 369–388, doi:10.1007/s10021-001-0018-z, 2001.
- 2547 Reich, P. B., Hungate, B. A. and Luo, Y.: Carbon-Nitrogen Interactions in Terrestrial Ecosystems in
2548 Response to Rising Atmospheric Carbon Dioxide, *Annu. Rev. Ecol. Evol. Syst.*, 37(1), 611–636,
2549 doi:10.1146/annurev.ecolsys.37.091305.110039, 2006a.
- 2550 Reich, P. B., Hobbie, S. E., Lee, T., Ellsworth, D. S., West, J. B., Tilman, D., Knops, J. M. H., Naeem, S. and
2551 Trost, J.: Nitrogen limitation constrains sustainability of ecosystem response to CO₂, *Nature*, 440(7086),
2552 922–925, doi:10.1038/nature04486, 2006b.
- 2553 Riddick, S., Ward, D., Hess, P., Mahowald, N., Massad, R. and Holland, E.: Estimate of changes in
2554 agricultural terrestrial nitrogen pathways and ammonia emissions from 1850 to present in
2555 the\hack\newline Community Earth System Model, *Biogeosciences*, 13(11), 3397–3426, doi:10.5194/bg-
2556 13-3397-2016, 2016.
- 2557 Salvagiotti, F., Cassman, K. G., Specht, J. E., Walters, D. T., Weiss, A. and Dobermann, A.: Nitrogen
2558 uptake, fixation and response to fertilizer N in soybeans: A review, *Field Crops Res.*, 108(1), 1–13,
2559 doi:https://doi.org/10.1016/j.fcr.2008.03.001, 2008.

2560 Sanz-Sáez, Á., Erice, G., Aranjuelo, I., Nogués, S., Irigoyen, J. J. and Sánchez-Díaz, M.: Photosynthetic
2561 down-regulation under elevated CO₂ exposure can be prevented by nitrogen supply in nodulated alfalfa,
2562 *J. Plant Physiol.*, 167(18), 1558–1565, doi:<https://doi.org/10.1016/j.jplph.2010.06.015>, 2010.

2563 Still, C. J., Berry, J. A., Collatz, G. J. and DeFries, R. S.: Global distribution of C₃ and C₄ vegetation: Carbon
2564 cycle implications, *Glob. Biogeochem. Cycles*, 17(1), 6–1, doi:[10.1029/2001GB001807](https://doi.org/10.1029/2001GB001807), 2003.

2565 Swart, N. C., Cole, J. N. S., Kharin, V. V., Lazare, M., Scinocca, J. F., Gillett, N. P., Anstey, J., Arora, V.,
2566 Christian, J. R., Hanna, S., Jiao, Y., Lee, W. G., Majaess, F., Saenko, O. A., Seiler, C., Seinen, C., Shao, A.,
2567 Sigmund, M., Solheim, L., von Salzen, K., Yang, D. and Winter, B.: The Canadian Earth System Model
2568 version 5 (CanESM5.0.3), *Geosci. Model Dev.*, 12(11), 4823–4873, doi:[10.5194/gmd-12-4823-2019](https://doi.org/10.5194/gmd-12-4823-2019),
2569 2019.

2570 Thom, A. S.: Momentum, mass and heat exchange of plant communities, in *Vegetation and the*
2571 *atmosphere*, Vol. 1, Principles, edited by Monteith, J. L., Academic Press, London., 1975.

2572 Thornton, P. E., Lamarque, J.-F., Rosenbloom, N. A. and Mahowald, N. M.: Influence of carbon-nitrogen
2573 cycle coupling on land model response to CO₂ fertilization and climate variability, *Glob. Biogeochem.*
2574 *Cycles*, 21(4), doi:[10.1029/2006GB002868](https://doi.org/10.1029/2006GB002868), 2007.

2575 Tian, H., Yang, J., Lu, C., Xu, R., Canadell, J. G., Jackson, R. B., Arneth, A., Chang, J., Chen, G., Ciais, P.,
2576 Gerber, S., Ito, A., Huang, Y., Joos, F., Lienert, S., Messina, P., Olin, S., Pan, S., Peng, C., Saikawa, E.,
2577 Thompson, R. L., Vuichard, N., Winiwarter, W., Zaehle, S., Zhang, B., Zhang, K. and Zhu, Q.: The Global
2578 N₂O Model Intercomparison Project, *Bull. Am. Meteorol. Soc.*, 99(6), 1231–1251, doi:[10.1175/BAMS-D-17-0212.1](https://doi.org/10.1175/BAMS-D-17-0212.1), 2018.

2580 Tipping, E., Somerville, C. J. and Luster, J.: The C:N:P:S stoichiometry of soil organic matter,
2581 *Biogeochemistry*, 130(1), 117–131, doi:[10.1007/s10533-016-0247-z](https://doi.org/10.1007/s10533-016-0247-z), 2016.

2582 Tomasek, A., Kozarek, J. L., Hondzo, M., Lurndahl, N., Sadowsky, M. J., Wang, P. and Staley, C.:
2583 Environmental drivers of denitrification rates and denitrifying gene abundances in channels and riparian
2584 areas, *Water Resour. Res.*, 53(8), 6523–6538, doi:[10.1002/2016WR019566](https://doi.org/10.1002/2016WR019566), 2017.

2585 Versegny, D. L.: Class—A Canadian land surface scheme for GCMS. I. Soil model, *Int. J. Climatol.*, 11(2),
2586 111–133, doi:[10.1002/joc.3370110202](https://doi.org/10.1002/joc.3370110202), 1991.

2587 Versegny, D. L., McFarlane, N. A. and Lazare, M.: Class—A Canadian land surface scheme for GCMS, II.
2588 Vegetation model and coupled runs, *Int. J. Climatol.*, 13(4), 347–370, doi:[10.1002/joc.3370130402](https://doi.org/10.1002/joc.3370130402),
2589 1993.

2590 Vitousek, P. M.: Litterfall, Nutrient Cycling, and Nutrient Limitation in Tropical Forests, *Ecology*, 65(1),
2591 285–298, doi:[10.2307/1939481](https://doi.org/10.2307/1939481), 1984.

2592 Vitousek, P. M.: Beyond Global Warming: Ecology and Global Change, *Ecology*, 75(7), 1861–1876,
2593 doi:[10.2307/1941591](https://doi.org/10.2307/1941591), 1994.

2594 Vitousek, P. M. and Howarth, R. W.: Nitrogen limitation on land and in the sea: How can it occur?,
2595 *Biogeochemistry*, 13(2), 87–115, doi:[10.1007/BF00002772](https://doi.org/10.1007/BF00002772), 1991.

2596 Vitousek, P. M., Porder, S., Houlton, B. Z. and Chadwick, O. A.: Terrestrial phosphorus limitation:
 2597 mechanisms, implications, and nitrogen–phosphorus interactions, *Ecol. Appl.*, 20(1), 5–15,
 2598 doi:10.1890/08-0127.1, 2010.

2599 Vitousek, P. M., Menge, D. N. L., Reed, S. C. and Cleveland, C. C.: Biological nitrogen fixation: rates,
 2600 patterns and ecological controls in terrestrial ecosystems, *Philos. Trans. R. Soc. B Biol. Sci.*, 368(1621),
 2601 20130119, doi:10.1098/rstb.2013.0119, 2013.

2602 Wang, J., Liu, X., Zhang, X., Li, L., Lam, S. K. and Pan, G.: Changes in plant C, N and P ratios under elevated
 2603 [CO₂] and canopy warming in a rice-winter wheat rotation system, *Sci. Rep.*, 9(1), 5424,
 2604 doi:10.1038/s41598-019-41944-1, 2019.

2605 Wania, R., Meissner, K. J., Eby, M., Arora, V. K., Ross, I. and Weaver, A. J.: Carbon-nitrogen feedbacks in
 2606 the UVic ESCM, *Geosci. Model Dev.*, 5(5), 1137–1160, doi:10.5194/gmd-5-1137-2012, 2012.

2607 Wei, X., Shao, M., Gale, W. and Li, L.: Global pattern of soil carbon losses due to the conversion of
 2608 forests to agricultural land, *Sci. Rep.*, 4, 4062, 2014.

2609 Wiltshire, A. J., Burke, E. J., Chadburn, S. E., Jones, C. D., Cox, P. M., Davies-Barnard, T., Friedlingstein, P.,
 2610 Harper, A. B., Liddicoat, S., Sitch, S. A. and Zaehle, S.: JULES-CN: a coupled terrestrial Carbon-Nitrogen
 2611 Scheme (JULES vn5.1), *Geosci. Model Dev. Discuss.*, 2020, 1–40, doi:10.5194/gmd-2020-205, 2020.

2612 Xu-Ri and Prentice, I. C.: Terrestrial nitrogen cycle simulation with a dynamic global vegetation model,
 2613 *Glob. Change Biol.*, 14(8), 1745–1764, doi:10.1111/j.1365-2486.2008.01625.x, 2008.

2614 Zaehle, S.: Terrestrial nitrogen and carbon cycle interactions at the global scale, *Philos. Trans. R. Soc. B*
 2615 *Biol. Sci.*, 368(1621), 20130125, doi:10.1098/rstb.2013.0125, 2013.

2616 Zaehle, S. and Friend, A. D.: Carbon and nitrogen cycle dynamics in the O-CN land surface model: 1.
 2617 Model description, site-scale evaluation, and sensitivity to parameter estimates: SITE-SCALE
 2618 EVALUATION OF A C-N MODEL, *Glob. Biogeochem. Cycles*, 24(1), n/a-n/a, doi:10.1029/2009GB003521,
 2619 2010.

2620 Zaehle, S., Friend, A. D., Friedlingstein, P., Dentener, F., Peylin, P. and Schulz, M.: Carbon and nitrogen
 2621 cycle dynamics in the O-CN land surface model: 2. Role of the nitrogen cycle in the historical terrestrial
 2622 carbon balance: NITROGEN EFFECTS ON GLOBAL C CYCLING, *Glob. Biogeochem. Cycles*, 24(1), n/a-n/a,
 2623 doi:10.1029/2009GB003522, 2010.

2624 Zeng, H., Jia, G. and Epstein, H.: Recent changes in phenology over the northern high latitudes detected
 2625 from multi-satellite data, *Environ. Res. Lett.*, 6(4), 045508, 2011.

2626 Zhang, H., Goll, D. S., Manzoni, S., Ciais, P., Guenet, B. and Huang, Y.: Modeling the effects of litter
 2627 stoichiometry and soil mineral N availability on soil organic matter formation using CENTURY-CUE (v1.0),
 2628 *Geosci. Model Dev.*, 11(12), 4779–4796, doi:10.5194/gmd-11-4779-2018, 2018.

2629 Zhao, X., Yang, Y., Shen, H., Geng, X. and Fang, J.: Global soil–climate–biome diagram: linking surface soil
 2630 properties to climate and biota, *Biogeosciences*, 16(14), 2857–2871, doi:10.5194/bg-16-2857-2019,
 2631 2019.

2632 Zhu, Z., Piao, S., Myneni, R. B., Huang, M., Zeng, Z., Canadell, J. G., Ciais, P., Sitch, S., Friedlingstein, P.,
2633 Arneth, A., Cao, C., Cheng, L., Kato, E., Koven, C., Li, Y., Lian, X., Liu, Y., Liu, R., Mao, J., Pan, Y., Peng, S.,
2634 Penuelas, J., Poulter, B., Pugh, T. A. M., Stocker, B. D., Viovy, N., Wang, X., Wang, Y., Xiao, Z., Yang, H.,
2635 Zaehle, S. and Zeng, N.: Greening of the Earth and its drivers, *Nat. Clim Change*, 6(8), 791–795, 2016.

2636 Zinke, P. J., Stangenberger, A. G., Post, W. M., Emanuel, W. R. and Olson, J. S.: Global Organic Soil
2637 Carbon and Nitrogen, Tech. Rep. ORNL/TM-8857, Oak Ridge National Laboratory, Oak Ridge, Tennessee,
2638 USA. [online] Available from: <https://doi.org/10.3334/ORNLDAAAC/221>, 1998.

2639

2640

2641

Following earlier simpler approaches (Cao et al., 2001; Alexandrov and Oikawa, 2002), GPP can be expressed as a logarithmic function of $[\text{CO}_2]$

$$G_p(t) = G_0 \left(1 + \gamma_p \ln \frac{c(t)}{c_0} \right) \quad (1)$$

where the unconstrained or potential GPP at any given time, $G_p(t)$, is a function of its initial value G_0 , $[\text{CO}_2]$ at time t , $c(t)$, and its initial value c_0 . The rate of increase of GPP is determined by the parameter γ_p (where p indicates the “potential” rate of increase of GPP with $[\text{CO}_2]$). The parameter γ_p is calculated by fitting equation (1) to simulated GPP over the historical period. In the absence of any nutrient constraints, the rate of increase of carbon uptake per unit area of leaves is determined by the theoretical framework of Farquhar et al. (1980) and Collatz et al. (1992) for C_3 and C_4 photosynthetic pathways, respectively. The rate of increase of global GPP, however, also depends on how the model simulated LAI increases in response to increasing $[\text{CO}_2]$, which in turn depends on how photosynthate is allocated between leaves, stem, and root. Arora et al. (2009) compared the unconstrained simulated rate of increase of GPP per unit increase in $[\text{CO}_2]$ (their Figure 3) with that based on the theoretical framework to show that the model’s response to increasing $[\text{CO}_2]$ over the historical period is consistent with the theoretical framework, given specified time-independent V_{cmax} values for different PFTs. To parameterize downregulation of photosynthesis with increasing $[\text{CO}_2]$ for emulating nutrient constraints, the unconstrained or potential GPP (for each time step and each PFT in a grid cell) is multiplied by the global scalar $\xi(c)$

$$G = \xi(c) G_p \quad (2)$$

$$\xi(c) = \frac{1 + \gamma_d \ln(c/c_0)}{1 + \gamma_p \ln(c/c_0)} \quad (3)$$

where t is omitted for clarity and the parameter γ_d represents the downregulated rate of increase of GPP with $[\text{CO}_2]$ (indicated by the subscript d). When $\gamma_d < \gamma_p$ the modelled gross primary productivity (G) increases in response to $[\text{CO}_2]$ at a rate determined by the value of γ_d . In the absence of the N cycle, the term $\xi(c)$ thus emulates down-regulation of photosynthesis as CO_2 increases. For example, values of $\gamma_d=0.42$ and $\gamma_p=0.90$, from Arora et al. (2009), yield a value of $\xi(c) = 0.94$ (indicating a 6% downregulation) for $c=390$ ppm (corresponding to year 2010) and $c_0=285$ ppm.

$$\begin{aligned} \frac{d N_{NH_4}}{dt} = & B_{NH_4} + F_{NH_4} + P_{NH_4} + M_{D,NH_4} + M_{H,NH_4} \\ & - U_{NH_4} - (I_{NO_3} + I_{N_2O} + I_{NO}) - V_{NH_3} - O_{NH_4} \end{aligned} \quad (4)$$

$$\frac{d N_{NO_3}}{dt} = P_{NO_3} + I_{NO_3} - L_{NO_3} - U_{NO_3} - (E_{N_2} + E_{N_2O} + E_{NO}) - O_{NO_3} \quad (5)$$

and all fluxes are represented in units of $\text{gN m}^{-2} \text{day}^{-1}$. B_{NH_4} is the rate of biological N fixation which solely contributes to the NH_4^+ pool, F_{NH_4} is the fertilizer input which is assumed to contribute only to the NH_4^+ pool, and P_{NH_4} and P_{NO_3} are atmospheric deposition rates that contribute to the NH_4^+ and NO_3^- pools, respectively. Biological N fixation, fertilizer input, and atmospheric deposition are the three routes through which N enters the coupled soil-vegetation system. M_{D,NH_4} and M_{H,NH_4} are the mineralization flux from the litter and soil organic matter pools, respectively, associated with their decomposition. We assume mineralization of humus

and litter pools only contributes to the NH_4^+ pool. O_{NH_4} and O_{NO_3} indicate immobilization of N from the NH_4^+ and NO_3^- pools, respectively, to the humus N pool which implies microbes (that are not represented explicitly) are part of the humus pool. Combined together the terms $(M_{D,\text{NH}_4} + M_{H,\text{NH}_4} - O_{\text{NH}_4} - O_{\text{NO}_3})$ yield the net mineralization rate. V_{NH_3} is the rate of ammonia (NH_3) volatilization and L_{NO_3} is the leaching of N that occurs only from the NO_3^- pool. The positively charged ammonium ions are attracted to the negatively charged soil particles and as a result it is primarily the negatively charged nitrate ions that leach through the soil (Porporato et al., 2003; Xu-Ri and Prentice, 2008). U_{NH_4} and U_{NO_3} are uptakes of NH_4^+ and NO_3^- by plants, respectively. The nitrification flux from NH_4 to NO_3 pool is represented by I_{NO_3} which also results in the release of the nitrous oxide (N_2O), a greenhouse gas, and nitric oxide (NO) through nitrifier denitrification represented by the terms $I_{\text{N}_2\text{O}}$ and I_{NO} , respectively. Finally, E_{N_2} , $E_{\text{N}_2\text{O}}$, and E_{NO} are the gaseous losses of N_2 (nitrogen gas), N_2O , and NO from the NO_3^- pool associated with denitrification. N is thus lost through the soil-vegetation system via leaching in runoff and through gaseous losses of $I_{\text{N}_2\text{O}}$, I_{NO} , E_{N_2} , $E_{\text{N}_2\text{O}}$, E_{NO} , and V_{NH_3} .

The structural and non-structural N pools in root are written as $N_{R,S}$ and $N_{R,NS}$, respectively, and similarly for stem ($N_{S,S}$ and $N_{S,NS}$) and leaves ($N_{L,S}$ and $N_{L,NS}$), and together the structural and non-structural pools make the total N pool in leaf ($N_L = N_{L,S} + N_{L,NS}$), root ($N_R = N_{R,S} + N_{R,NS}$), and stem ($N_S = N_{S,S} + N_{S,NS}$) components. The rate change equation for structural and non-structural N pools in root are given by

$$\frac{d N_{R,NS}}{dt} = U_{\text{NH}_4} + U_{\text{NO}_3} + R_{L2R} - R_{R2L} - A_{R2L} - A_{R2S} - LF_{R,NS} - T_{R,NS2S} \quad (6)$$

$$\frac{d N_{R,S}}{dt} = T_{R,NS2S} - LF_{R,S} \quad (7)$$

Similar to the uptake of carbon by leaves and its subsequent allocation to root and stem components, N is taken up by roots and then allocated to leaves and stem. A_{R2L} and A_{R2S} represent the allocation of N from roots to leaves and stem, respectively. The terms R_{L2R} and R_{R2L} represent the reallocation of N between the non-structural components of root and leaves. R_{L2R} is the N reallocated from leaves to root representing resorption of a fraction of leaf N during leaf fall for deciduous tree PFTs. R_{R2L} indicates reallocation of N from roots to leaves (termed reallocation in Figure 2) at the time of leaf-out for deciduous tree PFTs. At times other than leaf-out and leaf-fall and for other PFTs these two terms are zero. $T_{R,NS2S}$ is the one way transfer of N from the non-structural to the structural root pool, and similar to the carbon pools, once N is converted to its structural form it cannot be converted back to its non-structural form. Finally, the litterfall due to turnover of roots occurs from both the structural ($LF_{R,S}$) and non-structural ($LF_{R,NS}$) N pools.

The rate change equations for non-structural and structural components of leaves are written as

$$\frac{d N_{L,NS}}{dt} = A_{R2L} - R_{L2R} - R_{L2S} + R_{R2L} + R_{S2L} - LF_{L,NS} - T_{L,NS2S} \quad (8)$$

$$\frac{d N_{L,S}}{dt} = T_{L,NS2S} - LF_{L,S} \quad (9)$$

where $T_{L,NS2S}$ is the one way transfer of N from the non-structural leaf component to its structural N pool and R_{S2L} indicates reallocation of N from stem to leaves (similar to R_{R2L}) at the time of leaf out for deciduous tree PFTs. Litterfall occurs from both the structural ($LF_{L,S}$) and non-structural ($LF_{L,NS}$) N pools of leaves, and all other terms have been previously defined.

Finally, the rate change equations for non-structural and structural components of stem are written as

$$\frac{d N_{S,NS}}{dt} = A_{R2S} + R_{L2S} - R_{S2L} - LF_{S,NS} - T_{S,NS2S} \quad (10)$$

$$\frac{d N_{S,S}}{dt} = T_{S,NS2S} - LF_{S,S} \quad (11)$$

where $LF_{S,NS}$ and $LF_{S,S}$ represent stem litter from the non-structural and structural components, $T_{S,NS2S}$ is the one way transfer of N from the non-structural stem component to its structural N pool. All other terms have been previously defined.

Adding equations (6) through (11) yields rate of change of N in the entire vegetation pool (N_V) as

$$\begin{aligned} \frac{d N_V}{dt} &= \frac{d N_{R,NS}}{dt} + \frac{d N_{R,S}}{dt} + \frac{d N_{L,NS}}{dt} + \frac{d N_{L,S}}{dt} + \frac{d N_{S,NS}}{dt} + \frac{d N_{S,S}}{dt} = \frac{d N_R}{dt} + \frac{d N_L}{dt} + \frac{d N_S}{dt} \\ \frac{d N_V}{dt} &= U_{NH4} + U_{NO3} - LF_{R,NS} - LF_{R,S} - LF_{L,NS} - LF_{L,S} - LF_{S,NS} - LF_{S,S} \\ &= U_{NH4} + U_{NO3} - LF_R \quad \quad \quad - LF_L \quad \quad \quad - LF_S \end{aligned} \quad (12)$$

which indicates how the dynamically varying vegetation N pool is governed by mineral N uptake from the NH_4^+ and NO_3^- pools and litterfall from the structural and non-structural components of the leaves, stem, and root pools. LF_R is the total N litter generation from the root pool and sum of litter generation from its structural and non-structural components ($LF_R = LF_{R,S} + LF_{R,NS}$), and similarly for the leaves (LF_L) and the stem (LF_S) pools.

The rate change equations for the organic N pools in the litter (N_D) and soil (N_H) pools are written as follows.

$$\frac{dN_D}{dt} = LF_R + LF_L + LF_S - H_{N,D2H} - M_{D,NH_4} \quad (13)$$

$$\frac{dN_H}{dt} = H_{N,D2H} + O_{NH_4} + O_{NO_3} - M_{H,NH_4} \quad (14)$$

where $H_{N,D2H}$ is the transfer of humidified organic matter from litter to the soil organic matter pool, and all other terms have been previously defined.

Sections A.1, A.2, and A.3 in the appendix describe how the individual terms of the rate change equations of the 10 prognostic N pools (equations 4 through 11, and equations 13 and 14) are specified or parameterized. The treatment of these terms are briefly described here. Biological N fixation (BNF, B_{NH_4}) is parameterized as a function of soil moisture and temperature with higher fixation rate per unit area for agricultural areas than natural vegetation. If externally specified information for ammonium (NH_4^+) and nitrate (NO_3^-) deposition rates is available then it is used otherwise deposition is assumed to be split equally between NH_4^+ and NO_3^- . Externally specified fertilizer application rates are same throughout the year in the tropics (between 30°S and 30°N), given multiple crop rotations in a given year in tropical regions. Between 30° and 90° latitudes in both northern and southern hemispheres, we assume that fertilizer application starts on the spring equinox and ends on the fall equinox. Plant N demand is calculated on the basis of the fraction of NPP allocated to leaves, stem, and root components and their specified minimum PFT-dependent C:N ratios. Both passive and active root uptakes of N are modelled. Passive uptake depends on transpiration and concentration of NH_4^+ and NO_3^- in the root zone water column. When passive N uptake cannot meet the N demand, active uptake compensates for reduced passive uptake though eventually they both depend on the amount of available N in the mineral pools. Plant N uptake by roots is allocated to stem and leaf components, which allows to

model leaf N content (N_L) as a prognostic variable. N contributions to litter through litterfall are based on C:N ratios of the vegetation components and the litterfall rates. Resorption of N before litterfall for deciduous tree species is also modelled. Decomposition of litter and soil organic matter releases C to the atmosphere as CO_2 and the mineralized N is moved to the NH_4^+ pool. Immobilization of mineral N from NH_4^+ and NO_3^- pools into the soil organic matter pool is meant to keep the soil organic matter C:N ratio ($C:N_H$) at its specified constant value of 13 for all PFTs.

Nitrification, the process converting ammonium to nitrate, is driven by microbial activity and depends both on soil temperature and moisture such that it is constrained both at high and low soil moisture contents. Gaseous fluxes of NO (I_{NO}) and N_2O (I_{N_2O}) are associated with nitrification and assumed to be directly proportional to the nitrification flux. Denitrification is modelled to reduce NO_3^- to NO, N_2O , and ultimately to N_2 . Unlike nitrification, however, denitrification is primarily an anaerobic process and therefore occurs primarily when soil is saturated. Leaching of NO_3^- (L_{NO_3}) is parameterized to be directly proportional to baseflow from the bottommost soil layer and the size of the NO_3^- pool. Finally, NH_3 volatilization (V_{NH_3}) is parametrized as a function of NH_4^+ pool size, soil temperature, soil pH, and aerodynamic and boundary layer resistances.

A1. N inputs

A1.1 Biological N fixation

Biological N fixation (BNF, B_{NH_4}) is caused by both free living bacteria in the soil and by bacteria symbiotically living within nodules of host plants' roots. Here, the bacteria convert free

nitrogen from the atmosphere to ammonium, which is used by the host plants. Like any other microbial activity, BNF is limited both by drier soil moisture conditions and cold temperatures. Cleveland et al. (1999) attempt to capture this by parameterizing BNF as a function of actual evapotranspiration (AET). AET is a function primarily of soil moisture (through precipitation and soil water balance) and available energy. In places where vegetation exists, AET is also affected by vegetation characteristics including LAI and rooting depth. Here, we parameterize BNF (B_{NH_4} , $\text{gN m}^{-2} \text{day}^{-1}$) as a function of modelled soil moisture and temperature to depth of 0.5 m following Xu-Ri and Prentice (2008) which yields a very similar geographical distribution of BNF as the Cleveland et al. (1999) approach as seen in Figure 4c.

$$\begin{aligned}
 B_{NH_4} &= \left(\sum_c \alpha_c f_c + \sum_n \alpha_n f_n \right) f(T_{0.5}) f(\theta_{0.5}) \\
 f(T_{0.5}) &= 2^{(T_{0.5}-25)/10} \\
 f(\theta_{0.5}) &= \min \left(0, \max \left(1, \frac{\theta_{0.5}-\theta_w}{\theta_{fc}-\theta_w} \right) \right)
 \end{aligned} \tag{A1}$$

where α_c and α_n ($\text{gN m}^{-2} \text{day}^{-1}$) are BNF coefficients for crop (c) and non-crop or natural (n) PFTs, which are area weighted using the fractional coverages f_c and f_n of crop and non-crop PFTs that are present in a grid cell, $f(T)$ is the dependence on soil temperature based on a Q_{10} formulation and $f(\theta)$ is the dependence on soil moisture which varies between 0 and 1. θ_{fc} and θ_w are the soil moisture at field capacity and wilting points, respectively. $T_{0.5}$ ($^{\circ}\text{C}$) and $\theta_{0.5}$ ($\text{m}^3 \text{m}^{-3}$) in equation (A1) are averaged over the 0.5 m soil depth over which BNF is assumed to occur. We do not make the distinction between symbiotic and non-symbiotic BNF since this requires explicit knowledge of geographical distribution of N fixing PFTs which are not represented separately in our base set of nine PFTs. A higher value of α_c is used compared to α_n to account for the use of N fixing plants over agriculture areas. Biological nitrogen fixation has been an essential

component of many farming systems for considerable periods, with evidence for the agricultural use of legumes dating back more than 4,000 years (O'Hara, 1998). A higher α_c than α_n is also consistent with Fowler et al. (2013) who report BNF of 58 and 60 Tg N yr⁻¹ for natural and agricultural ecosystems for present day. Since the area of natural ecosystems is about five times the current cropland area it implies BNF rate per unit land area is higher for crop ecosystems than for natural ecosystems. Values of α_c than α_n and other model parameters are summarized in Table A1.

Similar to Cleveland et al. (1999), our approach does not lead to a significant change in BNF with increasing atmospheric CO₂, other than through changes in soil moisture and temperature. At least two meta-analyses, however, suggest that an increase in atmospheric CO₂ does lead to an increase in BNF through increased symbiotic activity associated with an increase in both nodule mass and number (McGuire et al., 1995; Liang et al., 2016). Models have attempted to capture this by simulating BNF as a function of NPP (Thornton et al., 2007; Wania et al., 2012). The caveat with this approach and the implications of our BNF approach are discussed in Section 6.

A1.2 Atmospheric N deposition

Atmospheric N deposition is externally specified. The model reads in spatially- and temporally-varying annual deposition rates from a file. Deposition is assumed to occur at the same rate throughout the year so the same daily rate (gN m⁻² day⁻¹) is used for all days of a given year. If separate information for ammonium (NH₄⁺) and nitrate (NO₃⁻) deposition rates is available

then it is used otherwise deposition is assumed to be split equally between NH_4^+ and NO_3^- (indicated as P_{NH_4} and P_{NO_3} in equations 4 and 5).

A1.3 Fertilizer application

Geographically and temporally varying annual fertilizer application rates (F_{NH_4}) are also specified externally and read in from a file. Fertilizer application occurs over the C_3 and C_4 crop fractions of grid cells. Agricultural management practices are difficult to model since they vary widely between countries and even from farmer to farmer. For simplicity, we assume fertilizer is applied at the same daily fertilizer application rate ($\text{gN m}^{-2} \text{ day}^{-1}$) throughout the year in the tropics (between 30°S and 30°N), given the possibility of multiple crop rotations in a given year. Between the 30° and 90° latitudes in both northern and southern hemispheres, we assume that fertilizer application starts on the spring equinox and ends on the fall equinox. The annual fertilizer application rate is thus distributed over around 180 days. This provides somewhat more realism, than using the same treatment as in tropical regions, since extra-tropical agricultural areas typically do not experience multiple crop rotations in a given year.

A2. N cycling in plants and soil

Plant roots take up mineral N from soil and then allocate it to leaves and stem to maintain an optimal C:N ratio of each component. Litterfall from vegetation contributes to the litter pool and decomposition of litter transfers humified litter to the soil organic matter pool. Decomposition of litter and soil organic matter returns mineralized N back to the NH_4^+ pool, closing the soil-vegetation N cycle loop. Both active and passive plant uptakes of N (from both

the NH_4^+ and NO_3^- pools) are explicitly modelled. The modelled plant N uptake is a function of its N demand. Higher N demand leads to higher mineral N uptake from soil.

A2.1 Plant N demand

Plant N demand is calculated based on the fraction of NPP allocated to leaves, stem, and root components and their specified minimum PFT-dependent C:N ratios, similar to other models (Xu-Ri and Prentice, 2008; Jiang et al., 2019). The assumption is that plants always want to achieve their desired minimum C:N ratios if enough N is available.

$$\Delta_{WP} = \Delta_L + \Delta_R + \Delta_S$$

$$\Delta_i = \frac{\max(0, \text{NPP} \cdot a_{i,C})}{C:N_{i,\min}}, \quad i = L, S, R \quad (\text{A2})$$

where the whole plant N demand (Δ_{WP}) is the sum of N demand for the leaves (Δ_L), stem (Δ_S), and root (Δ_R) components, $a_{i,C}$, $i = L, S, R$ is the fraction of NPP (i.e. carbon as indicated by letter C in the subscript) allocated to leaf, stem, and root components, and $C:N_{i,\min}$, $i = L, S, R$ are their specified minimum C:N ratios (see Table A1 for these and all other model parameters). A caveat with this approach when applied at the daily time step, for biogeochemical processes in our model, is that during periods of time when NPP is negative due to adverse climatic conditions (e.g. during winter or drought seasons), the calculated demand is negative. If positive NPP implies there is demand for N, negative NPP cannot be taken to imply that N must be lost from vegetation. As a result, from a plant's perspective, N demand is assumed to be zero during periods of negative NPP. N demand is also set to zero when all leaves have been shed (i.e., when GPP is zero). At the global scale, this leads to about 15% higher annual N demand than would be the case if negative NPP values were taken into consideration.

A2.2 Passive N uptake

N demand is weighed against passive and active N uptake. Passive N uptake depends on the concentration of mineral N in the soil and the water taken up by the plants through their roots as a result of transpiration. We assume that plants have no control over N that comes into the plant through this passive uptake. This is consistent with existing empirical evidence that too much N in soil will cause N toxicity (Goyal and Huffaker, 1984), although we do not model N toxicity in our framework. If the N demand for the current time step cannot be met by passive N uptake then a plant compensates for the deficit (i.e., the remaining demand) through active N uptake.

The NH_4^+ concentration in the soil moisture within the rooting zone, referred to as $[\text{NH}_4]$ ($\text{gN gH}_2\text{O}^{-1}$), is calculated as

$$[\text{NH}_4] = \frac{N_{\text{NH}_4}}{\sum_{i=1}^{i \leq r_d} 10^6 \theta_i z_i} \quad (\text{A3})$$

where N_{NH_4} is ammonium pool size (gN m^{-2}), θ_i is the volumetric soil moisture content for soil layer i ($\text{m}^3 \text{m}^{-3}$), z_i is the thickness of soil layer i (m), r_d is the soil layer in which the 99% rooting depth lies as dynamically simulated by the biogeochemical module of CLASSIC following Arora and Boer (2003). The 10^6 term converts units of the denominator term to $\text{gH}_2\text{O m}^{-2}$. NO_3^- concentration ($[\text{NO}_3]$, $\text{gN gH}_2\text{O}^{-1}$) in the rooting zone is found in a similar fashion. The transpiration flux q_t ($\text{kgH}_2\text{O m}^{-2} \text{s}^{-1}$) (calculated in the physics module of CLASSIC) is multiplied by $[\text{NH}_4]$ and $[\text{NO}_3]$ ($\text{gN gH}_2\text{O}^{-1}$) to obtain passive uptake of NH_4^+ and NO_3^- ($\text{gN m}^{-2} \text{day}^{-1}$) as

$$\begin{aligned}
 U_{p,NH_4} &= 86400 \times 10^3 \beta q_t[NH_4] \\
 U_{p,NO_3} &= 86400 \times 10^3 \beta q_t[NO_3]
 \end{aligned}
 \tag{A4}$$

where the multiplier 86400×10^3 converts q_t to units of $gH_2O m^{-2} day^{-1}$, and β (see Table A1) is the dimensionless mineral N distribution coefficient with value less than 1 that accounts for the fact that NH_4 and NO_3 available in the soil are not well mixed in the soil moisture solution, and not completely accessible to roots, to be taken up by plants.

A2.3 Active N uptake

The active plant N uptake is parameterized as a function of fine root biomass and the size of NH_4^+ and NO_3^- pools in a manner similar to Gerber et al. (2010) and Wania et al (2012). CLASSIC does not explicitly model fine root biomass. We therefore calculate the fraction of fine root biomass using an empirical relationship that is very similar to the relationship developed by Kurz et al. (1996) (their equation 5) but also works below total root biomass of 0.33 Kg C m^{-2} (the Kurz et al. (1996) relationship yields a fraction of fine root more than 1.0 below this threshold). The fraction of fine root biomass (f_r) is given by

$$f_r = 1 - \frac{C_R}{C_R + 0.6}
 \tag{A5}$$

where C_R is the root biomass (KgC m^{-2}) simulated by the biogeochemical module of CLASSIC. Equation (A5) yields fine root fraction approaching 1.0 as C_R approaches 0, so at very low root biomass values all roots are considered fine roots. For grasses the fraction of fine root biomass is set to 1. The maximum or potential active N uptake is given by

$$\begin{aligned}
U_{a,pot,NH_4} &= \frac{\varepsilon f_r C_R N_{NH_4}}{k_{p,1/2} r_d + N_{NH_4} + N_{NO_3}} \\
U_{a,pot,NO_3} &= \frac{\varepsilon f_r C_R N_{NO_3}}{k_{p,1/2} r_d + N_{NH_4} + N_{NO_3}}
\end{aligned} \tag{A6}$$

where ε is the efficiency of fine roots to take up N per unit fine root mass per day ($\text{gN gC}^{-1} \text{day}^{-1}$), $k_{p,1/2}$ is the half saturation constant (gN m^{-3}), and N_{NH_4} and N_{NO_3} are the ammonium and nitrate pool sizes (gN m^{-2}) as mentioned earlier. Depending on the geographical location and the time of the year, if passive uptake alone can satisfy the plant demand the actual active N uptake of NH_4 ($U_{a,actual,NH_4}$) and NO_3 ($U_{a,actual,NO_3}$) is set to zero. Conversely, during other times both passive and potential active N uptakes may not be able to satisfy the demand and in this case actual active N uptake is equal to its potential rate. At times other than these, the actual active uptake is lower than its potential value. This adjustment of actual active uptake is illustrated in equation (A7).

$$\begin{aligned}
&\text{if } (\Delta_{WP} \leq U_{p,NH_4} + U_{p,NO_3}) \\
&\quad U_{a,actual,NH_4} = 0 \\
&\quad U_{a,actual,NO_3} = 0 \\
&\text{if } (\Delta_{WP} > U_{p,NH_4} + U_{p,NO_3}) \wedge (\Delta_{WP} < U_{p,NH_4} + U_{p,NO_3} + U_{a,pot,NH_4} + U_{a,pot,NO_3}) \\
&\quad U_{a,actual,NH_4} = (\Delta_{WP} - U_{p,NH_4} - U_{p,NO_3}) \frac{U_{a,pot,NH_4}}{U_{a,pot,NH_4} + U_{a,pot,NO_3}} \\
&\quad U_{a,actual,NO_3} = (\Delta_{WP} - U_{p,NH_4} - U_{p,NO_3}) \frac{U_{a,pot,NO_3}}{U_{a,pot,NH_4} + U_{a,pot,NO_3}} \\
&\text{if } (\Delta_{WP} \geq U_{p,NH_4} + U_{p,NO_3} + U_{a,pot,NH_4} + U_{a,pot,NO_3}) \\
&\quad U_{a,actual,NH_4} = U_{a,pot,NH_4} \\
&\quad U_{a,actual,NO_3} = U_{a,pot,NO_3}
\end{aligned} \tag{A7}$$

Finally, the total N uptake (U), uptake of NH_4^+ (U_{NH_4}) and NO_3^- (U_{NO_3}), are calculated as

$$\begin{aligned}
U &= U_{p,NH4} + U_{p,NO3} + U_{a,actual,NH4} + U_{a,actual,NO3} \\
U_{NH4} &= U_{p,NH4} + U_{a,actual,NH4} \\
U_{NO3} &= U_{p,NO3} + U_{a,actual,NO3}
\end{aligned}
\tag{A8}$$

A2.4 Litterfall

Nitrogen litterfall from the vegetation components is directly tied to the carbon litterfall calculated by the phenology module of CLASSIC through their current C:N ratios.

$$LF_i = \frac{(1-r_L)LF_{i,C}}{C:N_i}, i = L, S, R \tag{A9}$$

where $LF_{i,C}$ is the carbon litterfall rate (gC day^{-1}) for component i , calculated by the phenology module of CLASSIC, and division by its current C:N ratio yields the nitrogen litterfall rate, r_L is the leaf resorption coefficient that simulates the resorption of N from leaves of deciduous tree PFTs before they are shed and $r_i = 0, i = R, S$. Litter from each vegetation component is proportioned between structural and non-structural components according to their pool sizes.

A2.5 Allocation and reallocation

Plant N uptake by roots is allocated to leaves and stem to satisfy their N demand. When plant N demand is greater than zero, total N uptake (U) is divided between leaves, stem, and root components in proportion to their demands such that the allocation fractions for N ($a_i, i = L, S, R$) are calculated as

$$\begin{aligned}
a_i &= \frac{\Delta_i}{\Delta_{WP}}, i = L, S, R \\
A_{R2L} &= a_L (U_{NH4} + U_{NO3}) \\
A_{R2S} &= a_S (U_{NH4} + U_{NO3})
\end{aligned}
\tag{A10}$$

where A_{R2L} and A_{R2S} are the amounts of N allocated from root to leaves and stem components, respectively, as mentioned in the main text for equation (8). During periods of negative NPP due to adverse climatic conditions (e.g. during winter or drought seasons) the plant N demand is set to zero but passive N uptake, associated with transpiration, may still be occurring if the leaves are still on. Even though there is no N demand, passive N uptake still needs to be partitioned among the vegetation components. During periods of negative NPP allocation fractions for N are, therefore, calculated in proportion to the minimum PFT-dependent C:N ratios of the leaves, stem, and root components as follows.

$$a_i = \frac{1/C:N_{i,\min}}{1/C:N_{L,\min} + 1/C:N_{S,\min} + 1/C:N_{R,\min}}, i = L, S, R \quad (\text{A11})$$

For grasses, which do not have a stem component, equations (A10) and (A11) are modified accordingly by removing the terms associated with the stem component.

Three additional rules override these general allocation rule specifically for deciduous tree PFTs (or deciduous PFTs in general). First, no N allocation is made to leaves once leaf fall is initiated for deciduous tree PFTs and plant N uptake is proportioned between stem and root components based on their demands in a manner similar to equation (A10). Second, for deciduous tree PFTs, a fraction of leaf N is resorbed from leaves back into stem and root as follows

$$\begin{aligned} R_{L2R} &= r_L L F_L \frac{N_{R,NS}}{N_{R,NS} + N_{S,NS}} \\ R_{L2S} &= r_L L F_L \frac{N_{S,NS}}{N_{R,NS} + N_{S,NS}} \end{aligned} \quad (\text{A12})$$

where r_L is the leaf resorption coefficient, as mentioned earlier, and LF_L is the leaf litter fall rate. Third, and similar to resorption, at the time of leaf onset for deciduous tree PFTs, N is reallocated to leaves (in conjunction with reallocated carbon as explained in Asaadi et al. (2018)) from stem and root components.

$$\begin{aligned} R_{R2L} &= \frac{R_{R2L,C}}{C:N_L} \frac{N_{R,NS}}{N_{R,NS}+N_{S,NS}} \\ R_{S2L} &= \frac{R_{S2L,C}}{C:N_L} \frac{N_{S,NS}}{N_{R,NS}+N_{S,NS}} \end{aligned} \quad (A13)$$

where $R_{R2L,C}$ and $R_{S2L,C}$ represent reallocation of carbon from non-structural stem and root components to leaves and division by $C:N_L$ converts the flux into N units. The reallocation demand for N, at the time of leaf onset, is proportioned between non-structural pools of stem and root according to their sizes.

A2.6 N mineralization, immobilization, and humification

Decomposition of litter ($R_{h,D}$) and soil organic matter ($R_{h,H}$) releases C to the atmosphere and this flux is calculated by the heterotrophic respiration module of CLASSIC. The amount of N mineralized is calculated straightforwardly by division with the current C:N ratios of the respective pools and contributes to the NH_4^+ pool.

$$\begin{aligned} M_{D,\text{NH}_4} &= \frac{R_{h,D}}{C:N_D} \\ M_{H,\text{NH}_4} &= \frac{R_{h,H}}{C:N_H} \end{aligned} \quad (A14)$$

An implication of mineralization contributing to the NH_4^+ pool, in addition to BNF and fertilizer inputs that also contribute solely to the NH_4^+ pool, is that the simulated NH_4^+ pool is typically

larger than the NO_3^- pool. The exception is the dry and arid regions where the lack of denitrification, as discussed below in Section A.3.2., leads to a build up of the NO_3^- pool.

Immobilization of mineral N from the NH_4^+ and NO_3^- pools into the soil organic matter pool is meant to keep the soil organic matter C:N ratio ($C:N_H$) at its specified value of 13 for all PFTs in a manner similar to Wania et al. (2012) and Zhang et al. (2018). A value of 13 is within the range of observation-based estimates which vary from about 8 to 25 (Zinke et al., 1998; Tipping et al., 2016). Although $C:N_H$ varies geographically, the driving factors behind this variability remain unclear. It is even more difficult to establish if increasing atmospheric CO_2 is changing $C:N_H$ given the large heterogeneity in soil organic C and N densities, and the difficulty in measuring small trends for such large global pools. We therefore make the assumption that the $C:N_H$ does not change with time. An implication of this assumption is that as GPP increases with increasing atmospheric CO_2 rises, and plant litter becomes enriched in C with increasing C:N ratio of litter, more and more N is locked up in the soil organic matter pool because its C:N ratio is fixed. As a result, mineral N pools of NH_4^+ and NO_3^- decrease in size and plant N content subsequently follows. This is consistent with studies of plants grown in elevated CO_2 environment. For example, Cotrufo et al. (1998) summarize results from 75 studies and find an average 14% reduction in N concentration for above-ground tissues. Wang et al. (2019) find increased C concentration by 0.8–1.2% and a reduction in N concentration by 7.4–10.7% for rice and winter wheat crop rotation system under elevated CO_2 .

Immobilization from both the NH_4^+ and NO_3^- pools is calculated in proportion to their pool sizes, employing the fixed $C:N_H$ ratio as

$$\begin{aligned}
O_{NH_4} &= \max\left(0, \left(\frac{C_H}{C:N_H} - N_H\right) \frac{N_{NH_4}}{N_{NH_4} + N_{NO_3}}\right) \\
O_{NO_3} &= \max\left(0, \left(\frac{C_H}{C:N_H} - N_H\right) \frac{N_{NO_3}}{N_{NH_4} + N_{NO_3}}\right)
\end{aligned}
\tag{A15}$$

Finally, the carbon flux of humified litter from the litter to the soil organic matter pool ($H_{C,D2H}$) is also associated with a corresponding N flux that depends on the C:N ratio of the litter pool.

$$H_{N,D2H} = \frac{H_{C,D2H}}{C:N_D} \tag{A16}$$

A3. N cycling in mineral pools and N outputs

This section presents the parameterizations of nitrification (which results in transfer of N from the NH_4^+ to the NO_3^- pool) and the associated gaseous fluxes of N_2O and NO (referred to as nitrifier denitrification), gaseous fluxes of N_2O , NO , and N_2 associated with denitrification, volatilization of NH_4 into NH_3 , and leaching of NO_3^- in runoff.

A3.1 Nitrification

Nitrification, the oxidative process converting ammonium to nitrate, is driven by microbial activity and as such constrained both by high and low soil moisture (Porporato et al., 2003). At high soil moisture content there is little aeration of soil and this constrains aerobic microbial activity, while at low soil moisture content microbial activity is constrained by moisture limitation. In CLASSIC, the heterotrophic respiration from soil carbon is constrained similarly but rather than using soil moisture the parameterization is based on soil matric potential (Arora, 2003; Melton et al., 2015). Here, we use the exact same parameterization. In addition to soil moisture, nitrification ($gN\ m^{-2}\ day^{-1}$) is modelled as a function of soil temperature and the size of the NH_4^+ pool as follows

$$I_{NO3} = \eta f_I(T_{0.5})f_I(\psi) N_{NH4} \quad (A17)$$

where η is the nitrification coefficient (day^{-1}), $f_I(\psi)$ is the dimensionless soil moisture scalar that varies between 0 and 1 and depends on soil matric potential (ψ), $f_I(T_{0.5})$ is the dimensionless soil temperature scalar that depends on average soil temperature ($T_{0.5}$) over the top 0.5 m soil depth over which nitrification is assumed to occur (following Xu-Ri and Prentice, 2008), and N_{NH4} is the ammonium pool size (gN m^{-2}), as mentioned earlier. Both $f_I(T_{0.5})$ and $f_I(\psi)$ are parameterized following Arora (2003) and Melton et al. (2015). $f_I(T_{0.5})$ is a Q_{10} type function with a temperature dependent Q_{10}

$$f_I(T_{0.5}) = Q_{10,I}^{(T_{0.5}-20)/10}, Q_{10,I} = 1.44 + 0.56 (\tanh(0.075(46 - T_{0.5}))) \quad (A18)$$

The reference temperature for nitrification is set to 20 °C following Lin et al. (2000). $f_I(\psi)$ is parameterized as a step function of soil matric potential (ψ) as

$$f_I(\psi) = \begin{cases} 0.5 & \text{if } \psi \leq \psi_{sat} \\ 1 - 0.5 \frac{\log(0.4) - \log(\psi)}{\log(0.4) - \log(\psi_{sat})} & \text{if } 0.4 > \psi \geq \psi_{sat} \\ 1 & \text{if } 0.6 \geq \psi \geq 0.4 \\ 1 - 0.8 \frac{\log(\psi) - \log(0.6)}{\log(100) - \log(0.6)} & \text{if } 100 > \psi > 0.6 \\ 0.2 & \text{if } \psi > 100 \end{cases} \quad (A19)$$

where the soil matric potential (ψ) is found, following Clapp and Hornberger (1978), as a function of soil moisture (θ)

$$\psi(\theta) = \psi_{sat} \left(\frac{\theta}{\theta_{sat}} \right)^{-B}. \quad (A20)$$

Saturated matric potential (ψ_{sat}), soil moisture at saturation (i.e. porosity) (θ_{sat}), and the parameter B are calculated as functions of percent sand and clay in soil following Clapp and

Hornberger (1978) as shown in Melton et al. (2015). The soil moisture scalar $f_I(\psi)$ is calculated individually for each soil layer and then averaged over the soil depth of 0.5 m over which nitrification is assumed to occur.

Gaseous fluxes of NO (I_{NO}) and N₂O (I_{N2O}) associated with nitrification, and generated through nitrifier denitrification, are assumed to be directly proportional to the nitrification flux (I_{NO3}) as

$$\begin{aligned} I_{NO} &= \eta_{NO} I_{NO3} \\ I_{N2O} &= \eta_{N2O} I_{NO3} \end{aligned} \quad (A21)$$

where η_{NO} and η_{N2O} are dimensionless fractions which determine what fractions of nitrification flux are emitted as NO and N₂O.

A3.2 Denitrification

Denitrification is the stepwise microbiological reduction of nitrate to NO, N₂O, and ultimately to N₂ in complete denitrification. Unlike nitrification, however, denitrification is primarily an anaerobic process (Tomasek et al., 2017) and therefore occurs when soil is saturated. As a result, we use a different soil moisture scalar than for nitrification. Similar to nitrification, denitrification is modelled as a function of soil moisture, soil temperature and the size of the NO₃⁻ pool as follows to calculate the gaseous fluxes of NO, N₂O, and N₂.

$$\begin{aligned} E_{NO} &= \mu_{NO} f_E(T_{0.5}) f_E(\theta) N_{NO3} \\ E_{N2O} &= \mu_{N2O} f_E(T_{0.5}) f_E(\theta) N_{NO3} \\ E_{N2} &= \mu_{N2} f_E(T_{0.5}) f_E(\theta) N_{NO3} \end{aligned} \quad (A22)$$

where μ_{NO} , μ_{N2O} , and μ_{N2} are coefficients (day⁻¹) that determine daily rates of emissions of NO, N₂O, and N₂. The temperature scalar $f_E(T_{0.5})$ is exactly the same as the one for nitrification

($f_I(T_{0.5})$) since denitrification is also assumed to occur over the same 0.5 soil depth. The soil moisture scalar $f_E(\theta)$ is given by

$$\begin{aligned} f_E(\theta) &= 1 - \tanh\left(2.5 \left(\frac{1-w(\theta)}{1-w_d}\right)^2\right) \\ w(\theta) &= \max\left(0, \min\left(1, \frac{\theta-\theta_w}{\theta_f-\theta_w}\right)\right) \end{aligned} \quad (\text{A23})$$

where w is the soil wetness that varies between 0 and 1 as soil moisture varies between wilting point (θ_w) and field capacity (θ_f), and w_d is the threshold soil wetness for denitrification below which very little denitrification occurs. Since very little denitrification occurs when soil wetness is below w_d this leads to build up of the NO_3^- pool in arid regions.

A3.3 NO_3^- leaching

Leaching is the loss of water-soluble ions through runoff. In contrast to positively charged NH_4^+ ions (i.e. cations), the NO_3^- ions do not bond to soil particles because of the limited exchange capacity of soil for negatively charged ions (i.e. anions). As a result, leaching of N in the form of NO_3^- ions is a common water quality problem, particularly over cropland regions. The leaching flux (L_{NO_3} , $\text{gN m}^{-2} \text{ day}^{-1}$) is parameterized to be directly proportional to baseflow (b_t , $\text{Kg m}^{-2} \text{ s}^{-1}$) calculated by the physics module of CLASSIC and the size of the NO_3 pool (N_{NO_3} , gN m^{-2}). Baseflow is the runoff rate from the bottommost soil layer.

$$L_{\text{NO}_3} = 86400 \varphi b_t N_{\text{NO}_3} \quad (\text{A24})$$

where the multiplier 86400 converts units to per day, and φ is the leaching coefficient ($\text{m}^2 \text{ Kg}^{-1}$) that can be thought of as the soil particle surface area (m^2) that 1 Kg of water (or about 0.001 m^3) can effectively wash to leach the nutrients.

A3.4 NH₃ volatilization

NH₃ volatilization (V_{NH_3} , gN m⁻² day⁻¹) is parametrized as a function of pool size of NH₄⁺, soil temperature, soil pH, aerodynamic and boundary layer resistances, and atmospheric NH₃ concentration in a manner similar to Riddick et al. (2016) as

$$V_{NH_4} = \vartheta \ 86400 \frac{1}{r_a+r_b} (\chi - [NH_{3,a}]) \quad (A25)$$

where ϑ is the dimensionless NH₃ volatilization coefficient which is set to less than 1 to account for the fact that a fraction of ammonia released from the soil is captured by vegetation, r_a (s m⁻¹) is the aerodynamic resistance calculated by the physics module of CLASSIC, χ is the ammonia (NH₃) concentration at the interface of the top soil layer and the atmosphere (g m⁻³), $[NH_{3,a}]$ is the atmospheric NH₃ concentration specified at 0.3×10⁻⁶ g m⁻³ following Riddick et al. (2016), 86400 converts flux units from gN m⁻² s⁻¹ to gN m⁻² day⁻¹, and r_b (s m⁻¹) is the boundary layer resistance calculated following Thom (1975) as

$$r_b = 6.2 u_*^{-0.67} \quad (A26)$$

where u_* (m/s) is the friction velocity provided by the physics module of CLASSIC. The ammonia (NH₃) concentration at surface (χ), in a manner similar to Riddick et al. (2016), is calculated as

$$\chi = 0.26 \frac{N_{NH_4}}{1+K_H+K_H[H^+]/K_{NH_4}} \quad (A27)$$

where the coefficient 0.26 is the fraction of ammonium in the top 10 cm soil layer assuming exponential distribution of ammonium along the soil depth (given by $3e^{-3z}$, where z is the soil depth), K_H (dimensionless) is the Henry's law constant for NH₃, K_{NH_4} (mol L⁻¹) is the dissociation equilibrium constant for aqueous NH₃, and H^+ (mol L⁻¹) is the concentration of hydrogen ion

that depends on the soil pH ($H^+ = 10^{-pH}$). K_H and K_{NH_4} are modelled as functions of soil temperature of the top 10 cm soil layer ($T_{0.1}$) following Riddick et al. (2016) as

$$\begin{aligned} K_H &= 4.59 T_{0.1} \exp\left(4092 \left(\frac{1}{T_{0.1}} - \frac{1}{T_{ref,v}}\right)\right) \\ K_{NH_4} &= 5.67 \times 10^{-10} \exp\left(-6286 \left(\frac{1}{T_{0.1}} - \frac{1}{T_{ref,v}}\right)\right) \end{aligned} \tag{A28}$$

where $T_{ref,v}$ is the reference temperature of 298.15 K.